NOTICE

The quality of this microform is heavily dependent upon the quality of the original thesis submitted for microfilming. Every effort has been made to ensure the highest quality of reproduction possible.

If pages are missing, contact the university which granted the degree.

Some pages may have indistinct print especially if the original pages were typed with a poor typewriter ribbon or if the university sent us an inferior photocopy.

Reproduction in full or in part of this microform is governed by the Canadian Copyright Act, R.S.C. 1970, c. C-30, and subsequent amendments.

AVIS

La qualité de cette microforme dépend grandement de la qualité de la thèse soumise au microfilmage. Nous avons tout fait pour assurer une qualité supérieure de reproduction.

S'il manque des pages, veuillez communiquer avec l'université qui a conféré le grade.

La qualité d'impression de certaines pages peut laisser à désirer, surtout si les pages originales ont été dactylographiées à l'aide d'un ruban usé ou si l'université nous a fait parvenir une photocopie de qualité inférieure.

La reproduction, même partielle, de cette microforme est soumise à la Loi canadienne sur le droit d'auteur, SRC 1970, c. C-30, et ses amendements subséquents.

CASE PILE WAVE EQUATION ANALYSIS
- CAPWAPC -

EVALUATION OF DRIVEN PILES

Robert D. Edde, P. Eng.

A Thesis
Submitted under the supervision of
Dr. Bengt H. Fellenius, P. Eng.
Professor

in partial fulfillment
of the requirements for the degree of
Master of Applied Science
in Civil Engineering

Department of Civil Engineering
Faculty of Science and Engineering
University of Ottawa

Ottawa, Canada

ISBN 0-315-75010-3

Canada

UNIVERSITÉ D'OTTAWA
UNIVERSITY OF OTTAWA

ACKNOWLEDGEMENTS

This study has been partially supported by the Industrial Research Assistance Program, IRAP. The case history data were provided by Terratech, a division of SNC Inc.

The Author expresses his appreciation for the technical support provided by Pile Dynamics Inc., in particular Dr. Frank Rausche and Mr. Garland Likins. Sincere appreciation for the overall support of Dr. Bengt H. Fellenius. The Author wishes to express his sincere thanks and gratitude for the special support from his beloved wife and cherished parents.

SUMMARY

One of the most important aspects of a piled foundation is the bearing capacity of the individual piles. Correct quantitative evaluation of the pile capacity during pile driving requires the use of dynamic monitoring by means of the Pile Driving Analyzer. These monitoring data are combined with a wave equation analysis and processed using a special software called CAPWAP. The CAPWAP analysis is an iterative procedure whereby the calculated force trace is adjusted to agree with the one measured. CAPWAP analysis requires a close examination of the dynamic behavior of the pile coupled with knowledge of the soil conditions at a particular site. Normally, only one blow is selected for analysis. Yet, different results may be obtained from different blows, even if they are chosen contiguously within the same soil layer. Thus, engineers are faced with the problem of choosing a representative blow for analysis to determine the pile bearing capacity, but the degree is unknown to which the pile bearing capacity depends on the blow analyzed. The bearing capacity determined by CAPWAP is claimed by many to be approximately equal to the capacity determined in static test, while others caution against the reliance on the method because several unknowns are involved in the CAPWAP analysis and the method includes a substantial amount of engineering judgment. Therefore, an investigation is warranted to determine the limitations of the CAPWAP method.

The main objective of the thesis study is to produce a statistical indication of the natural variation between the results from a CAPWAP analysis performed on blows within the same soil layer. More specifically, for three selected case histories, the natural variation is studied between contiguous blows of the pile capacity, the resistance distribution between the shaft and the toe, and of the soil dynamic parameters (quakes and damping) as determined in the CAPWAP analysis.

The first case history includes data from initial driving at Jones Island Advanced Facility: a 36.0 m long closed toe steel pipe pile driven by means of an air/steam hammer through a stratified soil layer varying from an organic clay material to dense clayey silty sand. The second case includes data from initial driving at CN Project, Jasper, Alberta: a 28.0 m long steel H-pile driven by means of a diesel

hammer through stratified layers of variable sizes of cemented sand and thin layers of fine silt. The third case includes data from restriking at National Aviation Museum, Ottawa: a closed-toe steel pipe pile driven by means of a diesel hammer to an embedment depth of 57.0 m through a layer of sand and clay fill into a stratified layer of silty clay.

In each case, the analyzed measurements were recorded when the pile toe penetrated a uniform soil layer over a distance not exceeding 300 mm at initial driving condition and 100 mm at restriking in order to alleviate the effect of depth on the analyses, to exclude the effect of variations of hammer performance, and when the pile has sufficient penetration per blow so that the pile capacity is fully mobilized. All selected blows were analyzed in a random order to eliminate any influence that might result from analyzing the blows contiguously.

In the CAPWAP analysis, all pile segments are assumed unstressed at the end of each impact blow. However, as reported by many (e.g., Holloway et al., 1978; Rausche et al., 1986; and Goble and Rausche, 1986), it is probable that each blow builds in a precompression or pretension condition causing residual load in the pile element from the next blow. Then, the result of the CAPWAP analysis, when assuming no residual loads, may be offset from the true soil resistance and quake values acting on the pile element. Authier and Fellenius (1983) stated that as the pile forces are in equilibrium, the overestimation for one element will be compensated by an underestimation for other pile elements. However, the ultimate soil resistance will be unaffected, but not the resistance distribution between the pile elements, and/or the shaft and toe. Horvath and Killeavy (1988) showed that the total resistance at end-of-initial-driving computed by CAPWAPC, even if the selected blow is poorly chosen, is within 10% of the mean value referred to as the "true value".

All selected blows included in the study were first processed by means of the DATPRO program to evaluate the CMES results, energy transferred, and impact stress and maximum stress, and then, analyzed by means of the CAPWAPC program. The J-factor for the CMES-RMX capacity was selected based on the type of soils at the site and by checking resistance versus time for a varying J-value as

recommended by Goble et al. (1989). The ratio of normalized CMES-RMX and CAPWAPC capacity to normalized impact force, FIMP, and the normalized CMES-RMX and CAPWAPC capacity versus transferred energy are produced to evaluate the influence of the driving system. Also, to isolate the variation effect of total capacity from variation of resistance distribution, a graphical illustration of the ratio of shaft and toe re sistance to capacity was produced.

For the three cases, qualitative evaluation of the wave propagation for each blow record and the graphical illustration of the compiled results from the DATPRO and CAPWAPC analysis show that the selection criteria for the blows are satisfied.

The analysis of the two cases at initial driving indicates that the pile capacity computed by CAPWAPC varies within a range of 10%. The results agree with the mentioned findings of Horvath and Killeavy (1988). Also for the case studied at restrike a range of about 10% is obtained.

Further, the results of the analysis of total resistance indicate that there exists a cyclic behavior ranging within a series of about 3 to 8 blows, noting that analysis was performed at random order by the same CAPWAP operator. This cyclic behavior may be attributed, amongst other, to the effect of varying amount of residual stress between blows which conclusion is supported by the observed variation in calculated distribution of resistance between the shaft and the toe of the pile. At initial driving, the results suggest that the resistance distribution found for the shaft and toe varies up to 15% and 45%, respectively. This variation may be the result of residual stress developed within blows during driving. At restrike, the analyses indicates a variation up to 33% and 68% for the shaft and the toe, respectively. However, this larger variation is mainly influenced by the effect of the breakdown of soil set-up.

The results of the CAPWAPC analysis show also variation in the soil dynamic parameters (quakes and damping) for the cases. The computed soil dynamic parameters vary by up to 40% at initial driving condition. The applied dynamic values demonstrate no particular trend and show to be insensitive to the computed capacity at easy driving condition. At restrike, the Smith damping values along the

.../v

shaft and at the toe demonstrate a trend inverse to that of the shaft and toe resistance, respectively. The quake values along the shaft show a trend proportional to that of the shaft resistance. Case damping and quake values at the toe demonstrate no particular trend.

Further work is recommended to quantitatively evaluate the effect of residual stress on the dynamic analysis of piles from force and velocity measurements with regard to the variation of resistance distribution and soil parameters.

.../vi

TABLE OF CONTENTS

	Page
ACKNOWLEDGEMENTS	i
SUMMARY	ii
TABLE OF CONTENTS	vi
LIST OF TABLES	ix
LIST OF FIGURES	x
LIST OF APPENDICES	xiv
CHAPTER 1. INTRODUCTION	1
CHAPTER 2. THEORETICAL BACKGROUND AND LITERATURE REVIEW	6
CHAPTER 3. TECHNICAL BACKGROUND TO THE CASE STUDIES	37
CHAPTER 4. COMPILATION OF DATA AND ANALYSIS	41
CHAPTER 5. DISCUSSION AND CONCLUSIONS	49
REFERENCES	57
TABLES	
FIGURES	
APPENDICES	

CHAPTER Page

1. INTRODUCTION 1

1.1 General 1

1.2 Statement of the problem 3

1.3 Objectives of the investigation 3

1.4 Scope of the investigation 3

1.5 Outline of the thesis 4

2. THEORETICAL BACKGROUND AND LITERATURE REVIEW 6

2.1 Introduction 6

2.2 Methods of analysis 6

2.3 The Wave equation 9
2.3.1 Wave equation by TTI 11
2.3.2 Wave equation by WEAP 13
2.3.2.1 Pile driving hammers 13
2.3.2.2 Driving system 14
2.3.2.3 Pile model 15
2.3.2.4 Splice model 15
2.3.2.5 Soil model 15
2.3.2.6 Residual stresses 16

2.4 Dynamic monitoring 18
2.4.1 Pile driving analyzer 18
2.4.2 Wave propogation and analytical solutions 19
2.4.3 Case Method Estimate 21
2.4.3.1 Maximum resistance 22
2.4.3.2 Minimum resitance 23
2.4.3.3 Unloading resistance 23
2.4.3.4 Damping independent method 24

2.5 CAPWAP analysis 24
2.5.1 General 24
2.5.2 CAPWAP model 25
2.5.2.1 Pile model 25
2.5.2.2 Soil model 27
2.5.3 CAPWAP procedures 30
2.5.4 Dynamic measurements and CAPWAP analysis 33

2.6 Concluding remarks 35

CHAPTER Page

3. TECHNICAL BACKGROUND TO THE CASE STUDIES 37

3.1 General Background 37

3.2 Soil Description 38
3.2.1 Jones Island 38
3.2.2 CN project 38
3.2.3 National Aviation Museum 38

3.3 Pile Description 38
3.3.1 Jones Island 38
3.3.2 CN project 39
3.3.3 National Aviation Museum 39

3.4 Data Acquisition and data processing 39

4. COMPILATION OF DATA AND ANALYSIS 41

4.1 General 41

4.2 Datpro analysis 41
4.2.1 Jones Island 41
4.2.2 CN project 42
4.2.3 National Aviation Museum 43

4.3 CAPWAP analysis 43
4.3.1 Jones Island 44
4.3.2 CN project 44
4.3.3 National Aviation Museum 44

4.4 Data compilation and evaluation 44
4.4.1 Total activated resistance 44
4.4.2 Resistance distribution 46
4.4.3 Dynamic parameters 47

5. DISCUSSION AND CONCLUSIONS 49

5.1 Discussion 49
5.1.1 Total activated resistance 49
5.1.2 Resistance distribution 52
5.1.3 Dynamic parameters 53

5.2 Conclusions 54

LIST OF TABLES

TABLES	TITLE
2.1	Commonly used dynamic pile driving formulas (after Lawton et al., 1987)
2.2	Pile driving analyzer output quantities
2.3	CAPWAPC unknows
3.1	Soil profile - Jones Island, Milwaukee
3.2	Soil profile - CN Jasper, Alberta
3.3	Soil profile - National Aviation Museum, Ottawa
4.1	Summary of dynamic measurements - Datpro analysis Jones Island, Milwaukee, Pile A1
4.2	Summary of dynamic measurements - Datpro analysis Jasper Alberta, Bent 3, Pile 4
4.3	Summary of dynamic measurements - Datpro analysis Aviation Museum, Pile Q13X-4, 1st retrike
4.4	Summary of total static resistance - CAPWAP analysis Jones Island, Milwaukee, Pile A1
4.5	Summary of total static resistance - CAPWAP analysis Jasper Alberta, Bent 3, Pile 4
4.6	Summary of total static resistance - CAPWAP analysis Aviation Museum, Pile Q13X-4, 1st retrike
4.7	Summary of CAPWAPC resistance distribution Jones Island, Milwaukee, Pile A1
4.8	Summary of CAPWAPC resistance distribution Jasper Alberta, Bent 3, Pile 4
4.9	Summary of CAPWAPC resistance distribution Aviation Museum, Pile Q13X-4, 1st retrike
4.10	Summary of CAPWAPC dynamic parameters shaft and toe Jones Island, Milwaukee, Pile A1
4.11	Summary of CAPWAPC dynamic parameters shaft and toe Jasper Alberta, Bent 3, Pile 4
4.12	Summary of CAPWAPC dynamic parameters shaft and toe Aviation Museum, Pile Q13X-4, 1st retrike

LIST OF FIGURES

FIGURES	TITLE
2.1	Smith pile model (after Smith, 1960)
2.2	Load-Deformation for internal spring (after Smith, 1960)
2.3	Load-Deformation for soil spring (after Smith, 1960)
2.4	Stress-strain relationship at the pile toe (after Smith, 1960)
2.5	Stress-strain diagram for stiffness "k" and coefficient of restitution "e" (after Authier and Fellenius, 1983)
2.6	Comparison of Smith and Case damping (after Authier and Fellenius, 1983)
2.7	Actual stress-strain behavior for cushions — fir (after Lowery et al., 1969)
2.8	Basic components of an external combustion hammer (after Goble and Rausche, 1986)
2.9	Basic components of a single acting diesel hammer (after Goble and Rausche, 1986)
2.10	Diesel hammer model by TTI (after Hirsh and Edwards, 1966)
2.11	The complete wave equation model (after Goble and Rausche, 1980)
2.12	WEAP hammer–driving system model for EHC hammers (after Goble and Rausche, 1986)
2.13	Working principle of a single acting air/steam hammer (after Goble and Rausche, 1986)
2.14	WEAP model for an open end deisel hammer (after Goble and Rausche, 1986)
2.15	Operation cycle for a diesel hammer (after Goble and Rausche, 1986)
2.16	WEAP liquid fuel injection model (after Goble and Rausche, 1986)
2.17	WEAP atomized injection model (after Goble and Rausche, 1986)
2.18	Driving system components (after Goble and Rausche, 1986)

FIGURES TITLE

2.19 WEAP force–deformation curves, hammer and pile cushions (after Goble and Rausche, 1986)
2.20 WEAP pile and soil model (after Goble and Rausche, 1986)
2.21 Total, static, and dynamic soil resistance using case damping (after Authier and Fellenius, 1983)
2.22 Pile model in residual stress analysis (after Goble and Rausche, 1986)
2.23 WEAP static pile–soil model in residual stress analysis (after Goble and Rausche, 1986)
2.24 WEAP resistance versus displacement diagram (after Goble and Rausche, 1986)
2.25 Typical arrangement for attaching transducers (after ASTM D4945–89, 1989)
2.26 Schematic diagram for apparatus for dynamic monitoring of piles (after ASTM D4945–89, 1989)
2.27 Wave speed derivation (after Rausche, 1981)
2.28 Effects of soil resistance on force and VEA/c (after Hannigan, 1990)
2.29 CMES computation for RSP method (after Likins and Hussein, 1988)
2.30 CMES computation for RMX method (after Likins and Hussein, 1988)
2.31 CMES computation for RMN method (after Likins and Hussein, 1988)
2.32 CMES computation for RSU method (after Likins and Hussein, 1988)
2.33 Comparison of Smith and continuous pile model (after CAPWAPC manual, 1989)
2.34 Slack model (after CAPWAPC manual, 1989)
2.35 Comparison of Smith soil model (left) and CAPWAPC viscous damping model (right) (after CAPWAPC manual, 1989)
2.36 Static shaft resistance (after CAPWAPC manual, 1989)
2.37 Static toe resistance (after CAPWAPC manual, 1989)

FIGURES TITLE

2.38 CAPWAPC simulation and iteration procedure (after Hanningan, 1990)
2.39 CAPWAPC wave matching procedure (after Hanningan, 1990)
2.40 CAPWAPC wave matching intervals (after CAPWAPC manual, 1989)
2.41 CAPWAPC graphical output - Jones Island
2.42 CAPWAPC graphical output - CN Jasper
2.43 CAPWAPC graphical output - National Aviation Museum
3.1 Dynamic measurement record - Jones Island
3.2 Dynamic measurement record - CN Jasper
3.3 Dynamic measurement record - National Aviation Museum
3.4 Driving log diagram, Jones Island
3.5 Driving log diagram, CN Jasper
3.6 EOID driving log diagram, National Aviation Museum
4.1 Jones Island impact force
4.2 Jones Island transferred energy
4.3 Jones Island CMES capacity – RMX
4.4 Jones Island – RMX/FIMP
4.5 Jones Island transferred energy and RMX/FIMP
4.6 CN Jasper impact force
4.7 CN Jasper transferred energy
4.8 CN Jasper CMES capacity – RMX
4.9 CN Jasper RMX/FIMP
4.10 CN Jasper transferred energy and RMX/FIMP
4.11 Aviation Museum impact force
4.12 Aviation Museum transferred energy
4.13 Aviation Museum CMES capacity – RMX
4.14 Aviation Museum – RMX/FIMP
4.15 Aviation Museum transferred energy and RMX/FIMP
4.16 Jones Island CAPWAPC static resistance
4.17 Jones Island CAPWAPC static resistance / impact force
4.18 Jones Island CAPWAPC static resistance and transferred energy
4.19 Jones Island CAPWAPC and CMES static resistance
4.20 CN Jasper CAPWAPC static resistance
4.21 CN Jasper CAPWAPC static resistance / impact force
4.22 CN Jasper CAPWAPC static resistance and transferred energy
4.23 CN Jasper CAPWAPC and CMES static resistance
4.24 Aviation Museum CAPWAPC static resistance

FIGURES **TITLE**

4.25 Aviation Museum CAPWAPC static resistance / FIMP
4.26 Aviation Museum CAPWAPC static resistance and transf. energy
4.27 Aviation Museum CAPWAPC and CMES static resistance
4.28 Jones Island CAPWAPC static resistance distribution
4.29 Jones Island CAPWAPC resistance ratio - shaft and toe
4.30 CN Jasper CAPWAPC static resistance distribution
4.31 CN Jasper CAPWAPC resistance ratio - shaft and toe
4.32 Aviation Museum CAPWAPC static resistance distribution
4.33 Aviation Museum CAPWAPC resistance ratio - shaft and toe
4.34 Jones Island CAPWAPC dynamic parameters – shaft
4.35 Jones Island CAPWAPC dynamic parameters – toe
4.36 CN Jasper CAPWAPC dynamic parameters – shaft
4.37 CN Jasper CAPWAPC dynamic parameters – toe
4.38 Aviation Museum CAPWAPC dynamic parameters – shaft
4.39 Aviation Museum CAPWAPC dynamic parameters – toe

LIST OF APPENDICES

APPENDICES	TITLE
A1	Datpro analysis output – Jones Island , Pile A1
A2	Datpro analysis output – CN Jasper, Bent 3, Pile 4
A3	Datpro analysis output – Aviation Museum, Pile Q13x–4
B1	CAPWAPC analysis output – Jones Island , Pile A1
B2	CAPWAPC analysis output – CN Jasper, Bent 3, Pile 4
B3	CAPWAPC analysis output – Aviation Museum, Pile Q13x–4

CHAPTER 1

INTRODUCTION

1.1 GENERAL

Piles are used to support buildings, bridges, harbor piers, industrial chimneys, and other heavy structures. Primarily, piles are used to reduce or eliminate settlement of the structures.

One of the most important aspects of a piled foundation is the bearing capacity of the individual piles. Piles are usually driven or augered to a certain depth for a required capacity. Driven piles are installed by means of impacting the pile head with a pile driving hammer. The hammer can be a simple gravity drop hammer in the form of a solid ram mechanically hoisted over the pile head and released to fall by gravity, or a hydraulically operated weight, or a hammer where the lifting power is provided by a diesel combustion.

For each hammer impact, the pile is forced to penetrate into the ground. A progressively smaller penetration is often an indication of an increasing pile bearing capacity. However, from knowing only the penetration resistance, it is impossible to estimate correctly the pile capacity. Other related necessary information is the hammer size in terms of potential energy, the pile size, and the soil interaction during impact – a stiff pile in a strong soil will be able to absorb greater energy than a weak pile in a soft soil.

Several computer wave equation programs are available for estimating the bearing capacity of a driven pile. These computer programs include the hammer, the pile, and the soil in a mathematical model. The model simulates the pile as a series of lumped masses connected with elastic springs, and the soil as a series of elastic-plastic springs characterized by the plastic strength and the length of the elastic range (the quake). In addition, the soil viscous properties are simulated by means

.../2

of applying damping factors to the model. Although the theoretical model accurately represents pile-soil behavior, the difficulty in applying the analysis in practice lies with the choice of input parameters. However, for qualitative consideration, the wave equation analysis is a valuable tool in the foundation engineering analysis.

Correct quantitative evaluation of the pile capacity requires the use of measurement during actual pile driving. A hammer impact induces a strain wave in the pile travelling from the pile head down toward the pile toe. Dynamic monitoring of pile driving consists of monitoring the strain wave by measuring acceleration and force induced in the pile from each impact. By means of accelerometers and strain gages attached to the pile head, the dynamic monitoring measures what is actually delivered to the pile by the hammer. It can, therefore, quite reliably be used to determine the capacity of the monitored pile.

Dynamic monitoring data combined with a wave equation analysis are processed using a special software called CAPWAP. The analysis by means of CAPWAP provides information on the compressive and tensile forces induced in the pile, the behavior of the pile driving hammer, the energy transferred to the pile, the pile bearing capacity, and the soil dynamic properties, such as quake and damping.

In a CAPWAP analysis, the computer takes the measured velocity and converts it into force through application of wave dynamics. In an iterative procedure, the theoretical force trace is modelled to agree with the measured one. This is called the CAPWAP signal match, where the most important result is the bearing capacity of the pile.

The CAPWAP determined bearing capacity is claimed by many to be approximately equal to the capacity determined in static test, while others caution against the reliance on the method.

Dynamic monitoring and analysis are recommended in the Ontario Highway Bridge Design Code (1983) as well included in the Canadian Foundation Engineering Manual (1985).

1.2 STATEMENT OF THE PROBLEM

The CAPWAP analysis has tremendous technical and economical advantage over the conventional static pile testing. However, several unknowns are involved and the method includes a substantial amount of engineering judgment. Thus, more work needs to be carried out to investigate the limitations of the method.

Performing CAPWAP analysis requires a close examination of the dynamic behavior of the pile coupled with knowledge of the soil conditions at a particular site. Normally, only one blow is selected for analysis. Yet, different results may be obtained from different blows, even if they are chosen contiguously within the same soil layer. Also, engineers are faced with the problem of choosing a representative blow for analysis to determine the pile bearing capacity, but the degree is unknown to which the pile bearing capacity depends on the blow analyzed.

1.3 OBJECTIVE OF THE INVESTIGATION

The main objective of the investigation is to produce a statistical indication of the natural variation between the results from a CAPWAP analysis performed on blows within the same soil layer.

More specifically, the objective is to study the natural variation between contiguous blows of the pile capacity, the resistance distribution between the shaft and the toe, and of the soil dynamic parameters (quakes and damping) as determined in the CAPWAP analysis.

1.4 SCOPE OF THE INVESTIGATION

Three pile case histories with different soil conditions, pile properties, and driving conditions have been considered in the research work. From each site, dynamic

measurement data for one pile were closely examined. The analyzed measurements were recorded for a uniform soil layer over a penetration not exceeding 100 mm in order to alleviate the effect of depth on the analyses.

The investigations consisted of CAPWAP analysis of dynamic measurements taken at initial driving for the two first case histories, and at restriking for the third case history as follows;

Case 1, Jones Island Advanced Facility: a closed toe steel pipe pile driven by means of an air/steam hammer through a stratified soil layer varying from an organic clay material to dense clayey silty sand.

Case 2, CN Project, Jasper, Alberta: a steel H-pile driven by means of diesel hammer through stratified layers of variable sizes of cemented sand and thin layers of fine silt.

Case 3, National Aviation Museum, Ottawa: a closed-toe steel pipe pile driven by means of a diesel hammer through a layer of sand and clay fill into a stratified layer of silty clay.

For the three cases considered, the effect of variation between blows was investigated.

All selected blows were digitized from a four channel analog signal and were processed by means of a software called DATPRO (Goble et al., 1989). Then, each blow was analyzed by means of a Case Pile Wave Analysis Program Continuous Model, CAPWAPC (Goble et al., 1989). For each case history, the selected blows were analyzed in a random order to eliminate any influence that might result from analyzing a contiguous series of blows.

1.5 OUTLINE OF THE THESIS

The thesis work is reported thereafter in four chapters. Chapter 2 presents the

stress wave theory applied to pile driving, dynamic monitoring, and CAPWAP analysis. Chapter 3 presents factual technical background to the case studies. Chapter 4 presents compilation of processed data and results of the CAPWAP analysis. Chapter 5 presents discussion of the analysis in relation to the total activated resistance, resistance distribution, and dynamic soil parameters, and conclusions.

CHAPTER 2

THEORETICAL BACKGROUND AND LITERATURE REVIEW

2.1 INTRODUCTION

Pile foundations served the need over centuries to support heavy structures to prevent excessive settlement associated with shallow foundations. The widespread use of pile foundations both on land and offshore demonstrated the need to search for more reliable methods for analysis and design of piles.

In the mid 1800's, it was realized that capacity of driven piles is a function of the penetration resistance in terms of penetration distance per blow. It was later found that the capacity was also a function of the efficiency and impact of driving system. Since then, many have attempted to quantify the pile capacity from the penetration resistance.

Early attempts to relate the penetration resistance to the pile capacity resulted in several dynamic formulae. As a results of the shortcomings of the dynamic formulae, later development resulted in what is called Wave Equation Analysis. Field measurements were performed to assess and verify the methods and their related assumptions. Such measurements, referred to as Dynamic Monitoring, were carried out by means of a data acquisition system called the Pile Driving Analyzer. Coupling the Wave Equation Analysis with dynamic monitoring resulted in what is known today by the term CAPWAP analysis – Case Pile Wave Equation Analysis.

2.2 METHODS OF ANALYSIS

A pile driving formula is an attempt to evaluate the pile capacity as a function of the nominal energy and penetration resistance. Such formulae are based on Newton's law of impact and the principle of conservation of energy and are modified to account for energy losses during impact and during the propagation of stresses.

In 1820, 170 years ago, Eytelwein proposed the first dynamic formula by equating the total energy of the ram at impact to the work done to drive the pile (Jumikis, 1971). That is, the product of the ram weight and the stroke was assumed directly proportional to the product of the ultimate resistance and the distance the pile head moved.

In 1859, Redtenbacher proposed a dynamic formula termed by Jumikis (1971) "the pure, classical, complete dynamic pile driving formula". Other dynamic pile driving formulae are simplifications of Redtenbacher's formula, except those based on empirical results, by introducing correction for the energy loss through the hammer and pile cushion, pile, and soil. Where applicable, the use of the derived formulae normally result in an overly conservative and costly foundation.

Many formulae, as illustrated in Table 2.1, are still in use today. Their applications are restricted to a particular soil, pile, and driving condition for which correlation factors have been derived. Then, they are considered to yield a calculated bearing capacity that agrees with capacities observed in static loading tests. The problem is choosing an appropriate formula, and, unfortunately, in many cases no dynamic formula yields acceptable results, because, pile driving is not a simple problem that can be solved by the direct application of Newton's Law, as also reported by many e.g., Cummings (1940); Smith (1960); Forehand and Reese (1964); Lowery et al. (1969); Thompson and Thompson (1979); and Lawton et al. (1987).

Not only bearing capacity determination, but also, driving stresses are of major importance in the design of piles. Compressive stresses are determined by dividing the maximum driving force by the cross-sectional area at the pile head. However, conventional pile driving formulae are unable to calculate stresses.

Further development to evaluate the pile bearing capacity considered the principles of wave propagation in piles. That is, for a long slender rod free at both ends, when struck at one end, a tensile wave will be reflected from the opposing end with a magnitude that equals twice the impact velocity. For a slender long rod having one rigidly fixed end, when struck at the free end, the resulting wave reflection is twice the impact force. Thus, the reflected wave resulting from an impact at one end provides information regarding the resistance at the opposing end. The time

required for the wave to travel the rod length and back to the impact end is 2L/c; where L is the length of the rod and c is the wave speed. Reflections reaching the impact end prior to 2L/c are caused by resistance along the length of the rod.

The method of analysis using the principles of a travelling wave are called Wave Equation Analysis and it was first incorporated in a practical computer program by Smith, 1960. Two common programs in use today are the TTI, developed by Lowery et al. (1969) at the Texas Transport Institute, and the WEAP, Wave Equation Analysis Program developed by Goble and Rausche (1976). The development of both programs was sponsored by the Federal Highway Administration, USA.

The advantage of the Wave Equation over a simple dynamic formula is the ability to consider more realistically the hammer/pile/soil system. Unlike dynamic formulae, compressive and tensile stresses are computed by the Wave Equation. The computer program requires input of soil properties, and of the pile and hammer model parameters. Although good agreement has been reached between theoretical and actual bearing capacity, difficulties arise not only from variations in the soil conditions within the same site, but also from inconsistency within the driving system. That is, for a pile driving hammer, the hammer parameters such as cushion, impact block assembly and mechanical operations of the hammers vary. Therefore, the need for verification of the analysis results by actual measurements is obvious.

Dynamic stress measurements in pile driving were first taken by Glanville et al. (1938). In 1960, Michigan Department of Highway started a large research project (Housel, 1965). In 1964, Case Institute of Technology (today Case Western Reserve University) began an extensive research and development programme of dynamic measurements. The measurements were performed by means of a quartz accelerometer and a strain transducer attached to the pile head. Records were stored on analog magnetic tape. Today, similar measurements are performed using advanced piezoelectric accelerometers and strain gages. The gages provide a measurement of force by means of a calibration factor applied to strain and of velocity by integration from acceleration. Records are processed in real time on site by means of a special equipment called the Pile Driving Analyzer and simultaneously stored on a seven–channel analog tape recorder.

The Pile Driving Analyzer is a computer specially designed for data acquisition and processing of the measurements in the field. Later research at Case sponsored by the Ohio Department of Transportation continued and assisted in further developing and implementing the Pile Driving Analyzer in the design and construction of pile foundations.

From the dynamic measurements, quantities such as compressive and tensile stresses, transferred energy, and capacities are obtained. The bearing capacity is computed by means of empirical relationships called Case Method Estimate, CMES, developed at Case Institute of Technology (Goble et al., 1975) that includes a socalled Jfactor. Capacities for piles with large toe damping or long piles are underpredicted in comparison with static tests as reported by Goble et al. (1975). Riker and Fellenius (1983) reported that the sensitivity of the CMES capacity to the J-factor is a function not only of the driving condition but also of the pile type. The use of the Case Method Estimate is limited where the need arises to evaluate shaft and toe resistance distribution.

Concurrently with the development of the Case Method Estimate, a Case Pile Wave Equation Analysis Program (CAPWAP) was produced (Goble et al., 1980). The program uses pile head force and velocity measurement along with a wave equation type soil and pile model. The method enables the user to check assumptions on dynamic properties against measured pile behavior (force and velocity versus time). The results of the CAPWAP analysis are the total activated capacity, distribution of static resistance between shaft and toe, compressive and tensile stresses, transferred energy, pile impedance change, and calibrated dynamic properties. As well, results from the CAPWAP analysis are used to calibrate the Case Method Estimate, to refine the assumptions used in Wave Equation analysis, and to evaluate the integrity of the pile.

2.3 THE WAVE EQUATION

The basic Wave Equation was developed over a hundred years ago by Saint Venant and Boussinesq for end impact on rods (Forehand and Reese, 1964). Isaacs (1931) pointed out that wave action occurred in a pile during driving and that one–dimensional wave mechanics could be applied for such analysis. A solution to

the wave equation was first published by Glanville et al. (1938) with a number of simplifying assumptions to facilitate computations. About thirty years ago, Smith (1960) published a mathematical model for the analysis that has become the basis for all modern wave equation computer programs.

The Smith pile model consists of a series of lumped masses connected with weightless spring and subjected to a soil resistance. The mass elements are infinitely stiff. The stiffness of the spring is represented by EA/L where "E" is the modulus of elasticity of the mass element, "A" is the cross sectional area, and "L" is the length. In addition, the model considers the physical characteristics of the driving system such as the ram, the hammer cushion, and the pile helmet. The model is illustrated in Fig. 2.1.

The Smith soil model is an elasto-plastic function of displacement and a dashpot dynamic damping which is a linear function of the pile velocity. The soil resistance during driving consists of two components: a dynamic portion and a static portion. The dynamic resistance is also called damping resistance. The static resistance is assumed equal to the static bearing capacity of the pile. For clay soils, Litkouhi and Poskitt (1980) reported that the assumed linear proportionality of the damping resistance with the pile velocity is incorrect and rather insensitive to the soil type or to the soil dynamic properties.

The internal spring load deformation characteristics used by Smith is illustrated in Figs 2.2 (a) and (b) for cases with and without damping. The external spring load deformation behavior assumed by Smith representing soil resistance along the shaft and at the toe of the pile is shown in Fig. 2.3. Arrows indicated in Figs 2.2 and 2.3 illustrate the load–deformation path in loading conditions.

To calculate the pile capacity, Smith accounted for the elastic soil compression called quake "q" (Fig. 2.4), the ultimate soil resistance "R_u", and the viscous damping "j_s". The Smith damping is a ratio between the velocity and the damping force. Smith assumed a viscous damping factor along the shaft and at the toe of the pile equal to 0.05 s/m and 0.15 s/m, respectively. The original Smith model applied a constant quake value equal to 2.5 mm (0.1 inch).

At impact, both the hammer and pile cushion behavior are represented by a stress-strain relationship illustrated in Fig. 2.5. The ratio at which driving energy is transferred to the pile head is called coefficient of restitution, "e". This coefficient "e" indicating the relative loss of energy is defined as the square root of the ratio between the energy reaching the material (A_1+A_2) and the energy leaving the material (A_2). It can also be presented as a function of the loading stiffness (slope), k_1, and unloading stiffness, k_2. Then, the coefficient of restitution is equal to the square root of k_1/k_2.

The wave equation computations start by initiating an initial hammer ram velocity as input from the pile driver parameters. A pile head displacement is calculated from the integral of the velocity during a short time interval. The displacement compresses the uppermost spring, and the resulting force is calculated using the spring constant, which is the corresponding element stiffness. An external spring force is computed from the relative difference between the displacement of the pile element spring and the plastic displacement of the soil element spring by using the soil spring constant and excluding the soil damping effect. The acceleration is then computed using the resultant force and the element mass, which gives the element velocity at the end of the time interval. Element by element, the computation cycle is carried down the pile for successive time intervals .

2.3.1 WAVE EQUATION BY TTI

The TTI (Texas Transportation Institute) wave equation program, originated from the approach by Smith (1960), was developed by Hirsh et al. (1976) in the mid-1970's and was modified to accommodate a large variation of field problems.

The TTI used Smith damping. However, as shown by Authier and Fellenius (1983), the Smith damping approach results in a zero damping force in unloading when the static resistance is zero (Fig. 2.6). This was undesirable, because at this point, the pile still has a velocity.

Smith original model does not account for the static weight of the pile. That is, at time zero, all internal and external springs exert zero force. The TTI program corrects this aspect by assigning initial forces to produce equilibrium of the system.

Through a series of dynamic and static tests on hammer and pile cushion material performed by Hirsch and Edwards (1966), it was concluded that the stress-strain curves are not linear as assumed by Smith (Fig. 2.5), but rather appear as shown in Fig. 2.7. The TTI program is not able to model actual measured stress-strain behavior. Instead, the program uses a linear force-deformation curve with the loading portion based on the secant modulus of elasticity for the material (as opposed to an averaged modulus of elasticity). The unloading portion of the curve is based on the actual coefficient of restitution. The program requires input for both the hammer and pile cushions material k_1 and e, and the program computed k_2.

One of the most important parameter involved in the wave equation modelling is the energy output of the hammer and the energy transferred to the pile head. A large variation between manufacturers' rated energy and the output energy have been measured in the field. The hammer energy output for air/steam and diesel hammers (Figs 2.8 and 2.9) can be controlled by regulating the steam pressure or the quantity of diesel fuel supplied to the hammer.

The TTI program is developed primarily for analysis of piles driven with air/steam hammers or drop hammers. In conventional single-acting steam hammers, the steam pressure or energy is used to raise the ram for each blow. The magnitude of the steam force is too small to force the pile downward and, consequently, it works only on the ram to restore the potential energy for the next blow.

Diesel hammers, in the TTI program, are simply modelled as drop hammers with the explosion acting in conjunction with the impact. The explosive pressure in diesel hammers used to raise the ram is considered relatively large for a short time duration and exerts force on the pile. In the TTI program, to account for the effect of the explosive force in a diesel hammer, the force between the ram and the impact block is assumed to reach some maximum and then decrease to a specified minimum. That is, the program assumes that the explosive pressure maintains a specified minimum force between the ram and the impact block for a given time, after which the force tapers off to zero (Fig. 2.10). However, New York State Department of Transportation encountered serious problems when TTI wave equation program was used for piles driven by diesel hammers. Unrealistic values for driving stresses were sometimes also obtained (Lawton et al., 1987).

In response to the shortcomings of the TTI program with regard to piles driven by a diesel hammer, further development was undertaken in the WEAP wave equation program.

2.3.2 WAVE EQUATION BY WEAP

The WEAP program was first released in 1976 under the Federal Highway Administration sponsorship. The program adopted Smith's original concept with various improvement on the soil and hammer models (Fig. 2.11). Holloway (1978) showed that the residual stresses during pile driving have a major effect on the pile stresses and blow count (Rausche et al., 1986). Therefore, in 1983, the WEAP program was modified at the University of Colorado to incorporate a residual stress analysis, and called CUWEAP. The revised version, May 1986, of the wave equation program by Goble and Rausche is called WEAP86.

WEAP86 includes all the features of the previous WEAP versions plus separate models for liquid and atomized fuel injection for diesel hammers; modification of the pile splice model; and modification of the residual stress analysis.

2.3.2.1 Modelling of Pile Driving Hammers

As in the TTI, the WEAP program considers two types of hammers: external combustion hammers (ECH), an external source of power such as drop or air/steam hammers; and internal combustion hammers (ICH), an internal source of power such as diesel combustion.

For ECH, the WEAP program models the ram by a single mass. The ram mass impacts against a spring which represents the hammer cushion. Also, the hammer assembly which consists of a cylinder, columns, and base plate is modelled as illustrated in Fig. 2.12.

The working principle of an air/steam hammer is illustrated in Fig. 2.13. Difficulties are encountered with these hammers when pressure enters the cylinder before the ram impact, causing a reduction of the ram impact velocity. This behavior is called preadmission and it impairs the hammer efficiency.

For ICH, the WEAP diesel model for long slender ram includes several ram segments and the impact block segment on top of the hammer cushion (Fig. 2.14). The working principle of an open-end diesel hammer is illustrated in Fig. 2.15.

Unlike the TTI, the WEAP realizes the presence of pressure between the ram and the impact block. This pressure is calculated according to the gas laws during compression and expansion. Two different types of fuel injection are used: liquid (LI) and atomized (AI).

The most common method is the LI or low-pressure fuel injection. The LI ignition occurs within a certain time after or at impact since the required atomization for ignition is produced by the impact (Fig. 2.16). This time interval is called the combustion delay. After ignition starts, the pressure is assumed to increase linearly with time for a short ignition duration to a maximum pressure value, p_{max}, determined by measurement or trial and error computational procedures.

The AI combustion requires high injection pressures that produce a very fine fuel spray which ignites shortly after injection (Fig. 2.17). At the time of impact, the full pressure, p_{max}, is reached and the chamber pressure remains at this value until the final volume of combustion is reached. After that time, adiabatic expansion takes place.

The stroke for the diesel ram increases as the pile driving becomes harder. In soils with high resistance but low stiffness, a "spongy" driving situation results that yields a relatively low stroke. A similar situation can occur on very long, flexible piles. In fact, practically all components of the hammer/pile/soil system have an effect on the diesel hammer performance.

2.3.2.2 Driving System

The driving system consists of the hammer cushion, helmet, and the pile cushion (Fig. 2.18). The helmet is assigned all the weight of the system and is considered a rigid mass. The stiffness, k_c of both the hammer and pile cushion are computed from the cushion material modulus E_c, area A_c, and thickness t ($k_c = E_c A_c / t$).

As an additional improvement over the TTI program, the force/deformation behavior of the cushion material was modelled including a roundout at low forces as found by Hirsch and Edwards (1966) (Fig. 2.7). That is, at low loading level, the extent of deformation, d_{SC}, is nonlinear (Fig. 2.19).

The dissipation of energy that occurs in the cushion material is represented by a coefficient of restitution, e. However, in contrast to the TTI program, the WEAP program requires input of the unloading stiffness, k_2, and the coefficient "e" to compute the loading stiffness, k_1, for both the hammer and pile cushions.

2.3.2.3 Pile Model

Piles may be uniform along their length or may have an enlarged pile toe area, tapered end, or stepwise reductions in cross-section. The pile length should be at least ten times its diameter for the laws of the one-dimensional wave equation to be applicable. The pile is modelled as a series of masses and springs representing the weight and stiffness of the pile over each segment (Fig 2.20).

2.3.2.4 Splice Model

For long piles where splices are used, additional modelling features are required. Splices are modelled like cushioning materials, with a non-linear force-deformation relationship and a limited slack zone where an extension is possible without tension force (Fig. 2.19).

2.3.2.5 Soil Model

As in Smith's model, a soil resistance force is assumed to act at each pile segment below grade. The soil resistance has both a static and dynamic component. The static soil resistance is proportional to the displacement of the pile segment up to a limiting deformation value which Smith called quake. That is, when the pile displacement exceeds the quake, the element moves without further increase in resistance. This elastic-plastic behavior is schematically represented by a spring with a friction element (Fig. 2.11). In case of rebound, the soil resistance decreases parallel to the loading slope (Fig. 2.3).

Both the WEAP86 and the TTI programs use Smith's approach for the dynamic resistance component, D. That is, D is proportional to the pile velocity, v_p, and the static soil resistance, R_s, as follows.

$$D = j_s v_p R_s \qquad \text{Eq. 2.1}$$

The quantity j_s is Smith damping value of dimension time/length. However, as mentioned earlier, this damping approach is undesirable because it suggests a zero damping force in unloading when the static resistance is zero (Fig. 2.6). To offset this, WEAP86 offers an alternative damping definition called "case damping" (Goble and Rausche, 1976) that yields a more realistic conditions (Fig. 2.21).

The case damping alternative is a dimensionless factor and the damping force is obtained by multiplying the velocity with the damping factor and the pile-material impedance, EA/c, where c is the wave velocity in the pile. In contrast to the Smith damping, the Case damping can more easily be related to the soil properties. However, with Case damping, the soil damping force becomes dependent on the particular pile material and cross-sectional area.

2.3.2.6 Residual stresses

During impact, the pile displaces a larger distance at the pile head than at the pile toe. In unloading, the shaft resistance prevents the pile from complete rebound and the pile remains compressed to some degree. The resulting stress is called residual stress and such stresses are common for a long, flexible pile subjected to high shaft resistance (Fig. 2.22). Because of the stiffer response, upon the next blow, larger stresses will be accumulated in the pile as compared to the previous blow, and a greater toe displacement will result. In long piles, both tensile and compressive stresses may remain after the duration of a blow. Therefore, the penetration distance resulting from the next blow will be related to the stress condition in the pile. That is, if the net residual stress in the pile is compressive, the resulting penetration distance from a consecutive blow will be larger as opposed to a condition where the net residual stress is tensile, and vice versa.

As reported by Holloway et al. (1978) and Rausche et al. (1986) when residual stresses are neglected, the capacity will be underpredicted; the shaft resistance distribution along the pile will be overestimated (Holloway et al. 1978).

Residual stress analysis (RSA) option computes the displacements and the static soil resistance values after the pile has completely come to rest. The pile/soil model used for the analysis is similar to that of conventional wave equation model, but does not use a dashpot (Fig. 2.23).

At the end of the dynamic cycle, a soil spring may be in one of four situations (Fig. 2.24) as follows;

- the spring deformation is within the elastic range and therefore loading and unloading will occur on the same path.

- the spring deformation reached the plastic range and the soil resistance is the ultimate resistance. The unloading will start from the Point D and will follow a path parallel to the loading line.

- the spring deformation reached the plastic range but started to unload. Further unloading will occur on the same slope. If the ultimate soil resistance in tension is reached, the unloading will follow the path of plastic behavior.

- the spring deformation reached the plastic range in compression, then in tension. Thus, the unloading will occur along the plastic line.

The mathematical solution of the problem involves a set of linear equations subject to the conditions of elastic-plastic springs. The residual stress analysis is found to produce lower penetration resistance values and higher pile stresses than observed (Goble and Rausche, 1986).

As reported by Goble and Rausche (1986), the effect of residual stress analysis becomes very large in soils with high resistance, i. e., when final penetration resistance is small. In those situations, the difference between the assumed elastic-plastic and the actual non-linear soil behavior are potentially large. Therefore,

further development work is required to model the effect of residual stress on pile driving and analysis.

2.4 DYNAMIC MONITORING

Dynamic monitoring of pile driving is performed to confirm assumptions and calculations made in the Wave Equation Analysis.

Dynamic monitoring involves taking measurements of force and velocity near the pile head. Such measurements are obtained by means of two strain gages and two accelerometers placed diametrically opposed near the head of the pile (Fig. 2.25).

The strain transducer consists of four foil gages attached at a stress concentration points in a flexible hexagonal aluminum transducer frame. The foil gages are 350 ohm gages connected in a full bridge.

The accelerometers are piezoelectric devices with built-in amplifiers to reduce electronic noise from the cable. The nominal range is 1000 g with a maximum shock limit of 5000 g. The nominal sensitivity is 5 millivolts/g and a frequency range between 1 through 5000 Hz. They are mounted on a specially designed aluminum block which provide electronic ground isolation. The block is a rigid base with characteristics to eliminate resonant frequencies greater than 20,000 Hz.

During dynamic monitoring, each driving record measured in the field is processed by means of the Pile Driving Analyzer (PDA), displayed on an oscilloscope, and stored on an analog tape recorder as illustrated in Fig. 2.26.

2.4.1 PILE DRIVING ANALYZER

The Pile Driving Analyzer is a portable field computer that processes both strain and accelerometer signals during the monitoring operation. The pile driving analyzer amplifies, filters, and processes the strain signal. The accelerometer signal is conditioned by a limited current supply and transmitted through a special integrator.

The Pile Driving Analyzer (PDA) converts the analog strain and acceleration signals into digital force and velocity waves versus time. For each blow, dynamic quantities are computed such as impact force, maximum compressive force, maximum tension force, maximum transferred energy into the pile at the gage location, Case Method Estimate capacity, etc. In all, thirty dynamic quantities are computed (Table 2.2).

2.4.2 WAVE PROPAGATION AND ANALYTICAL SOLUTIONS

The fundamentals of wave mechanics used in the PDA have been described by Rausche (1981). The following should be noted when deriving the relationship between the wave speed and the material properties, and the proportionality in wave propagation:

- the "wave speed" is the speed with which a compression or tension zone moves along a rod.
- The "particle speed" is the speed with which a particle in a rod moves as a wave propagates.

The stress wave in a rod struck by a mass is presented by small elements compressed in sequence transferring a strain, ϵ, along neighboring elements to the end of the rod (Fig. 2.27). Compression of the material, δ, results in a motion of the particles or in a particle velocity, V, over a time interval Δt:

$$V=\delta/\Delta t \qquad \text{Eq. 2.2}$$

Using Hooke's Law and Newton's Second Law (the element deformation and the particle velocity), this yields the relationship between the wave speed, c, and the material properties of the rod as follows (Fig. 2.27):

$$c^2=E/\rho \qquad \text{Eq. 2.3}$$

where E is Young's Modulus and ρ is the rod unit mass. In addition, the strain is proportional to the particle velocity at the same point in the rod material. That is, the stress wave during a time interval, Δt, after the rod being struck by a mass, travels a distance, ΔL (Fig. 2.27),

$$\Delta L = \Delta t\, c \qquad \text{Eq. 2.4}$$

Since the material below the point becomes compressed, the point moves a distance, δ. This deformation δ was caused by a strain ϵ over a distance ΔL, or

$$\epsilon = \delta / \Delta L \qquad \text{Eq. 2.5}$$

combining Eqs. 2.2, 2.4, and 2.5, and multiplying both sides of the equation by the Young's modulus, E, and the cross-sectional area, A, of the rod will yield the basic relationship of stress wave measurements,

$$F = V\, EA/c \qquad \text{Eq. 2.6}$$

"EA/c" is referred to as the pile impedance, Z.

The impedance for non uniform pile cross-sectional area is obtained by substituting Eq. 2.3,

$$Z = EA/c = Mc/L \qquad \text{Eq. 2.7}$$

where, M = pile mass
c = wave speed of the pile material
L = pile length

The magnitude of force and VEA/c are equal at impact. This relationship will no longer hold when the reflected soil resistance forces reaches the gage location on the pile, because reflections from the soil resistance will cause an increase in the force wave and a corresponding decrease in the VEA/c wave.

The time at which the stress wave travels down the pile and back up again to the location of the gages is 2L/c. Knowing the wave speed of the pile material and the length of the pile, the location of the soil resistance acting at one point along the length of the pile may be identified (Fig. 2.28).

2.4.3 CASE METHOD ESTIMATE

The Case Method Estimate (CMES) is a closed-form solution to the one-dimensional stress wave propagation to evaluate the pile capacity (ultimate resistance). Initially, from the rigid body equation, the total penetration resistance, RTL, was computed;

$$RTL = F(t) - Ma(t) \qquad \text{Eq. 2.8}$$

Where F(t) is the force and a(t) is the acceleration at the pile head measured as a function of time, and M is the pile total mass. Later studies by Rausche (1970) at Case Western Reserve University resulted in the basic CMES equation;

$$RTL = \tfrac{1}{2}(FT1 + FT2) + \tfrac{1}{2}(VT1 - VT2)Mc/L \qquad \text{Eq. 2.9}$$

where,
- RTL = total static and dynamic resistance
- FT1 = force and velocity at Time 1, that is, at peak
- FT2 = force at Time 2, that is, T1+(2L/c)
- VT1 = velocity at Time 1
- VT2 = velocity at Time 2

This solution, taking into account the travelling wave, was derived based on the assumption of a uniform pile cross-section, linear elastic pile behavior, and one-dimensional wave propagation.

Goble et. al. (1975) assumed that the dynamic driving resistance can be expressed as a linear function of the pile toe velocity. In turn, the pile toe velocity can be estimated from the pile head velocity obtained from dynamic measurements,

$$v_{toe} = (FT1 + Z\,VT1 - RTL)/Z \qquad \text{Eq. 2.10}$$

The dynamic resistance, R_d, caused by damping can be analytically expressed as,

$$R_d = j_c\,(Mc/L)\,v_{toe} \qquad \text{Eq. 2.11}$$

Where j_c = dimensionless Case Damping constant, also called J-factor

Thus, the total static resistance, RSP, called the damping factor method (Likins and Hussein, 1988) can be computed,

$$RSP = RTL - R_d \qquad \text{Eq. 2.12}$$

Or, substituting Eqs. 2.10 and 2.11,

$$RSP = RTL - j_c[VT1(Mc/L) + FT1 - RTL] \qquad \text{Eq. 2.13}$$

Expressing the equation in terms of force and velocity,

$$RSP = [(1-j_c)(FT1 + Z\,VT1) + (1+j_c)(FT2-Z\,VT2)]/2 \qquad \text{Eq. 2.14}$$

This approach worked well on pile driven into cohesive soils (Likins and Hussein, 1988). An illustrative example is provided in Fig. 2.29.

Other damping dependent relationships, such as Maximum Resistance (RMX), Minimum Resistance (RMN), and Unloading Resistance (RSU), have been derived to evaluate the capacity of piles with different characteristics of the force and velocity wave measured.

2.4.3.1 MAXIMUM RESISTANCE, RMX

To fully engage the pile capacity, the toe displacement should be larger or at least equal to the quake at the toe of the pile.

This approach is suitable for cases where the quake at the toe of the pile is large, the impact of the driving hammer is small, or the rise time to peak is short. That is, for evaluating the static capacity of displacement piles driven into saturated fine grained soils, or piles having large penetration resistance records. Therefore, it may be necessary to allow more time during the blow, that is beyond 2L/c, for the toe displacement to take place.

The computation is similar to that of RSP procedure, but with Time 2L/c being fixed and the location of T1 varied in intervals of 30 ms until Eq. 2.14 gives a maximum value. This procedure is illustrated in Fig. 2.30.

2.4.3.2 MINIMUM RESISTANCE, RMN

For piles having small penetration resistance values, smaller than 130 blows/meter (Likins and Hussein, 1988), this approach may be suitable.

The RMN computation is similar to that of RSP, but with T1 being fixed, T2 is varied through a ±20% window of Time 2L/c searching for a minimum value computed by Eq. 2.14. This procedure is illustrated in Fig. 2.31.

2.4.3.3 UNLOADING RESISTANCE, RSU

For long flexible piles having appreciable shaft resistance, the CMES standard equations may underestimate the pile capacity during hard driving if the pile head velocity becomes zero before Time 2L/c. That is, the pile head moves upward due to that some shaft resistance unloads before the resistance reflections from the toe reaches the pile head (Fig. 2.32).

In such cases, the time, t_u, between when the velocity becomes zero and Time 2L/c is determined first. Then, the difference between the force $F(t_u)$ and velocity $V(t_u)$ after impact is determined. Half of this difference represents a correction for unloading of shaft resistance (UN). That is,

$$t_u = 2t_p + 2L/c - t_0 \qquad \text{Eq. 2.15}$$

Where, t_p = time at peak
t_0 = time of zero velocity before time 2L/c

and,

$$2UN = \tfrac{1}{2}[F_{(tu)} - V_{(tu)}\frac{Mc}{L}] \qquad \text{Eq. 2.16}$$

Then, the static capacity is computed by,

$$RSU = [RTL + UN] - j_c[FT1 + VT1 - (RTL - UN)] \qquad \text{Eq. 2.17}$$

This procedure is illustrated in Fig. 2.32.

2.4.3.4 DAMPING INDEPENDENT METHODS

The damping independent methods are RAU and RA2. The RAU method is particularly suitable for piles that only experience toe resistance. That is, the computation assumes that the pile toe velocity is zero. This assumption yields zero damping and the computed resistance is completely static.

The RA2 method is proposed for piles where the resistance in the lower portion of the pile dominates. This method converts the shaft resistance to equivalent toe resistance and determines the capacity at zero toe velocity.

2.5 CAPWAP ANALYSIS

2.5.1 GENERAL

In 1970, in parallel with the development of the CMES, a computer program was developed called Case Pile Wave Equation Analysis Program, CAPWAP. The program analysis is based on the concept of wave propagation and signal matching of computed to measured traces of either force, velocity, or downward travelling wave.

The program combines the wave equation pile/soil model and the CMES using dynamic measurements. That is, the input to the CAPWAP program is strain and acceleration measured at the pile head during a hammer blow impact. No assumption on the hammer performance is required, rather, it is measured. The soil dynamic properties (quake, damping, soil resistance, etc.) are determined from the analysis.

In CAPWAP analysis, the program computes either a pile head force or velocity trace for a duration of one blow. The analysis is an iterative procedure since a large

number of input parameters is required for which a computed wave signal is matched to a measured wave signal. A solution is obtained when best possible agreement is reached between the computed (from CAPWAP) and measured wave signal (from dynamic monitoring). At the same time, the program compares the measured and computed penetration resistance. The CAPWAP results include the distribution of the static resistance, quake, and damping factors.

2.5.2 CAPWAP MODEL

2.5.2.1 PILE MODEL

Initially, the CAPWAP program employed the pile model of lumped masses proposed by Smith (1960). Further improvement on the CAPWAP yielded the CAPWAPC version that modelled the pile in a continuous segment (Fig. 2.33). This model seemed more suitable for long piles (Davis et al., 1987).

The pile segment length is chosen such that the wave travel time for each segment is equal. The default segment length is 1 m. The segment lengths are different only in piles composed of different materials, such as steel and concrete.

Since each pile segment is uniform and linearly elastic, the magnitude of a downward wave entering the top of the segment is equal to the wave exiting at the bottom of the same segment. Thus, reflections occurs only at the interfaces of segments due to different pile segment properties, resistance forces, and pile toe reflections.

The program assumes that all pile segments are unstressed prior to the hammer blow. In the analysis, both upward and downward propagation are accounted for. The superposition of both waves is performed according to basic wave mechanics yielding forces and velocities at the upper and lower boundary of each pile segment. The velocity is integrated to yield displacement of each segment.

For concrete piles mainly, cracks in the pile may develop during or prior to the installation. In addition, long piles may require splicing using either mechanical splicing or welded plates. Therefore, pile model in the CAPWAPC includes the option of a slack to represent either a crack or a splice. A crack, if closed, transmits

compressive waves followed by a cycle of tensile, S_t, and compressive waves, S_c. To more realistically represent a slack model, some force is always considered to be transmitted across a crack or a splice. Two models are presented in the CAPWAPC program.

The first is a round-out slack model as presented in WEAP. As two pile segments approach the end of a specified slack, the transmitted forces increase until they reach the state of force in the continuous model. The second model allows for a completely open slack with a constant minimum force between the two adjacent pile segments.

The first model is illustrated in Fig. 2.34 and expressed numerically for upward (u) wave as,

$$F_{u,i,j} = (-F_{d,i,j-1} - R_i/2)\,(1-r) + (F_u^*{}_{i,j})r \qquad \text{Eq.2.18}$$

with,

$$r = dd/s \qquad \text{Eq.2.19}$$

where, $F_u^*{}_{i,j}$ = the upward wave force computed for an unspliced segment
R_i = the total static resistance acting on each pile segment
i = the element sequence number
j = the time sequence
r = the round-out radius and limited to $0.2 \leq r \leq 1$
dd = the relative displacement
s = the compressive or tensile slack

For downward (d) wave,

$$F_{d,i+1,j} = (-F_{u,i+1,j-1} - R_i/2)\,(1-r) + (F_d^*{}_{i+1,j})r \qquad \text{Eq. 2.20}$$

For the second model, tensile and compressive slacks are interpreted as slack forces, F_S, and presented for upward and downward waves as,

$$F_{u,i,j} = F_{d,i,j-1} + R_i/2 + F_s \qquad \text{Eq. 2.21}$$

.../27

and,

$$F_{d,i+1,j} = -F_{u,i+1,j-1} - R_i/2 + F_s \qquad \text{Eq. 2.22}$$

Internal pile damping may be added to the pile model by computing the change of a wave and reducing the new wave by a specified constant. The recommended reduction factor is usually smaller than or equal to 0.02.

2.5.2.1 SOIL MODEL

The displacement and velocity of each pile segment is the basis for computing the soil resistance forces according to the Smith soil model.

The CAPWAPC program uses the Smith soil model which consists of an elastic-plastic spring and linear dashpot (Fig. 2.35) with some improvements. At each pile segment, a resistance force may act which is modelled by three parameters: soil resistance, quake, and viscous damping.

The pile segment considered in the analysis is usually small in length. To save computation time, the CAPWAPC analysis considers the soil resistance for the shaft segments to act at only every second or third pile segment and letting the last pile segment to represent both shaft and toe resistance. Thus, the number of the pile segment, i, may not be equal to the number of the soil element, s. The total bearing capacity, R_u, is the sum of soil resistance force, R_i, acting on each segment of the pile length. The total resistance acting on each pile segment, R_i, is the sum of both static and dynamic resistance. That is,

$$R_i = R_{si} + R_{di} \qquad \text{Eq. 2.23}$$

For a soil element, k, acting on a pile segment, i, using from dynamic measurement known input of the pile segment velocity, v_i, displacement, u_i, and assigning a viscous damping factor, J_k, the resistance force acting on the k^{th} pile segment is,

$$R_k = R_{sk} + J_k(v_i) \qquad \text{Eq. 2.24}$$

and,

$$R_{sk} = k_{sk}\, u_i \qquad \text{Eq. 2.25}$$

.../28

the limiting boundary is,

$$R_{nk} \leq R_{sk} \leq R_{uk} \qquad \text{Eq. 2.26}$$

where, k_{sk} = the soil stiffness of the k^{th} soil element.
R_{uk} = the static resistance of the k^{th} soil element.

The lower bound static resistance R_{nk} is defined by,

$$R_{nk} = -U_n R_{sk} \qquad \text{Eq. 2.27}$$

where,

$$0 \leq U_n \leq 1$$

The U_n is denoted as the unloading factor. For toe resistance, the U_n factor is always zero. For shaft resistance, this value may vary from 0 to 1. In the traditional wave equation analysis, it is considered equal to 1. In the CAPWAPC analysis, this value may vary based on measurements of force and velocity wave propagation.

The soil stiffness may vary in the case of loading and unloading conditions along the shaft. For downward (positive) velocities, the stiffness is presented as,

$$k_{sk} = R_{uk} / q_k \qquad \text{Eq. 2.28}$$

where, q_k being the range of the elastic deformation of the k^{th} soil element denoted as loading quake.

For upward (negative; rebound) velocities, a modified quake, q_{mk}, is computed,

$$q_{mk} = q_k c_k \qquad \text{Eq. 2.29}$$

The c_k factor is limited to values greater than zero and less or equal to 1.0. The c_k factor is the same for all soil segments along the shaft and may be different for the toe. This factor is denoted c_s for the shaft and c_t for the toe. Then, the stiffness at unloading is,

$$k_{sk} = R_{uk} / q_{mk} \qquad \text{Eq. 2.30}$$

Thus, for upward (negative) pile velocities, the quake may be smaller than during loading due to higher soil stiffness. Hence, the modified quake is denoted as unloading quake.

The Smith–model approach is expanded by a reloading option. This option specified the loading quake in a second or later loading cycle. That is, below a zone specified as the reloading level, the soil loading stiffness equals the soil's unloading stiffness for repeated cycle sequences. This is illustrated in Fig. 2.36 showing soil resistance versus deformation.

In cases where piles are installed on a very hard layer, a gap between the pile toe and the soil may exist. This problem is identified by a behavior similar to a large quake at the toe. That is, a gap allows for high tension in the presence of high resistance.

The CAPWAPC expanded the Smith soil resistance model to account for such conditions by introducing an option called toe gap. Such a condition at the pile toe causes a strain hardening type of resistance. That is, as the pile penetrates through the gap distance, the static toe resistance remains zero. Once the gap is closed, the toe resistance starts to increase linearly (Fig. 2.37). The static soil resistance subject to the gap is computed as,

$$R_{sk} = k_{sk} (u_i - g_t) \qquad \text{Eq. 2.31}$$

and,

$$g_t < u_i < g_t + g_k$$

Where, k = represent the toe soil element.
i = represent the pile toe element.
g_t = represent the toe gap deformation.

For a displacement that is smaller than the gap, the R_{sk} is zero and equal to the total static resistance, R_{uk}, for displacement greater than the sum of the gap and quake. During unloading conditions, the soil behavior at the toe follows the

unloading quake path (Fig. 2.37). In the wave equation analysis, the toe quake is modelled to equal the sum of gap distance and quake.

During the installation of the pile, a soil mass may adhere to the toe of the pile. This is referred to as a soil plug. In the CAPWAPC, it is modelled to act like an external passive resistance rather than a change in the pile model. The soil plug resistance force, R_{SM}, at Time j, acting against the pile toe is computed as,

$$R_{SM,j} = W_s (v_{t,j} - v_{t,j-1}) / (g\, dt) \qquad \text{Eq. 2.32}$$

where, W_s = the soil weight
v_t = the pile toe velocity
g = the gravitational acceleration
dt = the computational time increment

A typical the toe static resistance versus the pile toe displacement is illustrated in Fig. 2.37. A reloading level may also be specified, but the unloading level at the toe is always zero. To better represent wave dissipation at the toe, a damping option modelled by a dashpot at the toe is provided.

2.5.3 CAPWAPC PROCEDURES

The CAPWAPC method is based on the concept of travelling waves as described earlier. The CAPWAPC analysis separates shaft resistance from toe resistance based on the time at which the waves reach the pile head. The magnitude of the waves is related to the magnitude of the resistance forces.

The pile is divided into N_p segments. The shaft resistance is lumped into N_s soil resistance forces. The soil resistance element acts only every second or third pile element of the embedment length. The toe resistance of the pile is presented by an additional soil resistance force.

The "unknowns" in the CAPWAPC model are presented in Table 2.3. They consist of the soil resistance, R_{ui}, and the extensions of the CAPWAPC parameters of the pile and soil model. Also listed are the dimensions and the recommended or possible ranges of the parameters as provided in the CAPWAPC program manual.

The CAPWAPC program uses measurement input of either the force or the velocity at the pile head. As a first step, the program requests information of the pile model such as the cross-sectional area, the elastic modulus, wave speed of the pile material, and the pile length. Prior to the first analysis, the soil model parameters such as the soil resistance distribution, quakes, and damping along the shaft and at the toe as illustrated in Table 2.3 are assumed.

With the input of pile head measurement, either motion or force, and the assumed boundary conditions, the program computes either a force or a velocity wave trace at the pile head. This computed wave trace is compared to the measured wave trace by the Pile Driving Analyzer in the field. During iterative computer runs, the soil model parameters are adjusted until a best match is obtained between the CAPWAPC computed wave trace and the measured wave trace. A schematic sketch of the iteration process is illustrated in Figs. 2.38 and 2.39.

The shaft resistance can be directly determined from the force-velocity record portion between the time of impact and the time of the first wave return, 2L/c. The toe resistance and unloading quantities have to be determined from the later record portion.

The analysis time period is subdivided into four intervals for the purpose of match quality determination (Fig. 2.40).

1. The first period extends from the onset of impact over a period 2L/c. This period indicates how well the shaft resistance distribution was modelled. For long piles, this time period may easily take on a heavy weight compared to the next three intervals.

2. The second period starts at the end of the first one and lasts for a duration t_r plus 3 ms. The duration, t_r, is measured from the onset of impact until t_j, the time of maximum velocity. This time period is usually important for determination of the pile toe resistance.

3. The third time period starts 2L/c after t_i and extends over 5 ms. During this interval, the proper choice of R_u will be determined as a good match quality is obtained.

4. Last, the fourth interval is an interval of at most 20 ms, starting at the end of the second interval. During this portion of the record, the unloading behavior of the soil affects the pile head variables. Thus, a proper match in this zone reflects a selection of good model of the soil parameters

The overall evaluation of the match quality is based on the match quality within the four identified zones. A "best match" occurs when no further agreement between the measured and computed wave trace can be reasonably obtained. The uniqueness and accuracy of the match, and of the CAPWAP "unknown" variables (Table 2.3) may be checked by confirming that a best match is obtained for both measured force and velocity wave trace. Hussein (1986) performed a parametric study through which he demonstrated that the final best match is a unique solution that best describes the actual soil behavior at the time of testing.

The method used in the CAPWAPC analysis to evaluate the match quality is by summing the absolute values of the relative differences between the computed and the measured pile head variable. Thus, the match quality number, MQN, computed in a time interval, t, is,

$$MQN_t = SUM\ [\ ABS\ (f_{jc} - f_{jm})/F_m\ ] \qquad \text{Eq. 2.33}$$

Where, f_{jc} = the computed pile head force
f_{jm} = the measured pile head force
SUM = the summation over a time period
F_m = the maximum measured pile head force

The overlap of Zones 2 and 3 for match quality determination demonstrates the importance of properly matching the wave reflected from the pile toe. As a result of matching this overlap zones, the magnitude of R_u affects the MQN more than the soil parameters.

In addition to achieving best–match quality number to label a CAPWAP solution, an agreement of the computed and measured penetration resistance, blow count, must be checked. The blow count, BCT, is computed in two different ways as,

$$BCT_q = 1.0 / (u_{tm} - q_{av}) \qquad \text{Eq. 2.34}$$

$$BCT_f = 1.0 / u_{tf} \qquad \text{Eq. 2.35}$$

with,

$$q_{av} = SUM (q_i R_{ui}) / R_{ut} \qquad \text{Eq.2.36}$$

Where, u_{tm} = the maximum computed toe displacement
q_{av} = the average quake
u_{tf} = the computed final toe displacement

The computed blow count in Eq. 2.35 depends to a high degree on the end time of analysis. Thus, this value is rather less reliable than the computed blow count value from Eq. 2.34. Actual examples of CAPWAPC matches, from the three case studies in this resaerch work, are presented in Figs. 2.41 through 2.43.

2.5.4 DYNAMIC MEASUREMENTS AND CAPWAPC ANALYSIS

The CAPWAPC analysis is directly influenced by the results of the dynamic measurements. As stated, CAPWAPC depends on varying velocity and displacement during the impact event. Thus, the signal matching process depends on the varying velocity history during an impact. CAPWAPC signal matching analysis, match quality, and capacity are greatly influenced by soil damping parameter.

A very common source of concern is if the calculated ultimate resistance is an underestimated or overestimated value of the true pile capacity. This concern of pile capacity prediction is caused by either lack or excessive transfer of energy to the pile head, or a result of the soil conditions (soil set–up or relaxation), or a combination of both.

In the case of the driving hammer, the main concern is sufficient transfer of energy to the pile. This may be illustrated as follows. Considering a toe bearing pile having an ideal elastic-plastic toe behavior, a quake, u_t, and an ultimate resistance, R_u. The pile toe receives a total driving energy, E_t. As the pile toe penetrates into the ground, the soil resistance increase. The energy transferred to the soil after the toe quake, q_t, has been reached is,

$$E_t = R_u (u_t - q_t)/2 \qquad \text{Eq. 2.37}$$

An energy smaller than $R_u q_t/2$ cannot activate the ultimate soil resistance at the toe. The same argument is valid for shaft resistance. In addition to the soil resistance, transferred energy has to compress the pile and overcome dynamic resistance forces. Thus, insufficient transfer of energy would normally result in underestimation of the pile capacity. This is usually combined with a high penetration resistance.

Excessive transfer of energy through the pile head will result in very small penetration resistance. This will cause insufficient velocity variation, and therefore, what appears as static resistance may actually be damping forces. Hence, the capacity may be overestimated.

When performing dynamic measurements, difficulties encountered with the driving system are easily controlled by the operator of the pile driving hammer. However, shortcomings in calculating pile capacity are mostly caused by the soil properties and the soil load–movement behavior.

As reported by many, results from dynamic measurements and CAPWAPC analysis may either overestimate or underestimate capacities in cases of soils exhibiting relaxation or soil set–up, respectively. These shortcomings are influenced by soil characteristics rather than by the method of testing and analysis.

The effect of soil characteristics on dynamic measurement and CAPWAPC analysis may be accounted for by considering restrike conditions, energy transferred to the pile head and impact forces at time of dynamic testing. Authier and Fellenius (1981) reported dynamic measurements on piles driven in soil exhibiting soil set-up

and relaxation, as well as, the change of resistance distribution amongst blows at restrike conditions.

2.6 CONCLUDING REMARKS

Research on pile foundation resulted in the Wave Equation Analysis program for modelling and analysis of the pile installation. This analysis considered the effect of the driving system, soil conditions, and residual stresses that may develop during pile driving. However, the approach was limited to the choice and assumption on input variables for the analysis.

Further development enabled the measurements of force and velocity during the installation of piles. This provided actual information on the performance of the pile driving system in terms of energy transferred and impact stresses. As well, from the measured force and velocity, the pile capacity was computed using the Case Method Estimate empirical approach. This method overlooked the effect of residual stress in the analysis; assumed the magnitude of dynamic resistance; and computed the total capacity, only.

The CAPWAPC analysis combines both the Wave Equation analysis and the dynamic measurement. The results of the analysis are the pile capacity, resistance distribution along the shaft and at the toe, and quakes and damping parameters. The wave signal matching approach of computed to measured waves provided the users an appreciable degree of confidence in the results. Horvath and Killeavy (1988) reported that the total resistance at end-of-initial-driving computed by CAPWAPC, even if the selected blow is poorly chosen, is within 10% of the mean value referred to as the "true value".

Unlike the WEAP analysis, CAPWAPC analysis does not include the effect of residual stress, that is, in the CAPWAP analysis, all pile segments are assumed unstressed at the end of each impact blow. However, as discussed earlier in Section 2.3.2.6, it is probable that the previous blow have built–in a stress condition between the soil and the pile. That is, the pile movement has ceased before all the forces in the pile are equalized. Thus, a precompression or pretension condition develops causing residual load in the pile element. Then, the result of the CAPWAP analysis, when assuming no residual loads, may be offset from the true

.../36

soil resistance and quake values acting on the pile element. Residual stress shows a similar influence on the soil resistance distribution in the analysis of static loading test as reported by others (Khan, 1987).

Authier and Fellenius (1983) stated that as the pile forces are in equilibrium, the overestimation will be compensated by underestimation of other pile elements, which are subjected to residual tension and, therefore, causing the analysis to result in smaller than true soil resistance and quake values. However, they point out that the ultimate soil resistance will be unaffected, but not the resistance distribution between the pile elements, and/or the shaft and toe.

CHAPTER 3

TECHNICAL BACKGROUND TO THE CASE STUDIES

3.1 GENERAL BACKGROUND

Three pile case histories with different soil conditions, pile properties, and driving conditions have been selected for the research work. The investigations consist of dynamic measurements at initial-driving for two pile case histories, and at restriking for the third case history as stated below;

1. Case 1, Jones Island Advanced Facility, Milwaukee: dynamic measurement at initial driving.

2. Case 2, CN project, Jasper, Alberta: dynamic measurement at initial driving.

3. Case 3, National Aviation Museum, Ottawa: dynamic measurement at restriking.

For the three cases considered, the natural variation between blows was investigated. All blows were closely examined and selected based on the following criteria.

1. Selected blows are within a uniform soil layer.

2. Selected blows are free from the variations of hammer performance.

3. Selected blows at initial driving conditions are within a penetration not exceeding 300 mm to avoid the effect of depth on the analysis.

4. Selected blows at restrike are within a penetration of 100 mm to avoid the effect of depth on the analysis.

5. All selected blows should have sufficient penetration so that the mobilized resistance is equal to actual capacity of the pile (that is, no capacity underestimation).

3.2 SOIL DESCRIPTION

3.2.1 Case 1 - Jones Island

The soil consists of about 6 m of fill overlying a 19.5 m layer silty clay and clayey silt. Hereunder, lies a 56 m layer of mixed glacial soil ranging from sandy silt to clayey silt to a depth of about 81.5 m where a layer of dolomite bedrock exists at end of borehole. The blows were selected from initial–driving records taken when the pile toe was at a depth of 35.2 m. More detailed information is provided in Table 3.1.

3.2.2 Case 2 - Jasper

The soil consists of an upper layer of about 1.3 m of sandy gravel fill over a 2.3 m of sand with layers of silty sand. Hereunder, exists a 0.7 m of sandy gravel over a 23.6 m layer of sand with layers of fine silt to end of borehole. The blows were selected from initial–driving records taken when the pile toe was at a depth of 21.6 m. More detailed information is provided in Table 3.2.

3.2.3 Case 3 - National Aviation Museum

The soil consists of an upper 1.3 m layer of sand and clay fill over a 0.5 m thick layer of silty sand. Hereunder, exists a 46.2 m layer of silty clay to end of borehole. The blows were selected from Beginning of Restrike, BOR, records when the pile toe was at a depth of 57.0 m. More detailed information is provided in Table 3.3.

3.3 PILE DESCRIPTION

3.3.1 Case 1 - Jones Island

The pile selected for analysis is a 324 mm diameter steel pipe pile having a wall thickness of 9.5 mm. The pile was driven closed toe by means of an air-steam hammer, Vulcan 200C, and the blows were selected when the pile toe was at a depth of 35.2 m. The pile length above ground was 0.8 m.

3.3.2 Case 2 - Jasper

The pile selected for analysis is a W310x79 H-pile. The pile was driven by means of a diesel hammer, MKT DE 30B, and the blows were selected when the pile toe was at a depth of 21.6 m. The pile length above ground was 6.4 m.

3.3.3 Case 3 - National Aviation Museum

The pile selected for analysis is a 245 mm diameter steel pipe pile having a wall thickness of 14 mm. The pile was driven open ended by means of a diesel hammer, Bermingham B–300, to a final embedment depth of 57.0 m. The analyzed blows are from beginning of restrike.

3.4 DATA ACQUISITION AND PROCESSING

Dynamic measurement data were obtained by means of a Pile Driving Analyzer, model GB, and stored on a magnetic tape by means of an analog, four–channel recorder for later processing.

The selected blow records were digitized from the analog signal stored on the recorder using a Tecmar Labmaster analog to digital converter. The digitized records were then processed by means of a computer program called DATPRO. Figs. 3.1 through 3.3 presents representative wave traces from the three analyzed cases (beginning and end of records).

For Jones Island, twenty–five contiguous blow records at an embedment depth of 35.2 m through 35.5 m (115 ft through 116 ft) were selected and digitized for the purpose of this research work. The location of the selected blows within the embedment depth of the pile is indicated in the driving log diagram, Fig. 3.4. The corresponding penetration resistance for the selected blow records was about 25 blows per 0.3 m.

For Jasper, twenty–four contiguous blow records at an embedment depth between 21.6 m through 21.9 m (71 ft to 72 ft) were selected and digitized for the purpose of

this research work. The location of the selected blows within the embedment depth of the pile is indicated in the driving log diagram, Fig. 3.5. The corresponding penetration resistance for the selected blow records was about 24 blows per 0.3 m.

For National Aviation Museum, seventeen contiguous blow records starting at beginning of restrike at an embedment depth of 57.0 m (187 ft) were selected and digitized for the purpose of this research work. The driving log diagram at initial driving is presented in Fig. 3.6. The penetration resistance at end-of-initial driving was 160 blows per 1.0 m. At restriking, the equivalent penetration resistance for the selected blow records was 8 blows per 25 mm.

CHAPTER 4

COMPILATION OF DATA AND ANALYSIS

4.1 GENERAL

For the three case histories, each blow record is first processed by means of the DATPRO software program. Thereafter, all selected blows are subjected to the Case Pile Wave Equation Analysis, CAPWAPC. The CAPWAP analyses are performed at random order to eliminate the influence that may result from the analysis of a contiguous series of blows. A graphical output of the CAPWAPC analysis result for each of the case history is presented in Figs. 2.41 through 2.43. Finally, the results are compiled for statistical evaluation.

4.2 DATPRO ANALYSIS

All selected blows are processed by means of the DATPRO program to evaluate the CMES results, energy transferred, and impact stress and maximum stress, if they differ.

The DATPRO results are graphically produced versus time in terms of force and velocity, transferred energy and displacement, upward and downward travelling wave, and total static resistance curves. Also, a tabular print-out of the Case Method Estimate computations, energy, impact force, maximum force, and other values are produced. The J-factor for the CMES-RMX capacity is selected based on the type of soils at the site and by checking resistance versus time for varying J-value until the curve smoothens from any sharp peak as recommended by Goble et al. (1989).

4.2.1 Jones Island

The twenty-five contiguous blow records during initial driving are processed using the DATPRO program. A summary of the results is presented and compiled in Table 4.1

showing transferred energy, impact force, maximum force, and Case Method Estimate capacity, RMX, for a J–factor of 0.7.

A compilation of impact force, transferred energy, and CMES-RMX capacity are presented in a bar chart versus depth in Figs. 4.1 through 4.3. The ratio of normalized CMES-RMX capacity to normalized impact force, FIMP, and the normalized CMES-RMX capacity versus transferred energy are presented in Figs. 4.4 and 4.5 to evaluate the influence of the driving system. That is, each numerical value is divided by the mean value and plotted as a percentage.

The average CMES-RMX and transferred energy are 1160 KN and 23.8 KJ, respectively. The maximum force occurs at impact and is equal to 979 KN. The standard deviation is 5.0% for the CMES-RMX; 3.8% for impact force; and 2.5% for transferred energy. The data and compilation results presented in Figs. 4.1 through 4.5 show that the selection criteria (see Section 3.1) Nos. 1 and 2 are satisfied.

4.2.2 CN-Jasper project

The twenty–four contiguous blow records during initial driving are processed using the DATPRO program. A summary of the results is presented and compiled in Table 4.2 showing transferred energy, impact force, maximum force, and Case Method Estimate capacity, RMX, for a J-factor of 0.6.

A compilation of impact force, transferred energy, and CMES-RMX capacity are presented in a bar chart graphically versus depth in Figs. 4.6 through 4.8. The ratio of normalized CMES-RMX capacity to normalized impact force, FIMP, and the normalized CMES-RMX capacity versus transferred energy are presented in Figs. 4.9 and 4.10.

The average CMES-RMX and transferred energy are 757 KN and 8.4 KJ, respectively. The maximum force occurs at impact and is equal to 1200 KN. The standard deviation is 2.1% for the CMES-RMX; 1.9% for impact force; and 4.7% for transferred energy. Also for Case 2, The data and compilation results presented in Figs. 4.1 through 4.5 show that the selection criteria (see Section 3.1) Nos. 1 and 2 are satisfied.

4.2.3 National Aviation Museum

The seventeen blow records at beginning-of-restriking are processed using the DATPRO program. A summary of the results is presented and compiled in Table 4.3 showing transferred energy, impact force, maximum force, and Case Method Estimate capacity, RMX, for a J-factor of 0.4.

A compilation of impact force, transferred energy, and CMES-RMX capacity are presented in a bar chart graphically versus depth in Figs. 4.11 through 4.13. The ratio of normalized CMES-RMX capacity to normalized impact force, FIMP, and the normalized CMES-RMX capacity versus transferred energy are presented in Figs. 4.14 and 4.15 to evaluate the influence of the driving system.

The average CMES-RMX and transferred energy are 1866 KN and 28.5 KJ, respectively. The maximum force occurs at impact and is equal to 1920 KN. The standard deviation is 6.7% for the CMES-RMX; 3.6% for impact force; and 7.0% for transferred energy.

Figs 4.11 and 4.12 show that the impact force and transferred energy are consistent through the blow records. The CMES–RMX reduces and, therefore, the ratios to RMX do too. Yet, the selection criteria (see Section 3.1) are still satisfied.

4.3 CAPWAP ANALYSIS

Each blow is analyzed by means of a Case Pile Wave Analysis Program Continuous Model, CAPWAPC. For each case history, the selected blows are analyzed in a random order to escape the influence that might be built in by analyzing the blows contiguously.

The computer output is presented graphically in a time scale in terms of measured and computed force and velocity waves, measured force and velocity, and resistance distribution along the shaft of the pile and at the toe in a bar chart.

4.3.1 Jones Island

Twenty-five contiguous blow records during initial driving are subjected to the CAPWAPC analysis.

4.3.2 CN-Jasper project

Twenty-four contiguous blow records during end-of-initial driving are subjected to the CAPWAPC analysis.

4.3.3 National Aviation Museum

Seventeen blow records from beginning of restriking are subjected to the CAPWAPC analysis.

4.4 DATA COMPILATION AND EVALUATION

4.4.1 Total activated resistance

The total activated resistance resulting from the CAPWAPC analysis is compiled in Tables 4.4 through 4.6. For each case history, the mean, and standard deviation are computed. In addition, the difference in percent of the total static resistance for each blow to the mean value is tabulated.

The results are also graphically produced in a bar chart in terms of total resistance versus depth to illustrate the variation of total capacity as evaluated by the CAPWAPC analysis. Also, a ratio of normalized impact force to normalized total activated resistance and values of normalized transferred energy versus normalized total activated resistance are graphically produced to highlight the influence of the driving system on the natural variation of total resistance between blows within the same soil layer.

For Jones Island, the mean value of total static resistance is 1162 KN, and the maximum and the minimum total static resistance evaluated by the CAPWAPC method is 1358 KN

and 1012 KN, respectively. The difference in percent from the mean ranges from -13% through +17%. The corresponding standard deviation is 8%. Graphical illustration of the variation of capacity within depth is presented in Fig. 4.16. The capacity tends to decrease then increase within a series of cycles ranging from 2 through 4 blows. A total of 7 cycles is demonstrated in Fig. 4.16. Figs. 4.17 and 4.18 show that the selected criteria stated in Section 3.1 are satisfied. The comparison between the total static resistance as computed by the CMES and as evaluated by the CAPWAPC method is presented in Fig. 4.19.

For CN-Jasper project, the mean value of total static resistance is 726 KN, and the maximum and the minimum total static resistance evaluated by the CAPWAPC method is 785 KN and 705 KN, respectively. The difference in percent from the mean ranges from -3% through +8%. The corresponding standard deviation is 2.5%. Graphical illustration of the variation of capacity within depth is presented in Fig. 4.20. The capacity tends to decrease then increase within a series of cycles ranging from 6 through 8 blows. A total of 3 cycles is demonstrated in Fig. 4.20. Figs. 4.21 and 4.22 show that the selected criteria stated in Section 3.1 are satisfied. The comparison between the total static resistance as computed by the CMES and as evaluated by the CAPWAPC method is presented in Fig. 4.23.

For the National Aviation Museum, the mean value of total static resistance is 1911 KN, and the maximum and the minimum total static resistance evaluated by the CAPWAPC method is 2352 KN and 1635 KN, respectively. The difference in percent from the mean ranges from -14% through +23%. The corresponding standard deviation is 11%. Graphical illustration of the variation of capacity within depth is presented in Fig. 4.24. The capacity shows a decreasing trend with depth for the first 14 blows from a value of 2352 KN to a value of 1705 KN. In addition to the apparent trend (Fig. 4.24), the capacity tends to decrease then increase within a series of cycles ranging from 4 through 5 blows. A total of 3 cycles is demonstrated. Figs. 4.25 and 4.26 show that the impact force and transferred energy are practically consistent through the blow records. The capacity reduces and, therefore, the ratios to capacity do too. Yet, the selected criteria stated in Section 3.1 are still satisfied. The comparison between the total static resistance as computed by the CMES and as evaluated by the CAPWAPC method is presented in Fig. 4.27.

4.4.2 Resistance distribution

The resistance distribution between the shaft and the toe of the pile resulting from the CAPWAPC analysis are compiled in Tables 4.7 through 4.9. For each case history, the mean value, and standard deviation are computed. Also, a ratio of the percent shaft and the toe resistance to the total activated resistance are compiled and tabulated. The maximum and minimum values of the ratio is highlighted and the difference between the ratios is computed.

The results are also presented in a bar chart in terms of shaft and toe resistance versus depth to illustrate the variation and potential trends of shaft and toe resistances as evaluated by the CAPWAPC analysis. To isolate the variation effect of total capacity from resistance distribution, the ratio of shaft and toe resistance to capacity is presented.

For Jones Island, the mean shaft and toe resistance is 867 KN and 293 KN, respectively. The maximum and the minimum resistance as evaluated by CAPWAPC along the shaft is 1107 KN and 644 KN, and at the toe is 530 KN and 120 KN, respectively. The corresponding standard deviation is 14% for the shaft resistance and 29% for the toe resistance. The maximum and minimum ratios of shaft to total resistance are 90% and 55%, and toe to total resistance are 45% and 10%, respectively. The corresponding difference between maximum and minimum ratio is 35%. Graphical illustration of the shaft and the toe resistance within contiguous blows is presented in Fig. 4.28. Also, the shaft and toe resistance, independent of varying total capacity, is illustrated in a bar chart in Fig. 4.29. Both figures demonstrate a varying resistance distribution amongst the contiguous blows.

For CN-Jasper project, the mean shaft and toe resistance is 603 KN and 123 KN, respectively. The maximum and the minimum resistance as evaluated by CAPWAPC along the shaft is 681 KN and 508 KN, and at the toe is 278 KN and 42 KN, respectively. The corresponding standard deviation is 9% for the shaft resistance and 45% for the toe resistance. The maximum and minimum ratios of shaft to total resistance are 94% and 65%, and toe to total resistance are 35% and 6%, respectively. The corresponding difference between maximum and minimum ratio is 29%. Graphical illustration of the

shaft and the toe resistance within contiguous blows is presented in Fig. 4.30. Also, the shaft and toe resistance, independent of varying total capacity, is illustrated in a bar chart in Fig. 4.31. Both figures demonstrate a slight variation of resistance distribution amongst the contiguous blows.

For the National Aviation Museum, the mean shaft and toe resistance is 1479 KN and 432 KN, respectively. The maximum and the minimum resistance as evaluated by CAPWAPC along the shaft is 2342 KN and 955 KN, and at the toe is 815 KN and 10 KN, respectively. The corresponding standard deviation is 33% for the shaft resistance and 68% for the toe resistance. The maximum and minimum ratios of shaft to total resistance are 100% and 54%, and toe to total resistance are 46% and less than 1%, respectively. The corresponding difference between maximum and minimum ratio is 46%. Graphical illustration of the shaft and the toe resistance within contiguous blows is presented in Fig. 4.33. Also, the shaft and toe resistance, independent of varying total capacity, is illustrated in a bar chart in Fig. 4.34. Both figures show a trend of decreasing shaft resistance and increasing toe resistance within the contiguous blows. The shaft resistance trend (Fig. 4.32) agrees with the trend of total capacity (Fig. 4.27).

4.4.3 Dynamic parameters

The dynamic parameters, that is, Smith and Case damping and quakes along the shaft and at the toe of the pile applied in the CAPWAPC analysis are compiled in Tables 4.10 through 4.12. For each case history, the mean, and standard deviation, are computed.

The results are also presented in a bar chart for both the shaft and toe resistance in terms of damping and quakes versus blow number.

For Jones Island, the mean Case and Smith damping are: 0.16 and 0.075 s/m along the shaft; 0.35 and 0.61 s/m at the toe, respectively. The corresponding standard deviations are: 25.5% and 34% along the shaft; 4% and 32% at the toe, respectively. The mean value of quake is 19 mm along the shaft and 38 mm at the toe, respectively. The corresponding standard deviation is 22% along the shaft and at the toe. Figs. 4.34 and 4.35 demonstrate the variation of the dynamic parameters along the shaft and at the toe for the selected blows, respectively.

For CN-Jasper project, the mean Case and Smith damping are: 0.175 and 0.12 s/m along the shaft; 0.48 and 2.15 s/m at the toe, respectively. The corresponding standard deviations are: 20.5% and 24% along the shaft; 5% and 43% at the toe, respectively. The mean value of quake is 13 mm along the shaft and 37 mm at the toe, respectively. The corresponding standard deviation is 9% along the shaft and 27% at the toe, respectively. Figs. 4.36 and 4.37 demonstrate the variation of the dynamic parameters along the shaft and at the toe for the selected blows, respectively.

For the National Aviation Museum, the mean Case and Smith damping are: 0.94 and 0.29 s/m along the shaft; 0.06 and 0.24 s/m at the toe, respectively. The corresponding standard deviations are: 4% and 30% along the shaft; 57% and 124% at the toe, respectively. The mean value of quake is 23 mm along the shaft and 12 mm at the toe, respectively. The corresponding standard deviation is 17% along the shaft and 42% at the toe, respectively. Figs. 4.38 and 4.39 demonstrate the variation of the dynamic parameters along the shaft and at the toe for the selected blows, respectively.

CHAPTER 5

DISCUSSION AND CONCLUSIONS

5.1 DISCUSSION

5.1.1 TOTAL ACTIVATED RESISTANCE

Case 1 and 2 – Initial Driving Condition

For Jones Island, the maximum driving forces induced by the air-steam hammer vary slightly and the standard deviation is smaller than 7% (Fig. 4.4). The energy transferred to the pile head is virtually consistent and the standard deviation is smaller than 3% (Fig. 4.5). Fig. 4.17 shows a trend of impact driving force practically similar to that of the static capacity computed by CAPWAPC. Fig. 4.18 illustrates that no relationship exists between the transferred energy and static capacity computed by CAPWAPC. Qualitative evaluation of the wave propagation for each blow record indicates that no change existed within the boundary conditions. Figs. 4.4, 4.5, 4.17, and 4.18 show that the selected criteria are satisfied.

The total activated resistances computed by the CMES (J=0.7) and CAPWAPC analysis (Fig. 4.19) are practically similar and the corresponding standard deviation is about 5% and 8%, respectively.

The static capacity during initial driving (Figs 4.16 through 4.19) demonstrates a cyclic behavior between contiguous blows. That is, the capacity tends to increase then decrease within a series of about 2 to 4 contiguous blows. This cyclic behavior may either be due to the sequence of analysis, or more probably, is due to a varying degree of residual stress induced in the pile during driving. The maximum and minimum difference from the mean is about 30% (Table 4.4). The standard deviation of the total static resistance is about 8%. This suggests that the computed capacity will be within 8% of the "true" capacity value. That is, assuming the mean computed value is the "true" capacity.

For CN-Jasper project, the maximum induced driving force shows to be consistent (Fig. 4.9) with a standard deviation of about 2% and a trend similar to that of the activated static capacity (Fig. 4.21). The energy transferred to the pile head by the drop hammer for the selected blows varies (Figs. 4.10 and 4.22) and the corresponding standard deviation is about 5%. The variation in the driving energy may to a limited extent affect the activated capacity. However, such variation is of no practical concern. Qualitative evaluation of the wave propagation for each blow record indicates no change in the boundary conditions. Figs. 4.6, 4.7, 4.21, and 4.22 show that the selected criteria are satisfied.

The total activated resistance computed by the CMES (J=0.4) and CAPWAPC analysis (Fig. 4.23) shows a comparable trend. The static capacity during initial driving varies between contiguous blows. Noting that analysis are performed at random order by the same CAPWAP operator, the capacity cycle (Figs. 4.20 through 4.23) changes from lower to upper bound within a series of about 6 to 8 contiguous blows. The observed cycles may be attributed to the effect of residual stress induced amongst blows during driving. The maximum and minimum difference from the mean average (Table 4.5) is about 13%. The standard deviation of the total static resistance is about 2.5%. This suggests that the computed capacity will not exceed 3% of the "true" capacity.

For the two cases studied at initial driving condition, the variations amongst contiguous blows is more or less a similar behavior. Such variation may be contributed to the effect of accumulated tensile and compressive stresses during driving between contiguous blows, that is, residual stresses. If so, the results of the analysis confirms the statement by Holloway et al. (1978), and Rausche et al. (1986) that residual stresses influence the measured and computed capacity of a pile. It should be noted that similar affects from residual stresses was demonstrated in the analysis of static loading test by Khan (1987). A method of analysis stress similar to that of the WEAP and static analysis for residual should be established for analysis of dynamic measurements to confirm the hypothesis of cyclic behavior caused by residual stress.

For the Jones Island, a pile length of about 35 m and a penetration resistance of about 25 blows/0.3 m, the 7% standard deviation of capacity may be contributed to the length of pile and very easy driving conditions. For CN-Jasper, the shorter length pile (22 m), the standard deviation of capacity is about 2.5%. Eventhough the penetration resistance for

both cases is similar, the low standard deviation observed for the CN-Jasper case as opposed to the Jones Island case may be attributed to the shorter length of pile and probably somewhat to hammer performance.

The results from the two cases studied during initial driving indicate that the pile capacity computed by CAPWAPC is within a range of 10%. These results agrees with the findings of Horvath and Killeavy (1988) for end-of-initial driving conditions that capacity computed by CAPWAPC, regardless of the selected blow for analysis, will be within 10% of the true value.

Case 3 – Restrike Condition

For the National Aviation Museum, the energy transferred and impact driving force by the open end diesel hammer are practically consistent amongst the selected contiguous blows at restrike (Figs. 4.11 and 4.12). The corresponding standard deviation is about 7% and 4%, respectively. Qualitative evaluation of the wave propagation for each blow record cindicates that no change existed within the boundary conditions. Figs. 4.11, 4.12, 4.25, and 4.26 show that the selected criteria are mainly satisfied. The first 3 through 6 blows indicate that probably not enough energy was delivered to the pile head. This is apparent when comparing the results of resistance distribution, that is, the toe resistance is fully engaged only after fully mobilizing the shaft resistance (Figs 4.32 and 4.33).

The computed static capacities at beginning of restrike demonstrate a decreasing trend between contiguous blows (Fig. 4.24). Such decreasing trend of static capacity can only be attributed to loss of soil set-up, only. This support the findings of Authier and Fellenius (1981). The trend of the total activated resistance computed by the CMES (J=0.4) is similar to that resulting from the CAPWAPC analysis (Fig. 4.27). The range between the maximum and minimum capacity from the mean is about 35% and the standard deviation is about 11% (Table 4.6). Due to the loss of soil set-up, the value of 11% standard deviation is not representative of the variation in the CAPWAPC analysis. In such a case, one should use the CAPWAPC results from the first and last blow records, after fully engaging both the shaft and toe resistance, to properly evaluate the "true" pile capacity.

Also, Fig. 4.24 show that the capacity varies between contiguous blows within a series of about 4 to 5 blows as noted for the cases at initial driving condition. This cyclic behavior may be contributed to the effect of compressive residual stress at restrike. That is, compressive residual stresses develops at restrike since the pile capacity is progressively engaged, only (Figs. 4.24, 4.27, 4.32, and 4.33).

5.1.2 RESISTANCE DISTRIBUTION

Case 1 and 2 – Initial Driving Condition

For Jones Island, the resistance distribution between the shaft and the toe varies amongst contiguous blows (Fig. 4.28). There exist a trend of increasing shaft resistance as the pile embedment depth increase. The toe resistance shows a trend of uniform resistance. The standard deviation for the shaft and toe resistance is about 14% and 29%, respectively. The difference between the maximum and minimum normalized resistance distribution along the shaft and the toe is about 35% (Table 4.7 and Fig. 4.29).

For CN-Jasper, the resistance distribution between the shaft and the toe varies for the first six blows, and is consistent for the other eighteen contiguous blows excluding blow #18 (Fig. 4.30). The standard deviation for the shaft and the toe is about 9% and 45%, respectively. The difference between the maximum and minimum normalized resistance distribution along the shaft and the toe is about 29% (Table 4.8 and Fig. 4.31).

The variation in resistance distribution between the shaft and the toe for the initial driving condition is influenced by the variation in total capacity and the effect of residual stress. Variation of up to 15% and 45% is observed along the shaft and at the toe, respectively. These results confirms statements by Holloway et al. (1978), and Authier and Fellenius (1983) related to the effect of residual stresses on resistance distribution.

Case 3 – Restrike Condition

For the National Aviation Museum, the resistance distribution between the shaft and the toe demonstrate an apparent trend of exponentially reducing shaft resistance and

increasing toe resistance. Such a trend is normally observed on sites where soils exhibit set-up. The standard deviation for the shaft and the toe is about 33% and 68%, respectively. This high value of standard deviation reflects the soil set-up condition at restrike. The results suggest that the resistance distribution at restrike under similar conditions vary widely.

In addition to the apparent trend, there exists a variation amongst the contiguous blows (Fig. 4.32) somewhat similar to that of total capacity (Fig. 4.27). This variation amongst contiguous blows is influenced by the varying total capacity and the effect of residual stress.

5.1.3 DYNAMIC PARAMETERS

Case 1 and 2 – Initial Driving Condition

For Jones Island, variation in quakes and damping along the shaft and the toe exists amongst blows (Figs. 4.34 and 4.35). As Smith damping is proportional to velocity, variation of damping amongst contiguous blows is more apparent. The standard deviation for the shaft and toe quake is about 22%. For Smith and Case damping, the standard deviation is about 34% and 25% along the shaft, and is about 32% and 4% at the toe (Table 4.10), respectively. This suggest that the quake and damping values may vary from the "true value" by about 20% and 30%, respectively. That is, assuming the mean value is referred to as the "true value".

For CN-Jasper, quakes and damping along the shaft and the toe vary amongst blows (Figs. 4.36 and 4.37). The standard deviation for Case damping along the shaft and at the toe is about 20% and 5%, respectively. The corresponding standard deviation for Smith damping is about 24% and 43%, respectively. The standard deviation for the shaft and toe quake is about 10% and 26%, respectively (Table 4.11). This suggests that the computed quakes and damping may be within 25% and 40% of the "true value", respectively.

In general, the computed soil quake and damping values by CAPWAPC vary by up to 40% at initial driving condition, that is, easy driving condition. The applied dynamic values demonstrate no particular trend and show to be insensitive to the computed capacity at easy driving condition.

Case 3 – Restrike Condition

For the National Aviation Museum, the quake and damping values along the shaft and at the toe vary between the blows excluding Case damping along the shaft (Figs. 4.38 and 4.39). The standard deviation is about 17% and 42% for the shaft and toe quake, respectively. For Smith and Case damping, the standard deviation is about 30% and 4% along the shaft, and is about 125% and 57% at the toe (Table 4.12), respectively. This suggest that the quake and damping values may vary from the "true value" by about 40% and 125%, respectively.

At restrike condition, a penetration resistance of 8 blows per 25 mm, the Smith damping values along the shaft and at the toe demonstrate a trend inverse to that of the shaft and toe resistance, respectively. The quake values along the shaft show a trend proportional to that of the shaft resistance. Case damping and quake values at the toe demonstrate no particular trend.

5.2 CONCLUSIONS

The objectives of the study are reached, and the criteria for the selected blows from the three case studies are satisfied. A statistical evaluation of the natural variation between contiguous blows using the CAPWAPC analysis is performed.

The results of the CAPWAPC analysis indicates that there exists a slight variation in total activated resistance for the cases at initial driving and restrike conditions. Its magnitude is not significant from aspects of practical engineering.

The analysis of the two cases at initial driving indicates that the pile capacity computed by CAPWAPC varies within a range of 10%. The results agrees with the findings of Horvath and Killeavy (1988) for end-of-initial driving conditions that capacity computed by CAPWAPC, regardless of the selected blow for analysis, will be within 10% of the true value. In the third case studied at restrike, eventhough the analysis indicates a range of

about 10%, one should never overlook the effect of soil set-up and relaxation as demonstrated by Authier and Fellenius (1981).

Also, the results of the analysis of total resistance indicate that there exist a cyclic behavior ranging within a series of about 3 to 8 blows, noting that analysis was performed at random order by the same CAPWAP operator. This cyclic behavior may be contributed, amongst other, to the effect of residual stresses. However, to more confirm such hypothesis, a method of analysis for residual stress similar to that of WEAP and static analysis should be established for the analysis of dynamic measurements.

The results of the CAPWAPC analysis indicate that there exists a variation in resistance distribution between the shaft and the toe of the pile for the cases at initial driving and restrike conditions.

At initial driving, the results suggest that the resistance distribution vary by up to 15% and 45% along the shaft and the toe, respectively. This variation is the result of residual stress developed within blows during driving. At restrike, the analyses indicate that variation up to 33% and 68% along the shaft and the toe may exist, respectively. However, such variation is mainly contributed to the effect of soil set-up.

The results of the CAPWAPC analysis indicate that there exist a variation in the soil dynamic parameters (quakes and damping) for the cases at initial driving and restrike conditions.

The results show that the computed soil dynamic parameters by CAPWAPC vary by up to 40% at initial driving condition. The applied dynamic values demonstrate no particular trend and show to be insensitive to the computed capacity at easy driving condition. At restrike, the Smith damping values along the shaft and at the toe demonstrate a trend inverse to that of the shaft and toe resistance, respectively. The quake values along the shaft show a trend proportional to that of the shaft resistance. Case damping and quake values at the toe demonstrate no particular trend.

Further work is recommended to quantitatively evaluate the effect of residual stress on the dynamic analysis of piles from force and velocity measurements. Similarly, to further investigate variation of resistance distribution and soil parameters, one should isolate the effect of residual stresses.

REFERENCES

AMERICAN SOCIETY FOR TESTING AND MATERIALS, ASTM, 1989. Standard test method for high strain dynamic testing of piles, D4945-89, Annual Book of ASTM Standards, Vol. 04.08 pp. 1018-1028.

AUTHIER, J. and FELLENIUS, B. H., 1981. Pile integrity and soil set-up and relaxation. Second Seminar on the Dynamics of Pile Driving. Pile Research Laboratory, University of Colorado, Boulder, March 24-25, 9 p.

AUTHIER, J. and FELLENIUS, B. H., 1983. Wave equation analysis and dynamic monitoring of pile driving. Civil Engineering for Practicing and Design Engineers. Pergamon Press Ltd. Vol. 2, No. 4, pp. 387-407.

CANADIAN FOUNDATION ENGINEERING MANUAL, 1985. Part 3, Deep Foundations. The Canadian Geotechnical Society, 2nd Edition, 1985, pp 269-374.

CASE PILE WAVE ANALYSIS PROGRAM - CONTINUOUS MODEL, 1989. Goble Rausche Likins and Associates Inc. Cleveland, Ohio, 275 p.

CUMMINGS, A. E., 1940. Dynamic pile driving formulas. Journal of Boston Society of Civil Engineers, "Contributions to Soil Mechanics 1925-1940", Boston Society of Civil Engineers, pp. 392-413.

DAVIS, R. A., MURE, J. N., and KIGHTLEY, M. L., 1987. The dynamic analysis of pile foundation using the CAPWAP method. Ground Engineering, November 1987, pp. 16-22.

FOREHAND, P. W., and REESE,Jr., J. L., 1964. Prediction of pile capacity by the wave equation. American Society of Civil Engineers, ASCE Journal of Soil Mechanics and Foundation Engineering Division, No. SM2, pp. 1-25.

GLANVILLE, W. H., GRIME, G., FOX, E. N., DAVIES, W. W., 1938. An investigation of the stresses in reinforced concrete piles during driving. British Building Research Board, Technical Paper No. 20. (As referenced by Goble et al., 1980)

GOBLE, G. G., LIKINS, G. E. Jr., and RAUSCHE, F., 1975. Bearing capacity of piles from dynamic measurements. Case Western University, Department of Solid Mechanics, Structures and Mechanical Design. Final Report. 75 p.

GOBLE, G. G. and RAUSCHE, F., 1976. Wave equation analysis of pile driving–WEAP program. Federal Highway Administration, IP-76-14.1-4. Vol. 1-4.

GOBLE, G. G., RAUSCHE, F., and LIKINS, G. E. Jr., 1980. The analysis of pile driving a state-of-the-art. First International Seminar on the Application of Stress Wave Theory on Piles, pp. 131-161.

GOBLE, G. G. and RAUSCHE, F., 1986. Wave equation analysis of pile foundations - WEAP86 program, Vol. I - Background, Vol. II - General Users Manual. US. Departemnt of Transp.- Federal Highway Administration.

HANNIGAN, P. J., 1990. Dynamic monitoring and analysis of pile foundation installation. Deep Foundation Institute – Continuing Education Short Course Text, First Edition, 1990, 70 p.

HIRSCH, T. J., CARR, L., and LOWERY, L. L. Jr., 1976. Pile driving analysis wave equation user's manuals TTI Program. Federal Highway Administration, IP-76-13.1-4. Vol. 1-4.

HIRSCH, T. J. and EDWARDS, T. C., 1966. Impact load-deformation properties of pile cushioning materials. Research report 33-4, Texas A&M University, 12 p.

HOLLOWAY, D. M., CLOUGH, G. H., and VESIC, A. S., 1978. The effects of residual driving stresses on pile performance under axial loads. Proceeding 1978 Offshore Technology Conference, Huston, OTC 3306, 12 p.

HOLLOWAY, D. M., CLOUGH, G. H., and VESIC, A. S., 1978. A rational procedure for evaluating the behavior of impact driven piles. American Society for Testing and Materials, ASTM symposium on behavior of deep foundations, R. Lundgren, Editor, Special Technical Publication, STP 670, 1978, pp. 335-357.

HORVATH, R. G. and KILLEAVY, M., 1988. Variation of CAPWAP results with blows selected for analysis. Proceedings of the Third International Conference on Application of Stress-Wave Theory to Piles, B. H. Fellenius, Editor, 1988, pp. 735-747.

HOUSEL, W. S., 1965. Michigan study of pile driving hammers. Journal of Soil Mechanics and Foundations Division, Proceedings of the American Society of Civil Engineers, Vol. 91, SM5, pp. 33-64.

HUSSEIN, M., 1986. CAPWAPC - a parameter study. Eighth Pile Driving Analyzer User's Seminar, Cleveland, Ohio. pp. 1-24

JUMIKIS, A. R., 1971. Foundation Engineering. International Textbook Co., New York, pp. 598-609.

KHAN, N., 1987. Load distribution in test loaded instrumented steel piles. M.A.Sc. Thesis, University of Ottawa, Faculty of Science and Engineering, Department of Civil Engineering, 176 p.

LAWTON, E. C., FRAGASZY, R. J., HIGGINS, J. D., KILIAN, A. P., and PETERS, A., 1987. Review of methods for estimating pile capacity. Transportation Research Board Record No. 1105, pp. 32-40.

LIKINS, G. E., 1984. Field measurements and the pile driving analyzer. Second International Conference on the Application of Stress-Wave Theory on Piles, pp. 298-305.

LIKINS, G. E. and HUSSEIN, M., 1988. A summary of the pile driving analyzer capacity methods - past and present. The Eleventh Pile Driving Analyzer User's Seminar, Cleveland, Ohio.

LITKOUHI, S. and POSKITT, T. J., 1980. Damping constants for pile driveability calculations. Geotechnique, Vol. 30, No. 1, pp. 77-86.

LOWERY, L. L., HIRSCH, T. J., EDWARDS, T. C., and SAMSON, C. H., 1969. Pile driving analysis state of the art. Research Report 33-13, Texas A&M University, 77 p.

ONTARIO HIGHWAY BRIDGE DESIGN CODE, 1983. Section 6, Substructures and retaining walls, Code and Commentary. Ministry of Transportation and Communications, Toronto, Ontario, 46p.

PILE DRIVING ANALYZER MANUAL, 1989. Chapter 1, General Description. Pile Dynamics Inc., 1989, pp. 1-18.

RAUSCHE, F., 1970. Soil response from dynamic analysis and measurements on piles, Ph. D. Thesis, Case Western Reserve University, Cleveland, Ohio, 1970. (as referenced by Goble et al., 1980)

RAUSCHE, F., 1981. A short introduction to continuous and discrete wave mechanics. The Second Seminar on The Dynamics of Pile Driving, Boulder, pp. 1-16.

RAUSCHE, F., LIKINS, G. E. Jr., and HUSSEIN, M., 1986. Dynamic analysis of impact driven piles by WEAP86. Paper prepared for the Office of Implementation, Federal Highway Administration. McLean, Virginia. 45 p.

RIKER, R. E. and FELLENIUS, B. H., 1988. Case method capacity estimates for piles in glacial soils. Proceedings of the Third International Conference on Application of Stress-Wave Theory to Piles, B. H. Fellenius, Editor, 1988, pp. 565-578.

SMITH, E. A., 1960. Pile-driving analysis by the wave equation. Journal of Soil Mechanics and Foundations Division, Proceedings of the American Society of Civil Engineers, SM4, pp. 35-61.

THOMPSON, C. D., and THOMPSON, D. E., 1978. Influence of driving stresses on the development of high pile capacities. Symposium on the Behavior of Deep Foundations, ASTM, STP 670, R. Lundgren Editor, pp. 562-577.

TABLES

Table 2.1 – Commonly used dynamic pile driving formulas (after Lawton et al., 1987)

Formula Name	Equation	Reference Number	Year	Recommended Safety Factor
Eytelwein (Dutch)	$R_u = \frac{e_h E_h}{s\left(1 + \frac{w}{W}\right)}$ (drop hammers)	(3) (4)	1820	6
	$R_u = \frac{e_h E_h}{s + 0.1\frac{w}{W}}$ (steam hammers)			
Weisbach	$R_u = -\frac{AE}{L} + \sqrt{\frac{2e_h E_h AE}{L} + \left(\frac{AE}{L}\right)^2}$	(3)	1850	
Redtenbacher	$R_u = \frac{AE}{L}\left[-s + \sqrt{s^2 + e_h E_h \cdot \frac{W}{W+w} \cdot \frac{2L}{AE}}\right]$	(3) (5) (6)	1859	3
Engineering News-Record (ENR)	$R_u = \frac{e_h E_h}{s + z}$	(3) (4)	1888	6
Navy-McKay	$R_u = \frac{e_h E_h}{s\left(1 + 0.3\frac{w}{W}\right)}$	(4) (3)		
Gates	$R_u = 27\sqrt{e_h E_h}\,(1 - \log s)$	(3) (4)	1957	3
	$e_h = 0.75$ for drop hammers			
	$e_h = 0.85$ for all other hammers			
	R_u (kips), s (in), E_h (ft-kips)			
Rankine	$R_u = \frac{2AEs}{L}\left[\sqrt{1 + \frac{e_h E_h L}{s^2 EA}} - 1\right]$	(3)		
Hiley	$R_u = \frac{e_h E_h}{s + \frac{1}{2}(C_1 + C_2 + C_3)} \cdot \frac{W + n^2 w}{W + w}$	(7)		3
Janbu	$R_u = \frac{e_h E_h}{K_u s}$ $\quad K_u = C_d\left[1 + \sqrt{1 + \frac{\lambda}{C_d}}\right]$	(4)	1951	3-6
	$C_d = 0.75 + 0.15\frac{w}{W}$			
	$\lambda = \frac{e_h E_h L}{AEs^2}$			
Pacific Coast Uniform Building Code (PCUBC)	$R_u = \frac{e_h E_h \cdot \frac{W + kw}{W + w}}{s + \frac{R_u L}{2AE}}$ $\quad k = 0.25$ for steel piles, $= 0.10$ for all other piles	(4) (6)		4
Gow	$R_u = \frac{e_h E_h}{s + z + \frac{w}{W}}$	(7)		
Danish	$R_u = \frac{n\,e}{s + \sqrt{\frac{e_h E_h L}{2AE}}}$	(7)	1967	3-6
Rabe	$R_u = \frac{e_h E_h}{s + C} \cdot \frac{w}{w + \frac{W}{2}} + B$	(3)	1946	2
Modified ENR*	$\frac{e_h E_h}{s + z} \cdot \frac{W + n^2 w}{W + w}$	(6)	1965	6
Canadian National Building Code	$R_u = \frac{e_h E_h \cdot \frac{W + n^2(0.5w)}{W + w}}{s + \frac{R_u}{2A}\left(\frac{L}{E} + 0.0001\right)}$	(4) (8)		3

*There are several formulas that are modifications of the ENR formula and are known as Modified ENR. The Modified ENR presented here was proposed by the Michigan State Highway Commission in 1965.

Note: To be consistent, the net hammer energy is given in all equations as $e_h E_h$ even though many of the formulas were developed for drop hammers where the hammer energy is given by Wh. No units are given for any terms (except for empirical formulas) so that any consistent set of units can be used.

- A = cross-sectional area of pile.
- A' = cross-sectional area of cushion block.
- B = units supplement factor in Rabe's formula (10) for clarification).
- C = temporary compression loss in the cap, pile, and soil; used in Rabe's formula (see (10) for clarification).
- C_1, C_2, C_3 = coefficients for Hiley equation.
- e_h = efficiency of striking hammer (<1.0).
- E = Young's modulus of elasticity of pile.
- E' = Young's modulus of elasticity of the cushion block.
- E_h = manufacturer's hammer energy rating.
- F = factor of safety.
- h = height of free fall of hammer.
- k = a coefficient to account for elastic compression plus other losses in Redtenbacher's classical formula.
- L = length of pile
- L' = axial length of cushion block.
- n = coefficient of restitution.
- R_u = ultimate bearing capacity of pile in soil.
- R_a = safe bearing capacity of pile.
- s = pile penetration for last blow, also called "set".
- w = weight of pile.
- W = weight of hammer.
- z = 0.1 for steam hammers; 1.0 for drop hammers.

Table 2.2 – Pile driving analyzer output quantities

Quantity	Description
FMX	the maximum measured compression force at the transducer location.
VMX	the maximum downward velocity at the transducer location.
DMX	the maximum downward displacement at the transducer location.
EMX	the maximum value of the energy transferred past the transducers.
AMX	the maximum acceleration at the transducer location.
FT1	force value at "impact" time 1.
VT1	the velocity value at time 1.
DT1	the displacement value at time 1.
FT2	the pile head force at time 2, 2L/C after impact.
VT2	the pile head velocity at time 2, 2L/C after impact.
WDN	the value of the downward traveling force wave at time 1; [FT1 + (VT1 · MC/L)]/2.
WUP	the value of the upward traveling force wave at time 1; [FT1 - (VT1 · MC/L)]/2.
FTN	maximum measured tension force (negative) at the transducers.
CTN	maximum computed tension force below the transducers.
BPM	the hammer operating rate in blows per minute.
RSP	Case Method static resistance using damping (J) at time 1.
RMX	maximum Case Method resistance using J at any time during blow.
TMX	delay time after impact where Case Method is maximum, RMX.
WDX	wave down at time TMX; for adjusting RMX with different damping.
DBX	computed pile toe displacement at time TMX, estimate of toe quake.
RMN	minimum Case Method resistance using damping.
TMN	the 2L/C time with the minimum Case Method resistance, RMN.
RTL	Case Method RSP resistance for zero damping.
RSU	Case Method resistance using damping corrected for early unloading.
RAU	Case Method static resistance at time of zero damping for piles without skin friction.
RA2	Case Method resistance at time of zero damping for piles with shaft resistance.
BTA	pile integrity factor for damage analysis.
SFT	shaft resistance total - not reduced for damping.
CFB	computed compression force at the pile toe.
MFO	maximum ram momentum at impact from integral of force.
MWO	maximum ram momentum at impact from integral of wave down.
MF1	impulse of force at time 1.
MW1	impulse of wave down at time 1.
VRI	ram impact velocity computed from MFO and MRAM.
FCP	maximum computed force in hammer cushion (capblock).
DCP	maximum computed displacement in hammer cushion (capblock).

NOTE: The Pile Driving Analyzer computes several quantities identified by the following code words. The first letter indicates the variable type, i.e. C is computed force, D is displacement, E is energy, F is force, M is momentum, R is resistance, T is time, V is velocity and W is wave force.

Table 2.3 – CAPWAPC unknows

Quantity	Symbol	Dimension	Recommended Minimum	Recommended Maximum	Recommended Starting Value
Skin Quake	QSkn	inch/cm	.01/.025	max u[2]	0.1/0.25
Toe Quake	QToe	inch/cm	.01/.025	max u[2]	0.1/0.25
Skin Unld Quake[1]	CSkn	--	.01	1.0	1.0
Toe Unld Quake[1]	CToe	--	.01	1.0	1.0
Unloading Level[1]	UNld	--	0	1.0	1.0
Skin Reloading Level[1]	RSkn		-1.0	1.0	-1.0
Toe Reloading Level[1]	RToe	--	0.0	1.0	0
Skin Damping					
Case	JSkn	--	N/A	N_c	0.1
Smith	SSkn	s/ft s/m	0.025/.08	0.31/1.0[3]	N/A
Toe Damping					
Case	JToe	--	N/A	1.0	0.1
Smith	SToe	s/ft s/m	0.025/.08	0.31/1.0[3]	N/A
Smith Damping Option	OPtd	--	0	2.0	0
Pile Damping	PIld	--	0	0.03	0
Toe Soil Dashpot	BTdp	--	0.02	N/A	0
Plug Mass	PLug	Fu	0	3 toe weight	0
Toe Gap	TGap	inch/cm	0	max u_{toe} - q_{toe}	0

1 Multiplier

2 Max. displacement

3 Higher values are possible though uncommon

Table 3.1 – Soil profile - Jones Island, Milwaukee (pile embedment depth of 35.2 m)

DEPTH (m)	TYPE	Thickness (m)	Unit Weight (KN/m^3)	C_u (KPa)	Friction angle (°)
0.0	Miscellaneous earth fill	6.0	18	--	30
6.0	Soft to medium stiff compressible postglacial silty clay and clayey silt	19.5	17	40	37
25.5	Mixed glacial soil: sandy silt, sand, clayey silt	56.0	18	200	37
81.5	Dolomite bedrock End of borehole	-	-	-	-

Table 3.2 – Soil profile - CN Jasper, Alberta (pile embedment depth of 21.6 m)

DEPTH (m)	TYPE	Thickness (m)
0.0	Sandy gravel fill	6.0
1.3	Coarse to medium san with layers of silty sand and lenses of frost	2.3
3.6	Sandy gravel	0.7
4.3	Medium to fine compact brown sand with layers of fine silt	18.6
22.9	Fine and medium compact sand, trace silt	5.0
27.9	End of borehole	

Table 3.3 – Soil profile - National Aviation Museum, Ottawa.
(pile embedment depth of 58.2 m)

DEPTH (m)	TYPE	Thickness (m)
0.1	Fill: Sans and clay with pieces of weathered shale	1.3
1.4	Loose to medium dense silty fine sand	0.5
1.8	Medium soft to stiff fissured silty grey clay	16.2
18.0	Stiff to very stiff silty grey clay	30.0
48.0	Dense soil End of borehole	5.0

TABLE 4.1 – SUMMARY OF DYNAMIC MEASUREMENTS – DATPRO ANALYSIS

JONES ISLAND, MILWAUKEE, PILE A1, @ 115-116 FEET

BLOW #	TRANSFERRED ENERGY (KJ)	IMPACT FORCE (KN)	MAXIMUM FORCE (KN)	CMES – RMX J = .7 (KN)
1	23.71	966	966	1125
2	23.50	999	999	1187
3	23.36	939	939	1104
4	23.74	985	985	1099
5	23.46	940	940	1139
6	23.26	986	986	1125
7	23.72	1014	1014	1192
8	23.67	971	971	1127
9	23.66	948	948	1126
10	22.88	985	985	1164
11	23.59	980	980	1145
12	23.74	1000	1000	1233
14	23.67	1005	1005	1135
15	23.66	980	980	1140
16	23.28	984	984	1114
17	23.72	1020	1020	1255
18	23.87	961	961	1112
19	24.39	985	985	1155
20	23.70	954	954	1117
21	24.02	988	988	1136
22	23.79	955	955	1147
23	23.79	922	922	1155
24	25.64	981	981	1248
25	25.53	1112	1112	1353
MEAN AVG	23.81	981.67	981.67	1159.71
STD	0.60	36.11	36.11	58.25
% STD	2.54	3.68	3.68	5.02

TABLE 4.2 – SUMMARY OF DYNAMIC MEASUREMENTS – DATPRO ANALYSIS

JASPER, ALBERTA, BENT 3, PILE 4, @ 71-72 FEET

BLOW #	TRANSFERRED ENERGY (KJ)	IMPACT FORCE (KN)	MAXIMUM FORCE (KN)	CMES – RMX J = .6 (KN)
1	9.10	1256	1256	765
2	7.63	1170	1170	779
3	8.21	1192	1203	760
4	8.02	1168	1168	714
5	8.83	1215	1215	779
6	8.73	1196	1223	756
7	8.67	1214	1214	762
8	8.42	1186	1186	752
9	7.72	1179	1179	782
10	8.45	1184	1184	746
11	8.91	1238	1238	774
12	8.18	1207	1207	773
13	9.26	1237	1244	766
14	8.76	1228	1228	749
15	8.48	1214	1214	732
16	8.21	1202	1206	750
17	8.05	1186	1186	773
18	8.34	1172	1172	759
19	8.38	1204	1204	742
20	8.14	1183	1183	747
21	8.63	1186	1186	744
22	8.64	1212	1212	744
23	8.15	1172	1172	757
24	8.25	1217	1217	767
MEAN AVG	8.42	1200.75	1202.79	757.17
STD	0.39	23.26	24.04	15.91
% STD	4.66	1.94	2.00	2.10

TABLE 4.3 – SUMMARY OF DYNAMIC MEASUREMENTS – DATPRO ANALYSIS

AVIATION MUSEUM, OTTAWA, PILE Q13X-4, 1st RESTRIKE

BLOW #	TRANSFERRED ENERGY (KJ)	IMPACT FORCE (KN)	MAXIMUM FORCE (KN)	CMES – RMX J = .4 (KN)
1	24.46	1839	1869	1962
2	28.20	1964	1964	2089
3	29.51	1970	1970	2047
4	29.69	1958	1966	2009
5	30.49	1971	1978	1973
6	31.02	2013	2013	1995
8	28.80	1973	1973	1923
9	28.49	1909	1925	1847
10	30.65	1964	1987	1882
11	26.02	1953	1957	1818
13	24.72	1732	1732	1672
14	29.31	1854	1866	1761
15	25.66	1814	1814	1754
16	29.46	1892	1934	1772
17	28.21	1889	1889	1749
18	28.59	1894	1894	1738
19	30.55	1921	1929	1734
MEAN AVG	28.46	1912.35	1921.18	1866.18
STD	2.00	69.46	69.13	124.61
% STD	7.04	3.63	3.60	6.68

TABLE 4.4 – SUMMARY OF TOTAL STATIC RESISTANCE – CAPWAP ANALYSIS

JONES ISLAND, MILWAUKEE, PILE A1, @ 115-116 FEET

BLOW #	TRANSFERRED ENERGY (KJ)	MAX. = IMP. FORCE (KN)	CMES-RMX J=0.7 (KN)	TOTAL STATIC RESISTANCE CAPWAPC (KN)	% DIFFERENCE OF MEAN AVG Rult
1	23.71	966	1125	1111	-4.42%
2	23.50	999	1187	1174	1.02%
3	23.36	939	1104	1012	-12.90%
4	23.74	985	1099	1020	-12.20%
5	23.46	940	1139	1065	-8.39%
6	23.26	986	1125	1241	6.82%
7	23.72	1014	1192	1020	-12.20%
8	23.67	971	1127	1088	-6.35%
9	23.66	948	1126	1134	-2.42%
10	22.88	985	1164	1227	5.58%
11	23.59	980	1145	1164	0.17%
12	23.74	1000	1233	1282	10.30%
13				1116	-4.00%
14	23.67	1005	1135	1159	-0.23%
15	23.66	980	1140	1212	4.33%
16	23.28	984	1114	1173	0.95%
17	23.72	1020	1255	1050	-9.63%
18	23.87	961	1112	1240	6.73%
19	24.39	985	1155	1220	4.99%
20	23.70	954	1117	1090	-6.19%
21	24.02	988	1136	1207	3.84%
22	23.79	955	1147	1179	1.43%
23	23.79	922	1155	1336	14.94%
24	25.64	981	1248	1358	16.89%
25	25.53	1112	1353	1173	0.93%
MEAN AVG	23.81	981.67	1159.71	1162.04	MAX 16.89%
STD	0.60	36.11	58.25	91.44	MIN -12.90%
% STD	2.54	3.68	5.02	7.87	

TABLE 4.5 – SUMMARY OF TOTAL STATIC RESISTANCE – CAPWAP ANALYSIS

JASPER, ALBERTA, BNT 3, PILE 4, @ 71-72 FEET

BLOW #	TRANSFERRED ENERGY (KJ)	MAX.=IMP. FORCE (KN)	CMES-RMX J=0.6 (KN)	TOTAL STATIC RESISTANCE CAPWAPC (KN)		% DIFFERENCE OF MEAN AVG Rult
1	9.10	1256	765	719		-0.97%
2	7.63	1170	779	785		8.11%
3	8.21	1203	760	730		0.46%
4	8.02	1168	714	726		-0.02%
5	8.83	1215	779	741		2.02%
6	8.73	1223	756	723		-0.50%
7	8.67	1214	762	728		0.25%
8	8.42	1186	752	719		-1.01%
9	7.72	1179	782	728		0.25%
10	8.45	1184	746	754		3.78%
11	8.91	1238	774	747		2.79%
12	8.18	1207	773	747		2.79%
13	9.26	1244	766	734		1.00%
14	8.76	1228	749	729		0.39%
15	8.48	1214	732	706		-2.80%
16	8.21	1206	750	725		-0.23%
17	8.05	1186	773	708		-2.60%
18	8.34	1172	759	705		-2.90%
19	8.38	1204	742	709		-2.36%
20	8.14	1183	747	708		-2.60%
21	8.63	1186	744	708		-2.57%
22	8.64	1212	744	719		-1.04%
23	8.15	1172	757	712		-1.96%
24	8.25	1217	767	725		-0.26%
MEAN AVG	8.42	1202.79	757.17	726.36	MAX	8.11%
STD	0.39	24.04	15.91	18.18	MIN	-2.90%
% STD	4.66	2.00	2.10	2.50		

TABLE 4.6 – SUMMARY OF TOTAL STATIC RESISTANCE – CAPWAP ANALYSIS

AVIATION MUSEUM, OTTAWA, PILE Q13X-4, 1st RESTRIKE

BLOW #	TRANSFERRED ENERGY (KJ)	MAX.=IMP. FORCE (KN)	CMES-RMX J=0.4 (KN)	TOTAL STATIC RESISTANCE CAPWAPC (KN)		% DIFFERENCE OF MEAN AVG Rult
1	24.46	1869	1962	2352		23.04%
2	28.20	1964	2089	2321		21.43%
3	29.51	1970	2047	2164		13.23%
4	29.69	1966	2009	2048		7.14%
5	30.49	1978	1973	2008		5.07%
6	31.02	2013	1995	2062		7.91%
8	28.80	1973	1923	1979		3.57%
9	28.49	1925	1847	1764		-7.71%
10	30.65	1987	1882	1806		-5.48%
11	26.02	1957	1818	1805		-5.58%
13	24.72	1732	1672	1635		-14.44%
14	29.31	1866	1761	1705		-10.81%
15	25.66	1814	1754	1767		-7.53%
16	29.46	1934	1772	1782		-6.74%
17	28.21	1889	1749	1779		-6.92%
18	28.59	1894	1738	1743		-8.80%
19	30.55	1929	1734	1770		-7.37%
MEAN AVG	28.46	1921.18	1866.18	1911.16	MAX	23.04%
STD	2.00	69.13	124.61	209.61	MIN	-14.44%
% STD	7.04	3.60	6.68	10.97		

TABLE 4.7 – SUMMARY OF CAPWAPC RESISTANCE DISTRIBUTION

JONES ISLAND, MILWAUKEE, PILE A1, @ 115-116 FEET

BLOW #	TOTAL STATIC RESISTANCE CAPWAPC (KN)	SHAFT RESISTANCE (KN)	TOE RESISTANCE (KN)	RATIO SHAFT/Rult %	RATIO TOE/Rult %
1	1111	675	436	61%	39%
2	1174	644	530	55%	45%
3	1012	675	337	67%	33%
4	1020	802	219	79%	21%
5	1065	681	383	64%	36%
6	1241	963	278	78%	22%
7	1020	782	238	77%	23%
8	1088	740	348	68%	32%
9	1134	844	290	74%	26%
10	1227	1107	120	90%	10%
11	1164	899	265	77%	23%
12	1282	922	360	72%	28%
13	1116	795	321	71%	29%
14	1159	881	278	76%	24%
15	1212	933	279	77%	23%
16	1173	949	225	81%	19%
17	1050	901	151	86%	14%
18	1240	967	273	78%	22%
19	1220	945	275	77%	23%
20	1090	730	360	67%	33%
21	1207	967	240	80%	20%
22	1179	936	243	79%	21%
23	1336	964	372	72%	28%
24	1358	1072	286	79%	21%
25	1173	951	222	81%	19%
MEAN AVG	1162.04	868.96	293.13	MAX. 90%	45.00%
STD	91.44	123.67	85.20	MIN. 55%	10.00%
% STD	7.87	14.23	29.06	DIFF. 35%	35%

TABLE 4.8 – SUMMARY OF CAPWAPC RESISTANCE DISTRIBUTION

JASPER, ALBERTA, BENT 3, PILE 4, @ 71-72 FEET

BLOW #	TOTAL STATIC RESISTANCE CAPWAPC (KN)	SHAFT RESISTANCE (KN)	TOE RESISTANCE (KN)	RATIO SHAFT/Rult %	RATIO TOE/Rult %
1	719	512	207	71%	29%
2	785	508	278	65%	35%
3	730	507	220	70%	30%
4	726	579	147	80%	20%
5	741	559	182	75%	25%
6	723	681	42	94%	6%
7	728	628	101	86%	14%
8	719	624	95	87%	13%
9	728	636	92	87%	13%
10	754	668	86	89%	11%
11	747	652	95	87%	13%
12	747	649	98	87%	13%
13	734	631	103	86%	14%
14	729	643	86	88%	12%
15	706	624	83	88%	12%
16	725	633	92	87%	13%
17	708	596	112	84%	16%
18	705	493	212	70%	30%
19	709	629	81	89%	11%
20	708	581	126	82%	18%
21	708	613	95	87%	13%
22	719	624	95	87%	13%
23	712	619	93	87%	13%
24	725	583	141	81%	19%
MEAN AVG	726.36	602.96	123.34	MAX. 94%	35.00%
STD	18.18	51.67	55.22	MIN. 65%	6.00%
% STD	2.50	8.57	44.77	DIFF. 29%	29%

TABLE 4.9 – SUMMARY OF CAPWAPC RESISTANCE DISTRIBUTION

AVIATION MUSEUM, OTTAWA, PILE Q13X-4, 1st RESTRIKE

BLOW #	TOTAL STATIC RESISTANCE CAPWAPC (KN)	SHAFT RESISTANCE (KN)	TOE RESISTANCE (KN)	RATIO SHAFT/Rult %	RATIO TOE/Rult %
1	2352	2342	10	100%	0%
2	2321	2311	10	100%	0%
3	2164	2113	51	98%	2%
4	2048	1961	87	96%	4%
5	2008	1975	33	98%	2%
6	2062	1914	148	93%	7%
8	1979	1498	481	76%	24%
9	1764	1154	610	65%	35%
10	1806	1290	516	71%	29%
11	1805	1289	516	71%	29%
13	1635	1092	543	67%	33%
14	1705	1146	559	67%	33%
15	1767	1099	668	62%	38%
16	1782	1062	720	60%	40%
17	1779	1006	773	57%	43%
18	1743	938	805	54%	46%
19	1770	955	815	54%	46%
MEAN AVG	1911.16	1479.16	431.98	MAX. 99.57%	46.18%
STD	209.61	488.25	294.79	MIN. 53.97%	0.42%
% STD	10.97	33.01	68.24	DIFF. 46%	46%

TABLE 4.10 – SUMMARY OF CAPWAPC DYNAMIC PARAMETERS SHAFT AND TOE

JONES ISLAND, MILWAUKEE, PILE A1, @ 115–116 FEET

BLOW #	SHAFT				TOE			
	RESISTANCE (KN)	CASE DAMPING	SMITH DAMPING	QUAKE (cm)	RESISTANCE (KN)	CASE DAMPING	SMITH DAMPING	QUAKE (cm)
1	675	0.177	0.102	0.098	436	0.350	0.355	0.300
2	644	0.127	0.077	0.050	530	0.400	0.352	0.150
3	675	0.151	0.087	0.176	337	0.350	0.505	0.500
4	802	0.150	0.072	0.277	219	0.350	0.862	0.400
5	681	0.150	0.085	0.231	383	0.350	0.422	0.400
6	963	0.150	0.060	0.186	278	0.350	0.604	0.250
7	782	0.150	0.074	0.186	238	0.350	0.783	0.350
8	740	0.150	0.079	0.208	348	0.350	0.525	0.350
9	844	0.150	0.069	0.197	290	0.350	0.572	0.350
10	1107	0.150	0.052	0.174	120	0.350	1.233	0.350
11	899	0.150	0.065	0.174	265	0.350	0.599	0.350
12	922	0.150	0.063	0.174	360	0.350	0.448	0.350
13	795	0.150	0.073	0.174	321	0.350	0.502	0.350
14	881	0.150	0.066	0.186	278	0.350	0.655	0.350
15	933	0.150	0.062	0.186	279	0.350	0.612	0.350
16	949	0.150	0.061	0.186	225	0.350	0.712	0.350
17	901	0.150	0.065	0.186	151	0.350	0.994	0.350
18	967	0.150	0.060	0.186	273	0.350	0.596	0.350
19	945	0.150	0.061	0.186	275	0.350	0.590	0.350
20	730	0.350	0.186	0.161	360	0.300	0.407	0.500
21	967	0.200	0.080	0.211	240	0.350	0.673	0.500
22	936	0.200	0.083	0.214	243	0.350	0.640	0.400
23	964	0.200	0.080	0.214	372	0.350	0.447	0.500
24	1072	0.150	0.054	0.214	286	0.350	0.520	0.500
25	951	0.150	0.061	0.214	222	0.350	0.646	0.450
MEAN AVG	869	0.164	0.075	0.186	293	0.350	0.610	0.376
STD	124	0.042	0.025	0.041	85	0.014	0.195	0.081
% STD	14.23	25.47	33.78	22.10	29.06	4.04	31.93	21.65

TABLE 4.11 – SUMMARY OF CAPWAPC DYNAMIC PARAMETERS SHAFT AND TOE

JASPER, ALBERTA, BENT 3, PILE 4, @ 71-72 FEET

BLOW #	SHAFT				TOE			
	RESISTANCE (KN)	CASE DAMPING	SMITH DAMPING	QUAKE (cm)	RESISTANCE (KN)	CASE DAMPING	SMITH DAMPING	QUAKE (cm)
1	512	0.175	0.141	0.114	207	0.500	1.110	0.300
2	508	0.150	0.121	0.086	278	0.500	0.812	0.275
3	507	0.200	0.162	0.125	220	0.450	0.915	0.250
4	579	0.200	0.142	0.120	147	0.450	1.391	0.250
5	559	0.200	0.147	0.120	182	0.450	1.172	0.350
6	681	0.125	0.076	0.136	42	0.500	5.520	0.450
7	628	0.150	0.098	0.136	101	0.500	2.334	0.450
8	624	0.125	0.082	0.136	95	0.500	2.415	0.450
9	636	0.125	0.082	0.136	92	0.450	2.390	0.400
10	668	0.125	0.077	0.136	86	0.450	2.490	0.450
11	652	0.125	0.079	0.157	95	0.500	2.532	0.500
12	649	0.200	0.127	0.136	98	0.450	2.220	0.450
13	631	0.200	0.130	0.136	103	0.500	2.267	0.500
14	643	0.200	0.128	0.136	86	0.500	2.755	0.500
15	624	0.200	0.132	0.136	83	0.450	2.425	0.450
16	633	0.200	0.130	0.136	92	0.450	2.363	0.450
17	596	0.200	0.138	0.136	112	0.450	1.834	0.450
18	493	0.200	0.167	0.136	212	0.500	1.073	0.275
19	629	0.200	0.131	0.125	81	0.500	2.942	0.300
20	581	0.200	0.141	0.125	126	0.500	1.929	0.300
21	613	0.200	0.134	0.125	95	0.500	2.461	0.300
22	624	0.200	0.132	0.125	95	0.500	2.355	0.300
23	619	0.200	0.133	0.125	93	0.500	2.467	0.300
24	583	0.088	0.062	0.125	141	0.450	1.492	0.127
MEAN AVG	603	0.175	0.121	0.129	123	0.479	2.153	0.368
STD	52	0.036	0.029	0.012	55	0.025	0.931	0.100
% STD	8.57	20.49	23.76	9.62	44.77	5.14	43.27	27.10

TABLE 4.12 -- SUMMARY OF CAPWAPC DYNAMIC PARAMETERS SHAFT AND TOE

AVIATION MUSEUM, OTTAWA, PILE Q13X-4, 1st RESTRIKE

BLOW #	SHAFT				TOE			
	RESISTANCE (KN)	CASE DAMPING	SMITH DAMPING	QUAKE (cm)	RESISTANCE (KN)	CASE DAMPING	SMITH DAMPING	QUAKE (cm)
1	2342	0.950	0.167	0.313	10	0.020	0.868	0.100
2	2311	0.950	0.169	0.289	10	0.020	0.860	0.125
3	2113	0.950	0.185	0.289	51	0.050	0.430	0.125
4	1961	0.950	0.199	0.254	87	0.050	0.254	0.125
5	1975	0.950	0.198	0.254	33	0.050	0.667	0.125
6	1914	0.800	0.172	0.254	148	0.175	0.521	0.050
8	1499	0.950	0.260	0.254	481	0.075	0.069	0.050
9	1154	0.950	0.338	0.241	610	0.075	0.054	0.050
10	1290	0.950	0.303	0.193	516	0.050	0.042	0.050
11	1289	0.950	0.303	0.193	516	0.050	0.042	0.175
13	1092	0.950	0.357	0.193	545	0.050	0.040	0.150
14	1146	0.950	0.341	0.217	559	0.100	0.078	0.075
15	1099	0.950	0.355	0.193	668	0.050	0.033	0.125
16	1062	0.950	0.367	0.193	720	0.050	0.030	0.125
17	1006	0.950	0.388	0.193	773	0.050	0.028	0.175
18	938	0.950	0.416	0.193	805	0.050	0.027	0.220
19	955	0.950	0.409	0.193	815	0.050	0.026	0.175
MEAN AVG	1479	0.941	0.290	0.230	432	0.060	0.239	0.119
STD	488	0.035	0.088	0.040	295	0.034	0.298	0.050
% STD	33.01	3.75	30.39	17.46	68.24	56.83	124.43	41.89

FIGURES

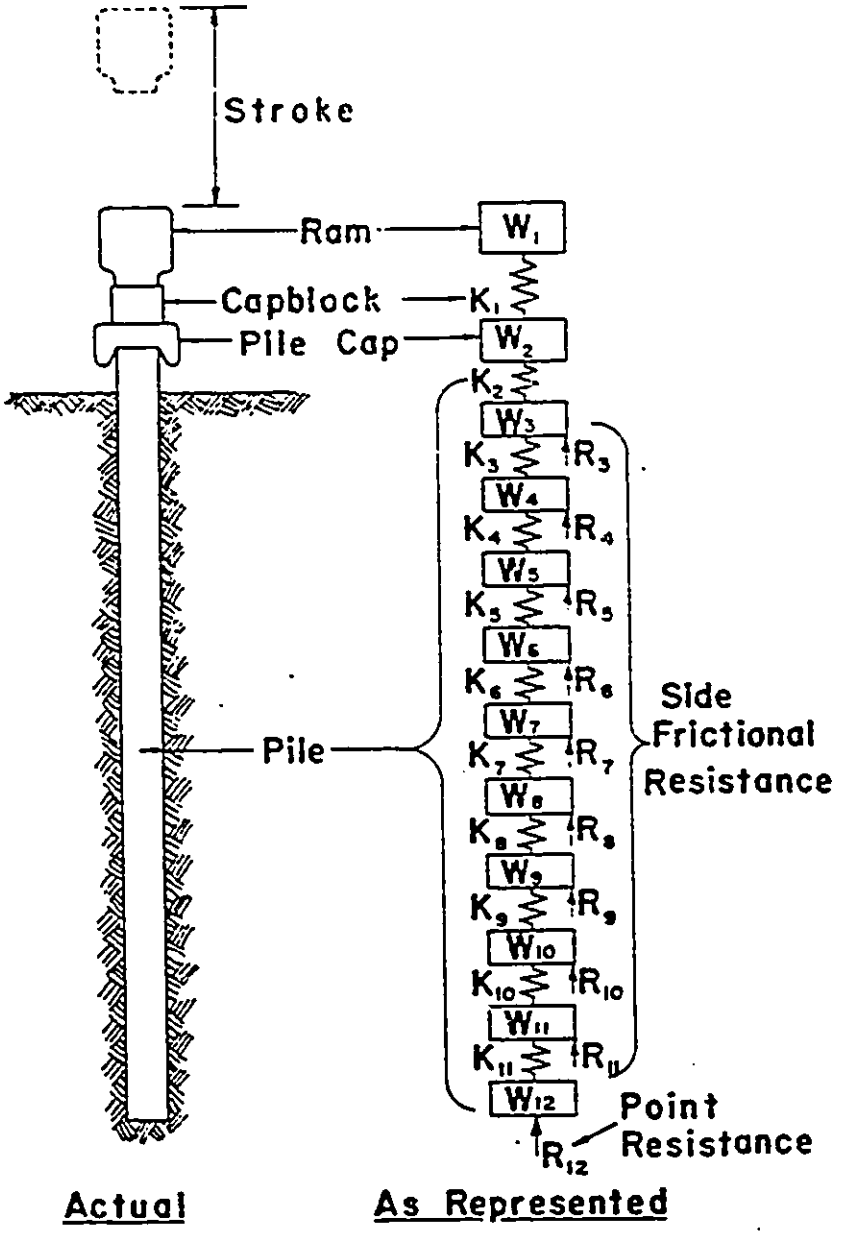

Fig. 2.1 Smith pile model (after Smith, 1960)
caplock = hammer cushion
pile cap = helmet

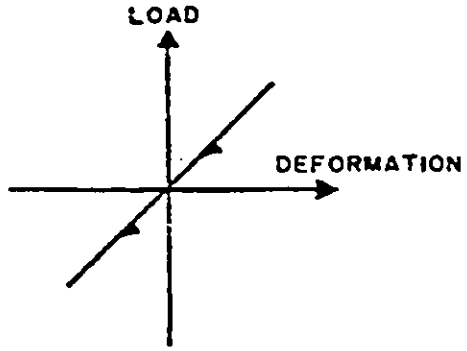

(a) - NO INTERNAL DAMPING

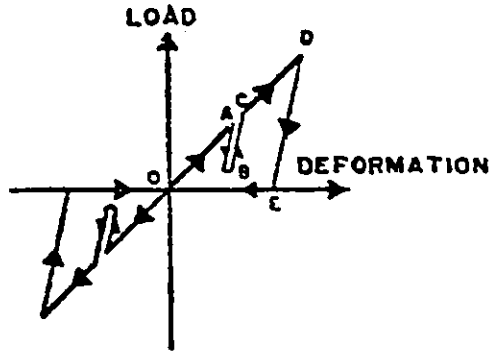

(b) INTERNAL DAMPING PRESENT

Fig. 2.2 Load-Deformation for internal spring (after Smith, 1960) arrows indicate path of load–deformation

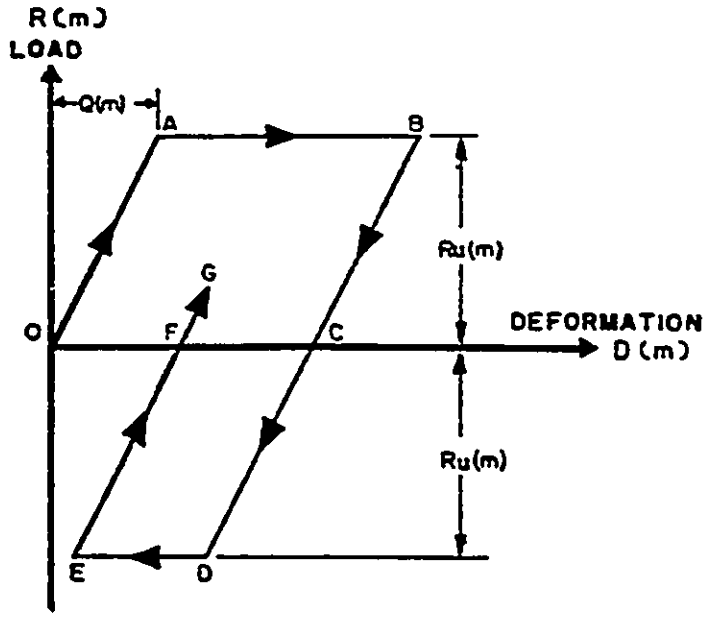

Fig. 2.3 Load Deformation for soil spring (after Smith, 1960) arrows indicate path of load–deformation

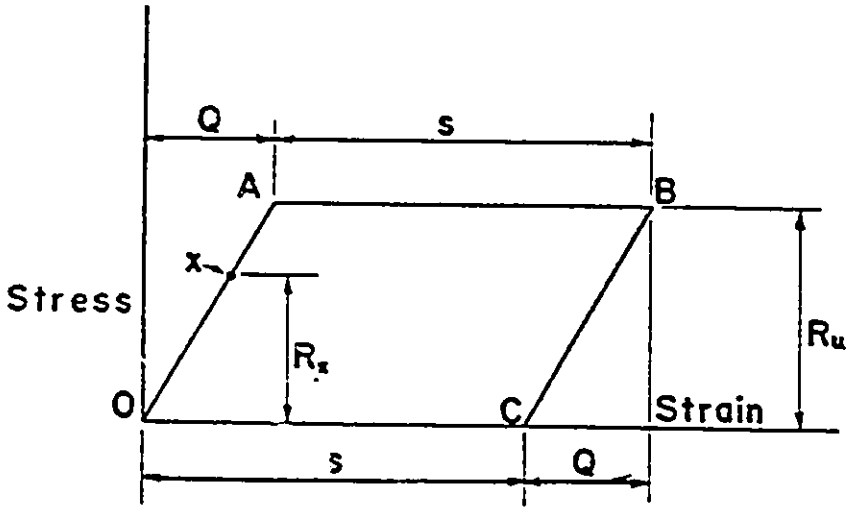

Fig. 2.4 Stress-strain relationship at the pile toe (after Smith, 1960)

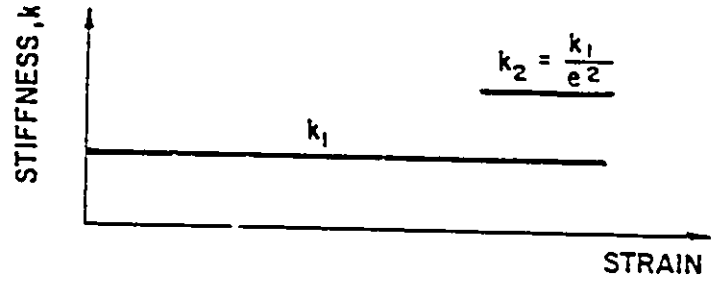

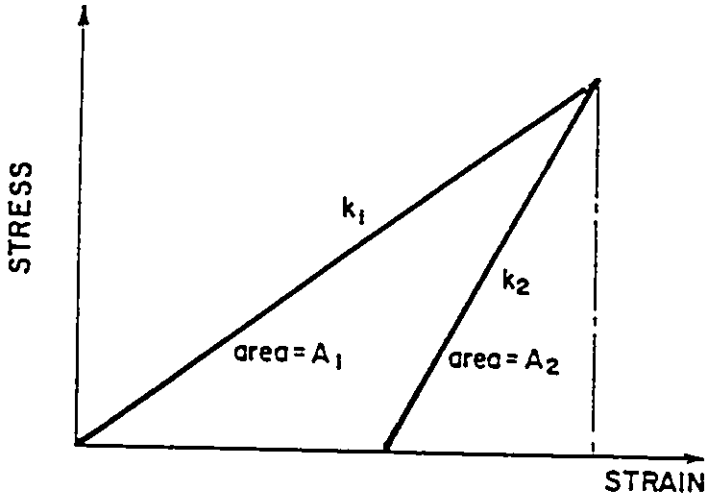

ENERGY INPUT = $A_1 + A_2$

ENERGY OUTPUT = A_2

COEFFICIENT OF RESTITUTION $e = \sqrt{\frac{A_2}{A_1 + A_2}} = \sqrt{\frac{k_1}{k_2}}$

Fig. 2.5 Stress-strain diagram
for stiffness "k" and coefficient of restitution "e"
(after Authier and Fellenius, 1983)

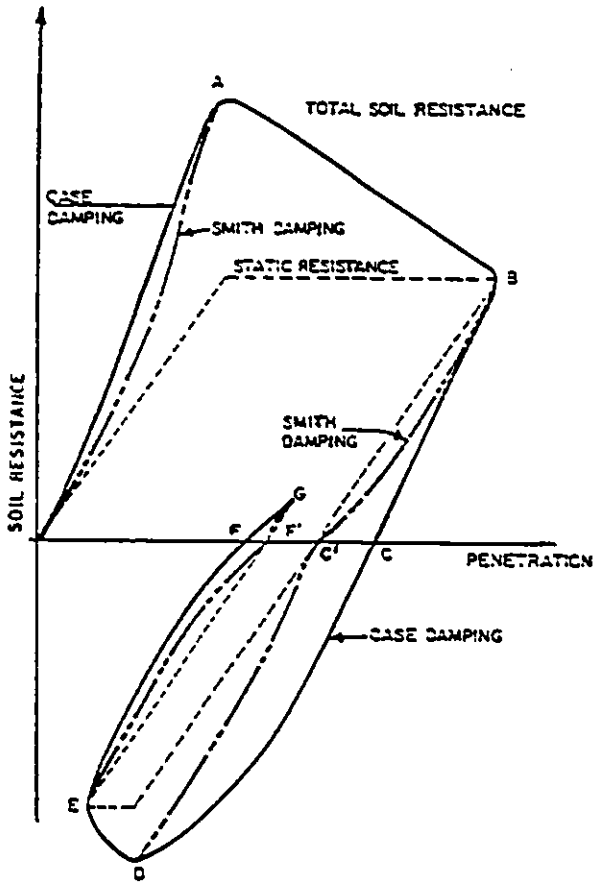

Fig. 2.6 Comparison of Smith and Case damping (after Authier and Fellenius, 1983)

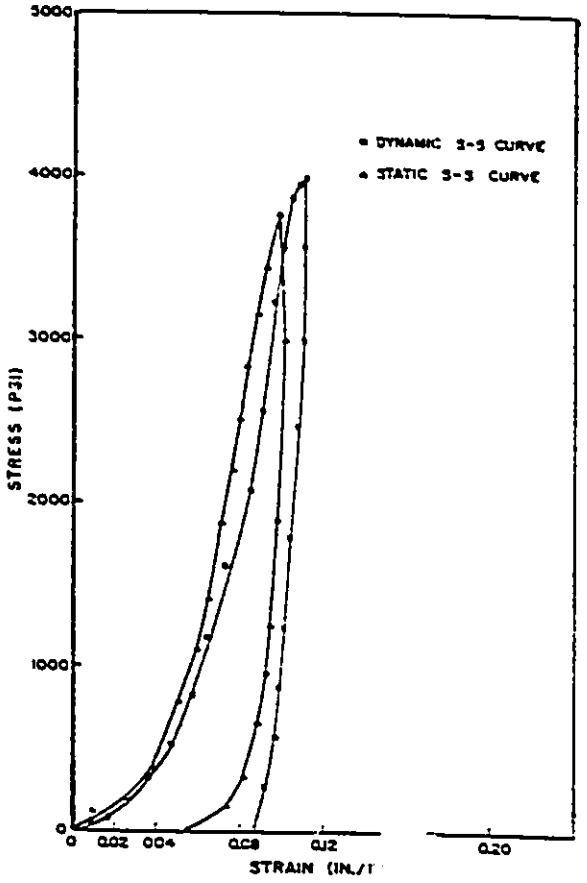

Fig. 2.7 Actual stress-strain behavior for cushions — fir (after Lowery et al., 1969)

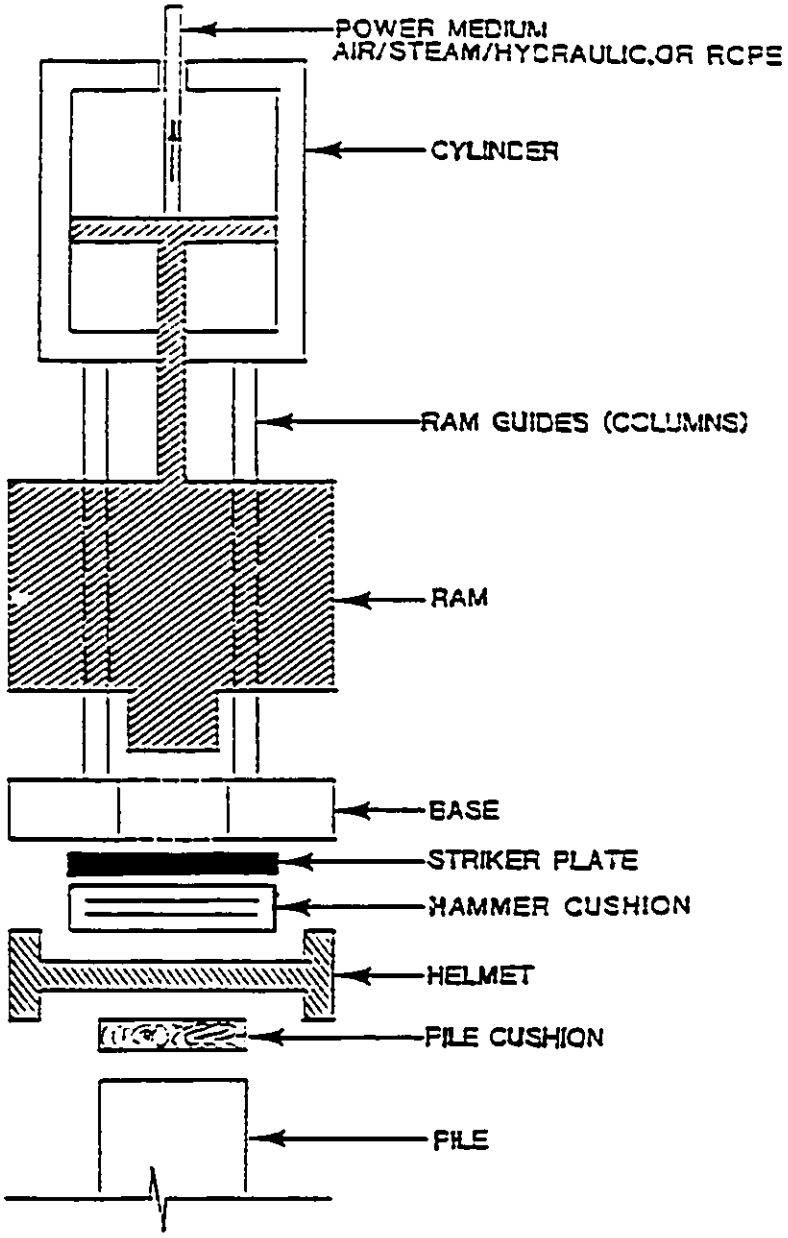

Fig. 2.8 Basic components of an external combustion hammer (after Goble and Rausche, 1986)

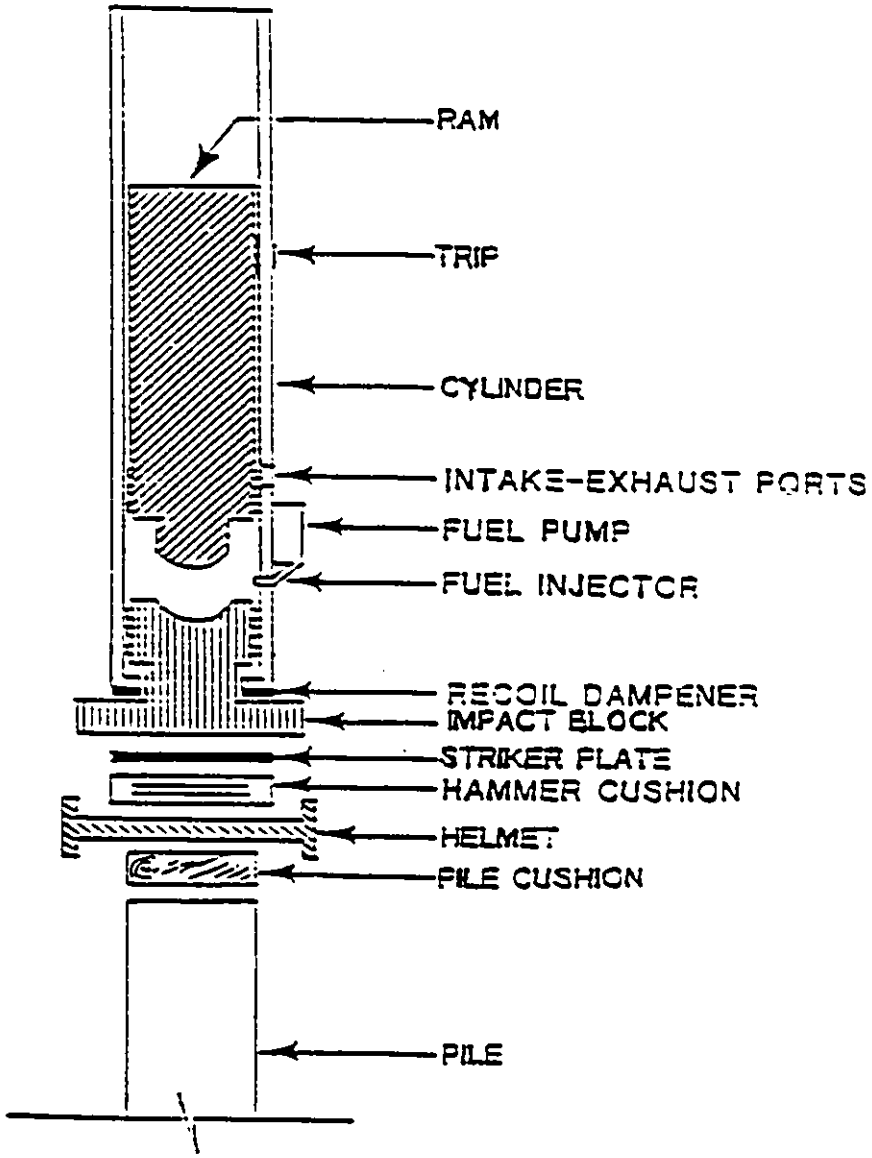

Fig. 2.9 Basic components of a single acting diesel hammer (after Goble and Rausche, 1986)

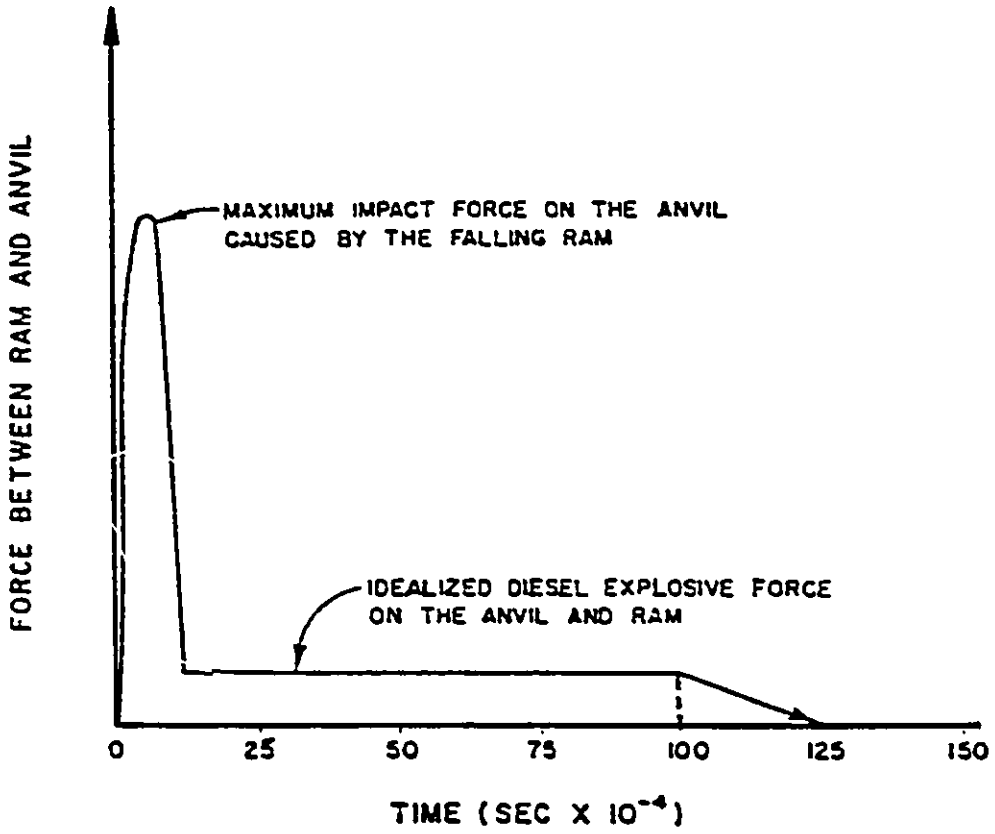

Fig. 2.10 Diesel hammer model by TTI (after Hirsh and Edwards, 1966)

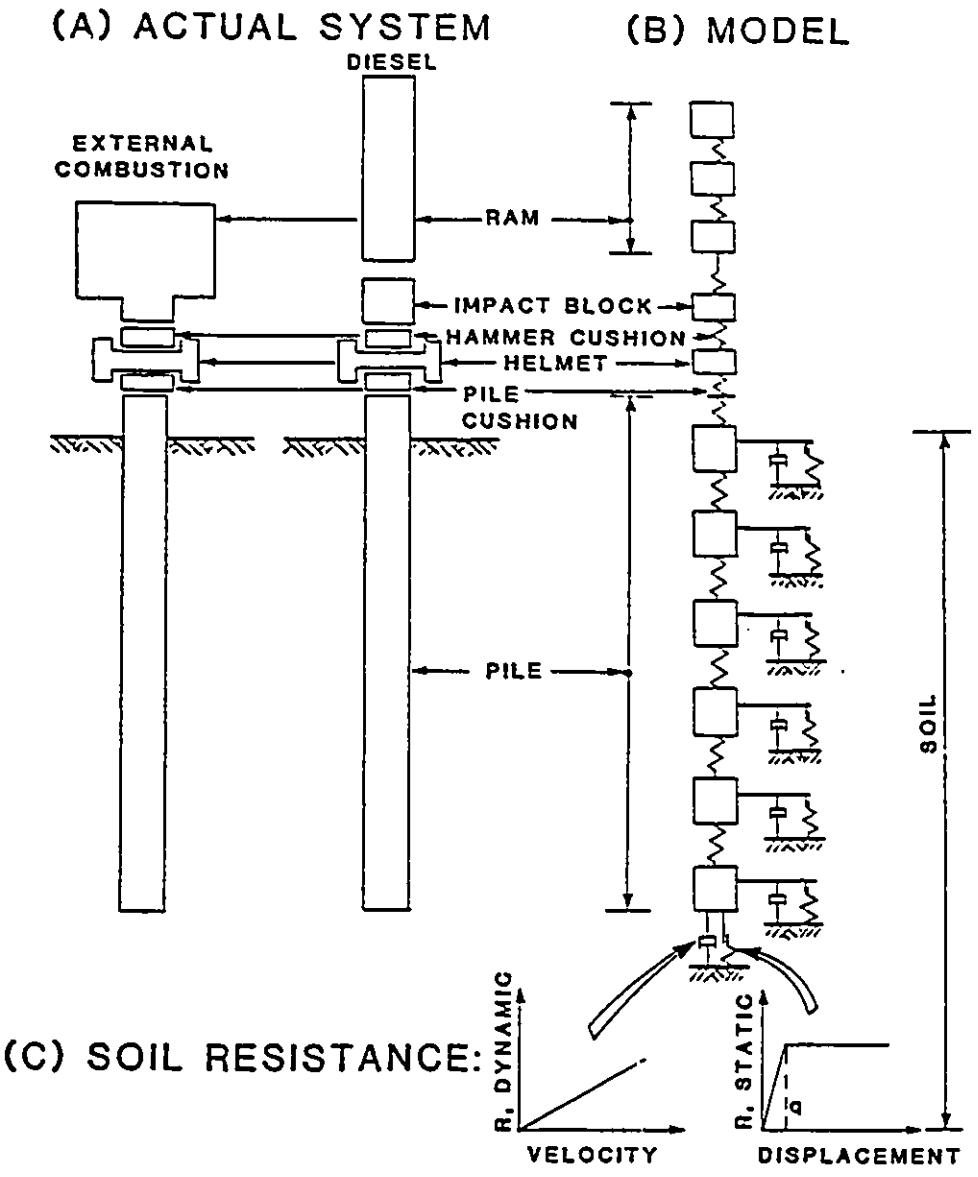

Fig. 2.11 The complete wave equation model
(after Goble and Rausche, 1980)

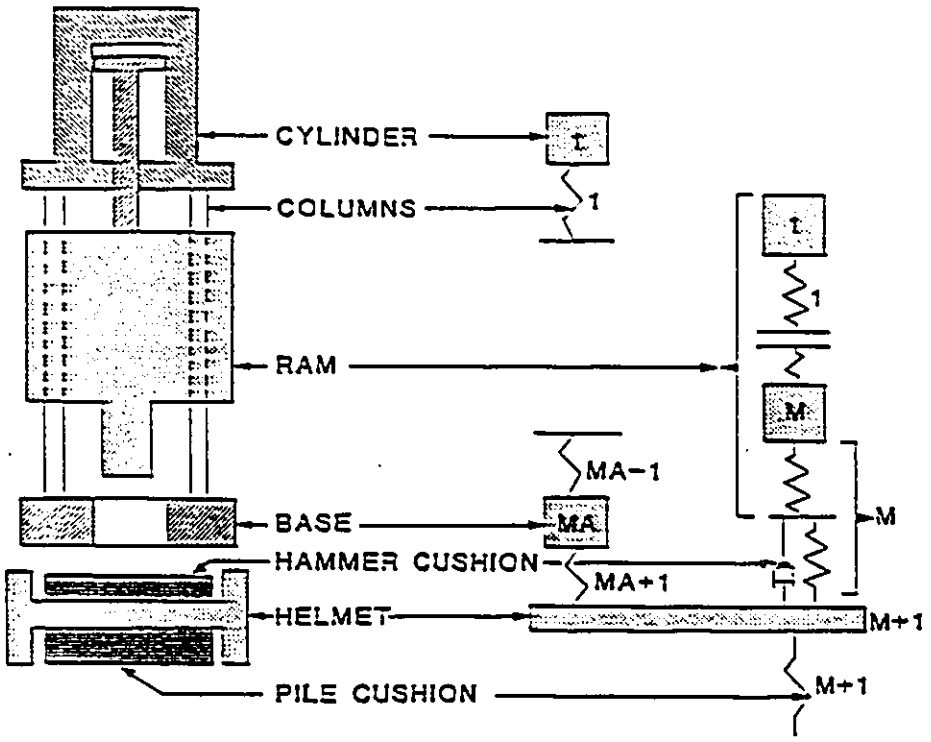

Fig. 2.12 WEAP hammer–driving system model for EHC hammers (after Goble and Rausche, 1986)

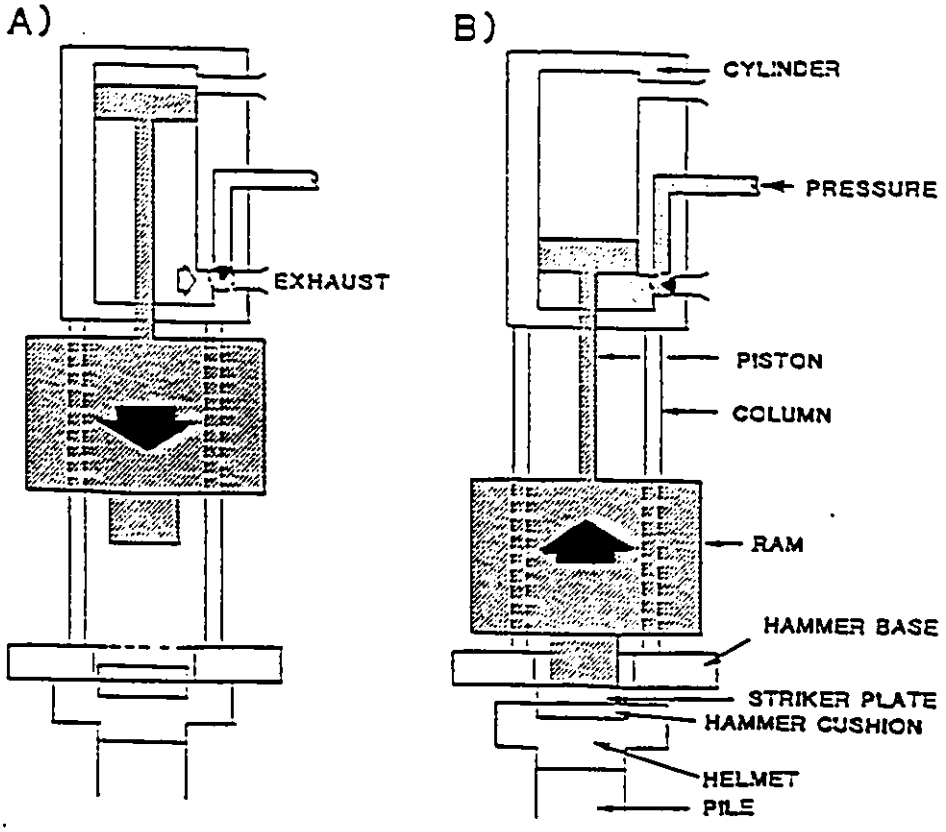

A) Exhaust valve is opened and ram falls.
B) Inlet valve is opened and ram is lifted back up.

Fig. 2.13 Working principle of a single acting air/steam hammer (after Goble and Rausche, 1986)

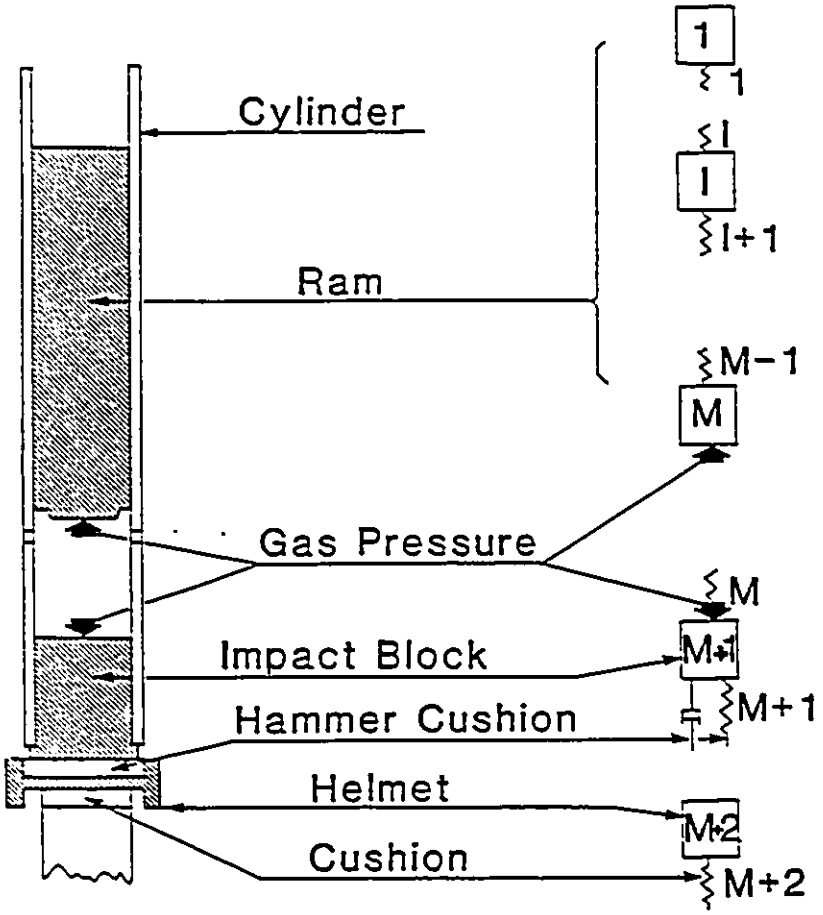

Fig. 2.14 WEAP model for an open end deisel hammer (after Goble and Rausche, 1986)

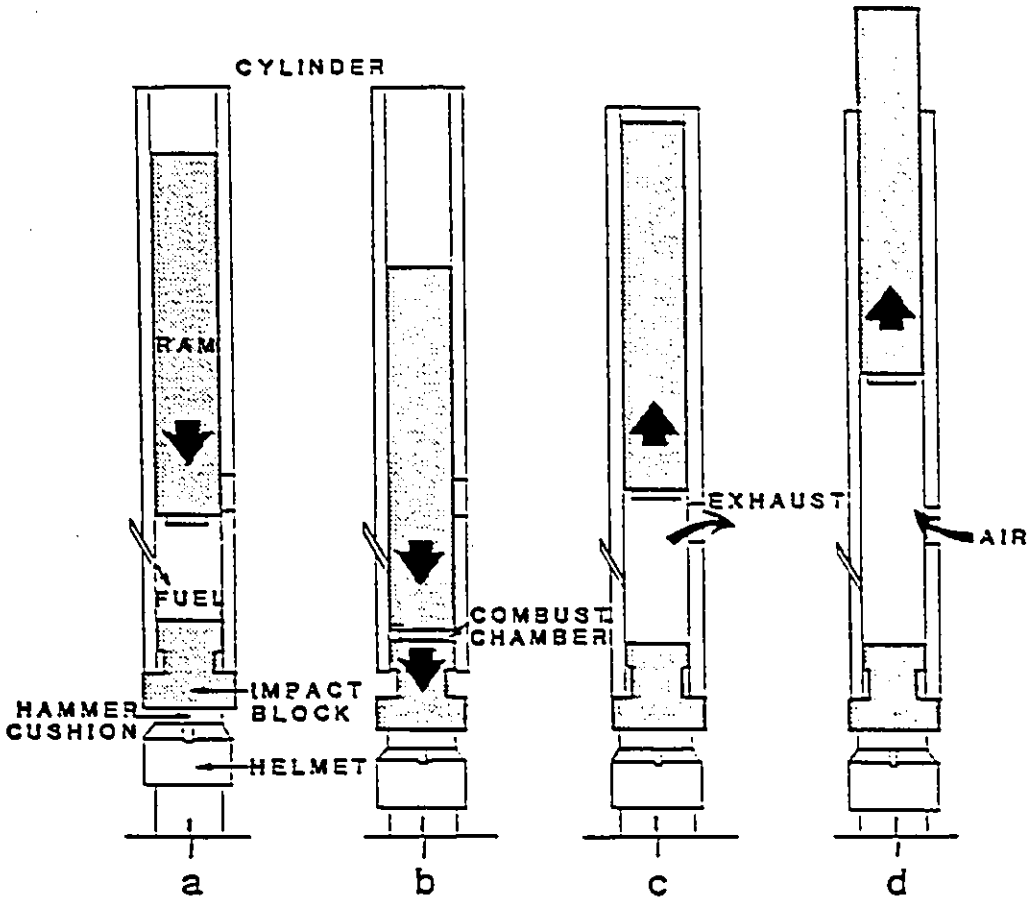

a) FREE FALL & FUEL INJECTION
b) IMPACT & IGNITION
c) EXHAUST
d) SCAVENGING

Fig. 2.15 Operation cycle for a diesel hammer (after Goble and Rausche, 1986)

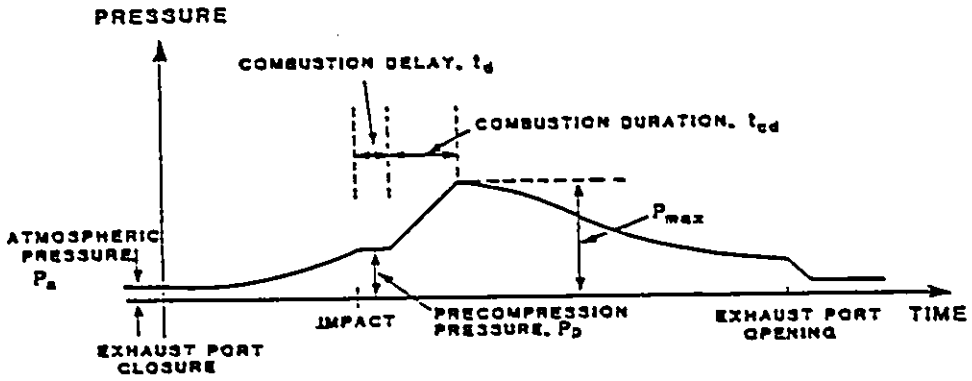

Pressure vs. time relationship for liquid fuel injection model.

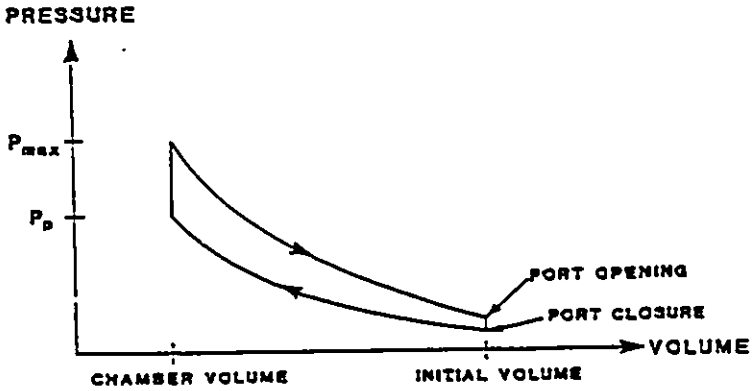

Pressure vs. volume relationship for liquid fuel injection model.

Fig. 2.16 WEAP liquid fuel injection model (after Goble and Rausche, 1986)

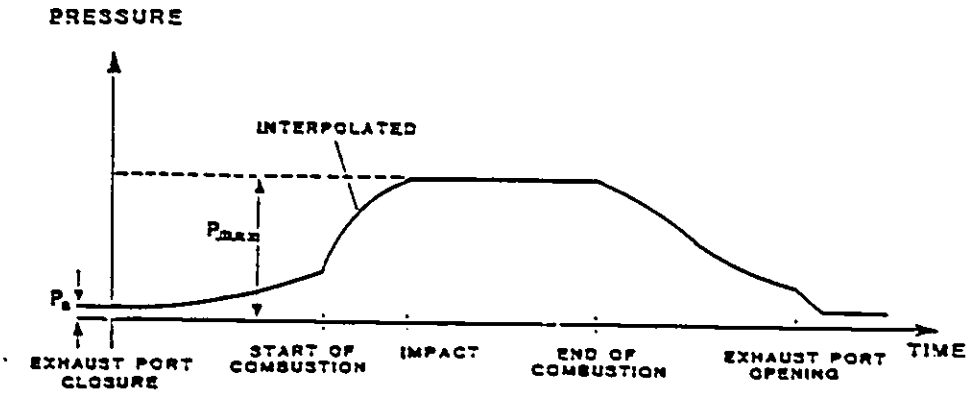

Pressure vs. time relationship for atomized injection model.

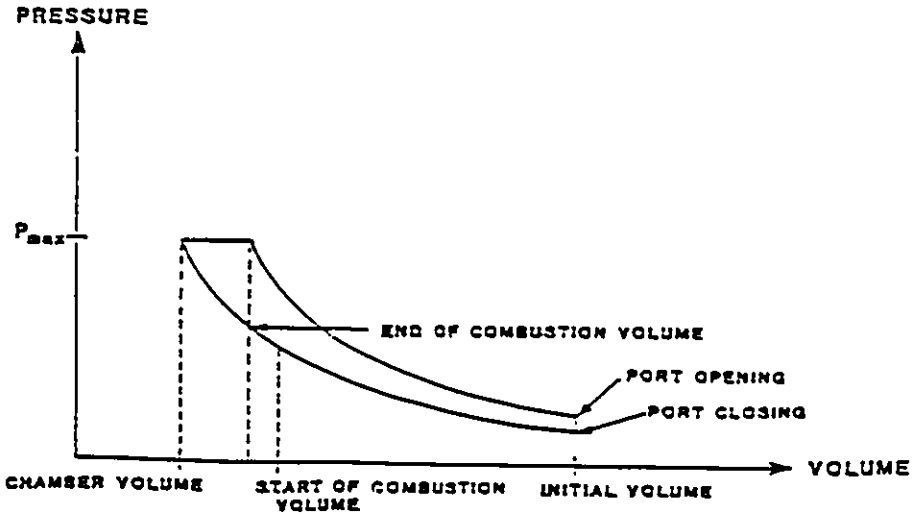

Pressure vs. volume relationship for atomized injection model.

Fig. 2.17 WEAP atomized injection model
(after Goble and Rausche, 1986)

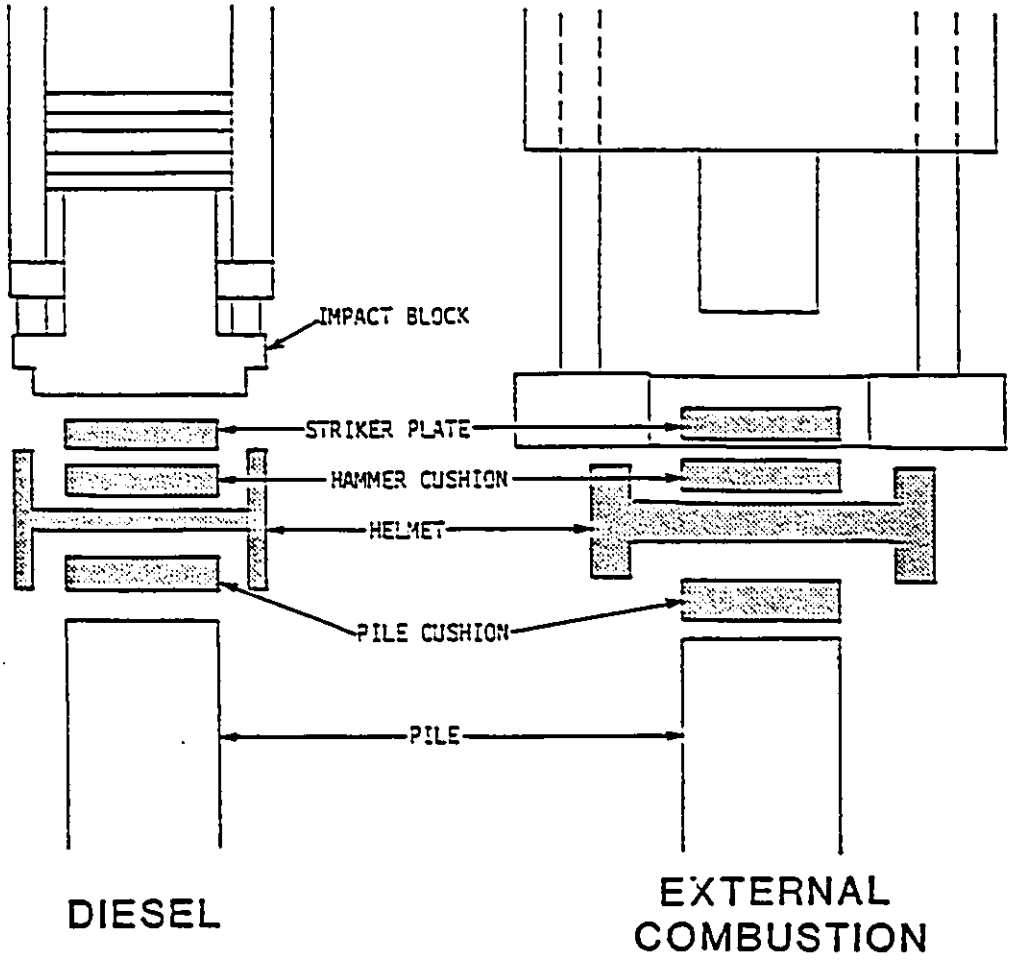

Fig. 2.18 Driving system components (after Goble and Rausche, 1986)

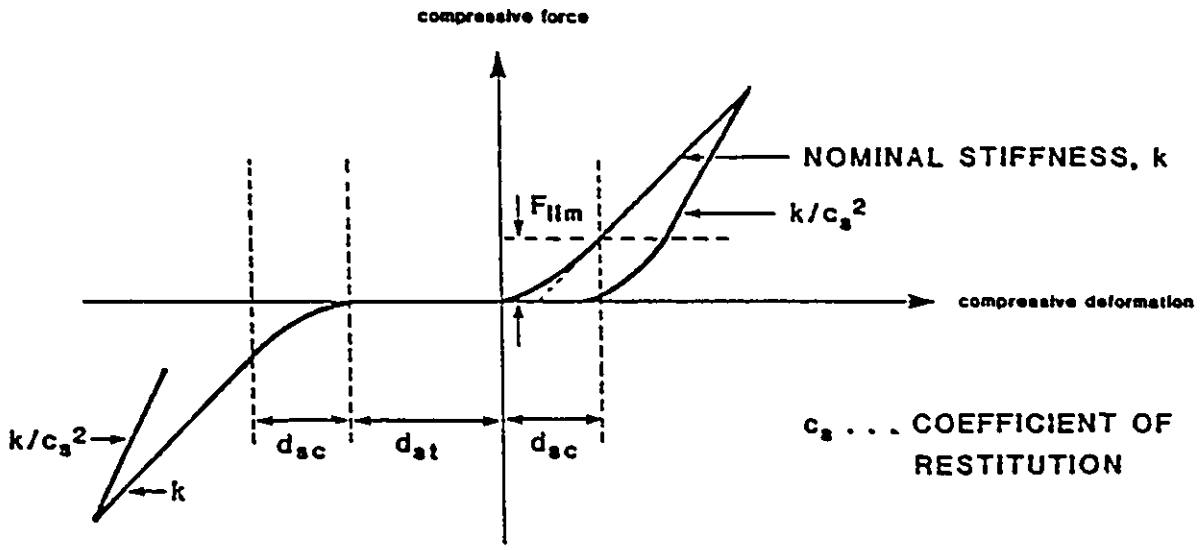

Fig. 2.19 WEAP force–deformation curves, hammer and pile cushions (after Goble and Rausche, 1986)

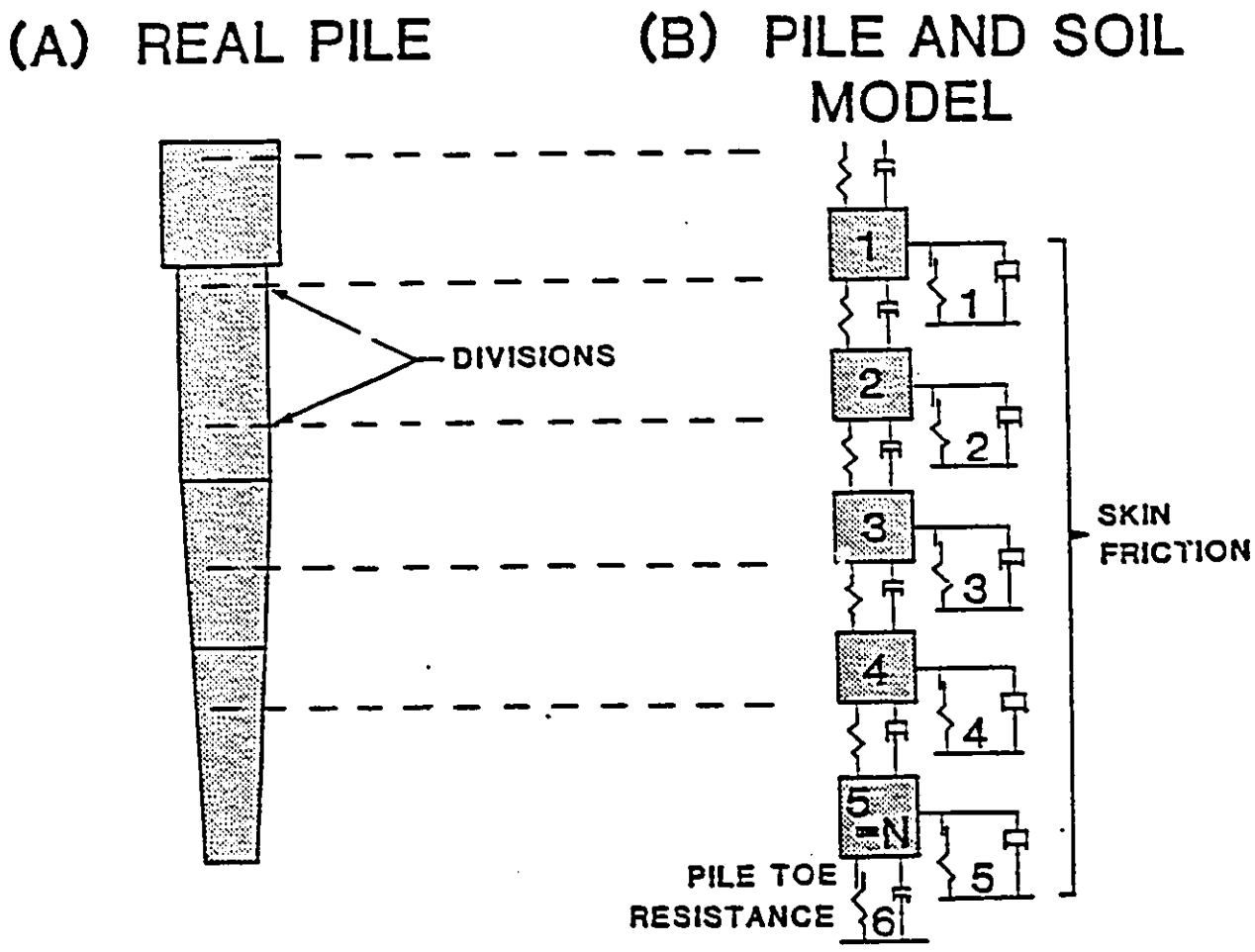

Fig. 2.20 WEAP pile and soil model (after Goble and Rausche, 1986)

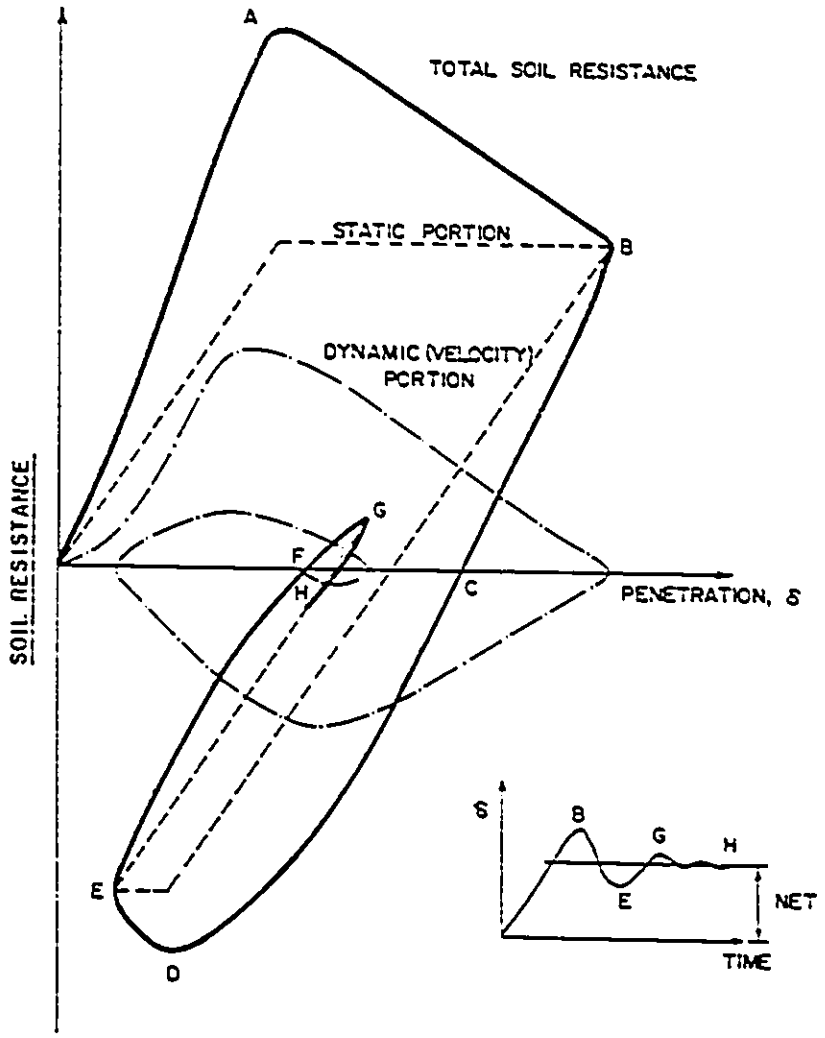

Fig. 2.21 Total, static, and dynamic soil resistance using case damping (after Authier and Fellenius, 1983)

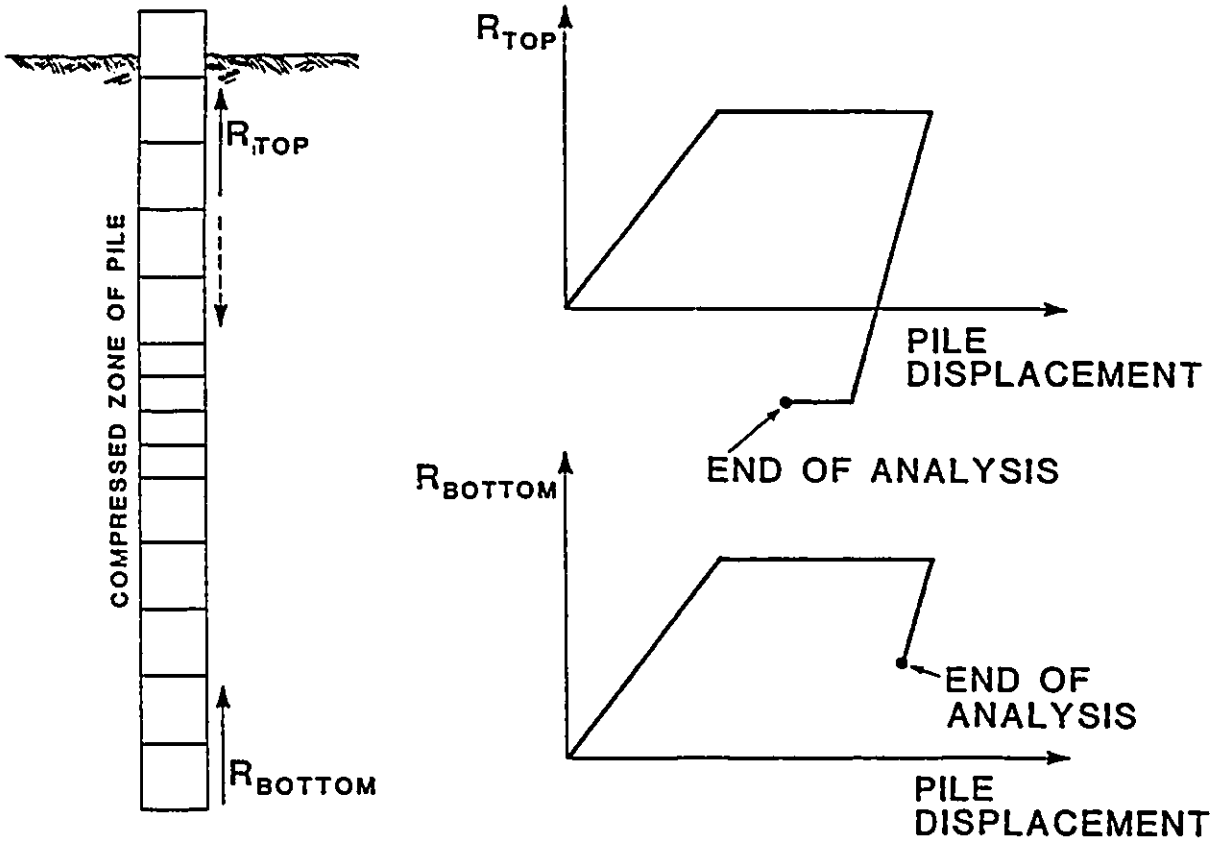

Fig. 2.22 Pile model in residual stress analysis (after Goble and Rausche, 1986)

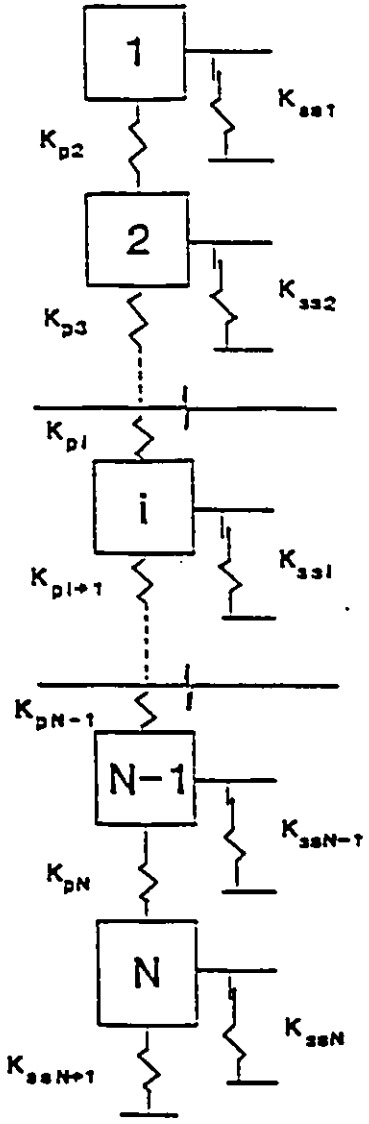

Fig. 2.23 WEAP static pile–soil model in residual stress analysis (after Goble and Rausche, 1986)

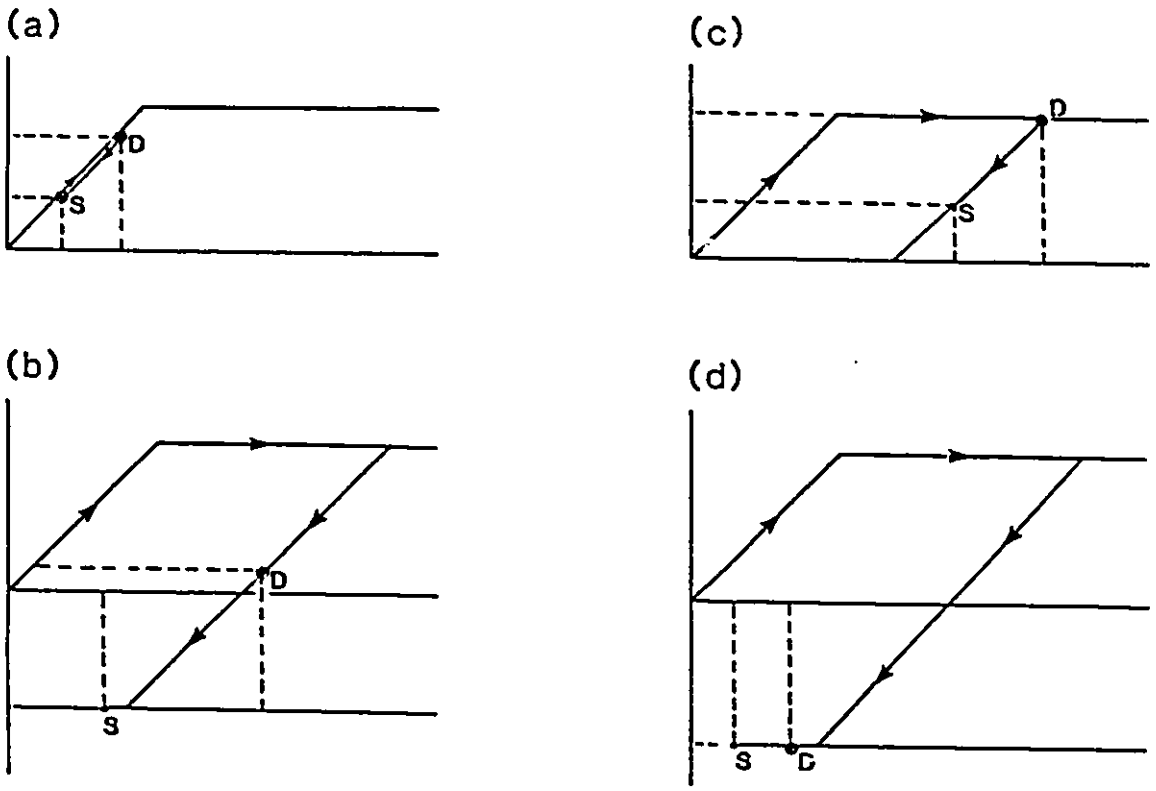

Fig. 2.24 WEAP resistance versus displacement diagram
(after Goble and Rausche, 1986)

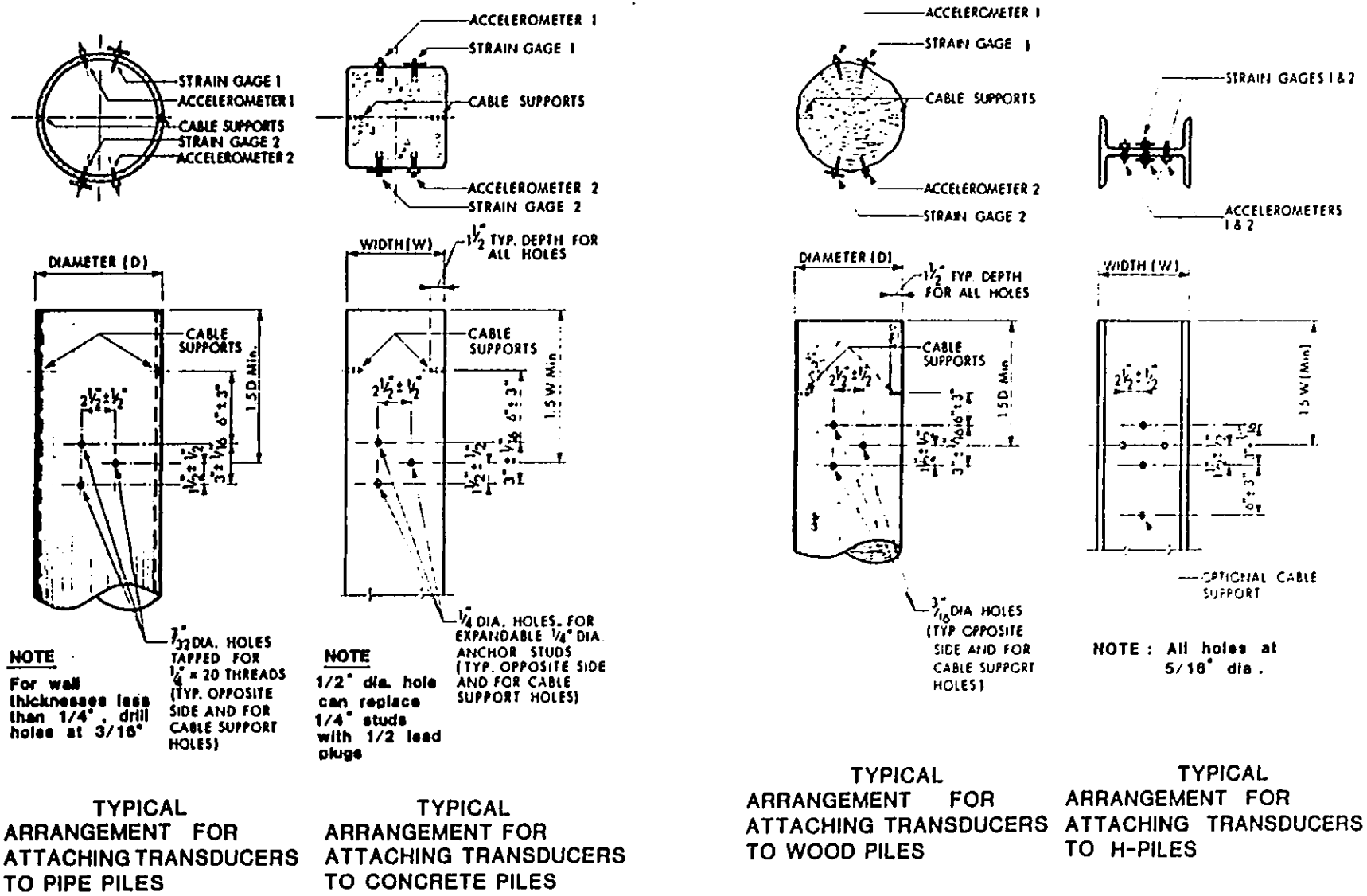

Fig. 2.25 Typical arrangement for attaching transducers (after ASTM D4945-89, 1989)

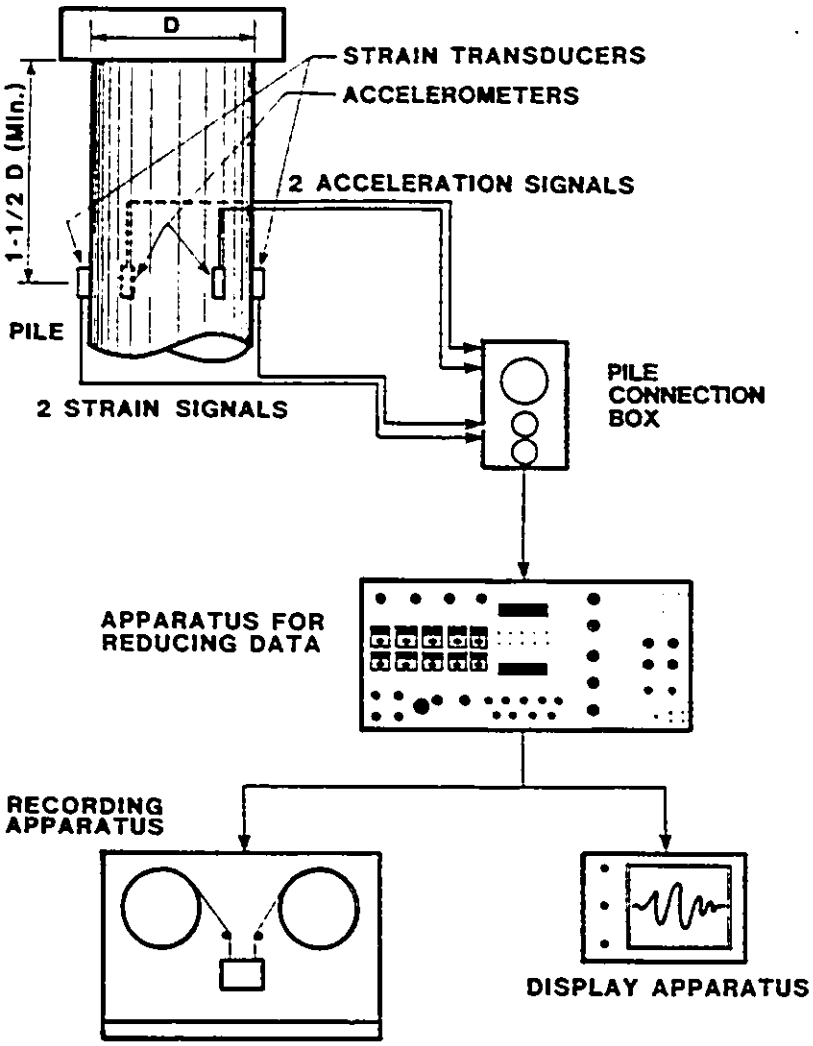

Fig. 2.26 Schematic diagram for apparatus for dynamic monitoring of piles (after ASTM D4945–89, 1989)

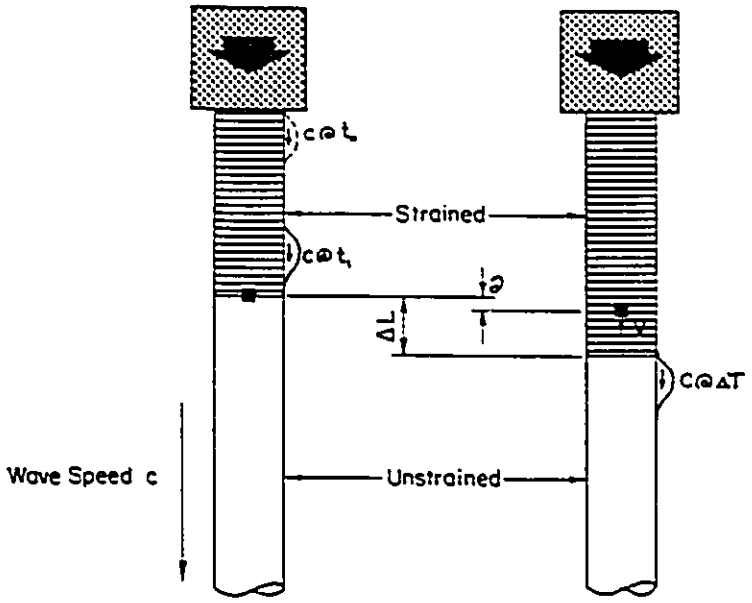

$$\Delta L = C\Delta T$$

$$\varepsilon = \frac{\partial}{\Delta L} = \frac{\partial}{C\Delta T}$$

$$\frac{\partial}{\Delta T} = V \quad \text{(particle velocity)}$$

$$\varepsilon = \frac{V}{C}$$

$$\varepsilon E = \sigma = \frac{VE}{C}$$

$$\varepsilon EA = F = \frac{VEA}{C}$$

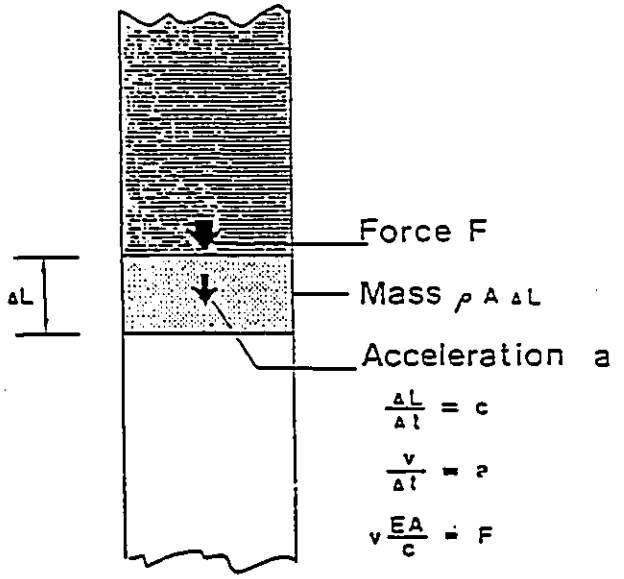

$$\frac{\Delta L}{\Delta t} = c$$

$$\frac{v}{\Delta t} = a$$

$$v\frac{EA}{C} = F$$

Force = (Mass)(Acceleration)

$$v\frac{EA}{C} = \rho A \Delta L \frac{v}{\Delta t}$$

$$\boxed{C^2 = \frac{E}{\rho}}$$

Fig. 2.27 Wave speed derivation (after Rausche, 1981)

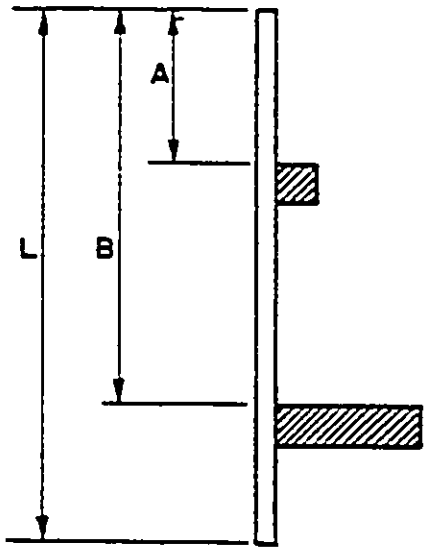

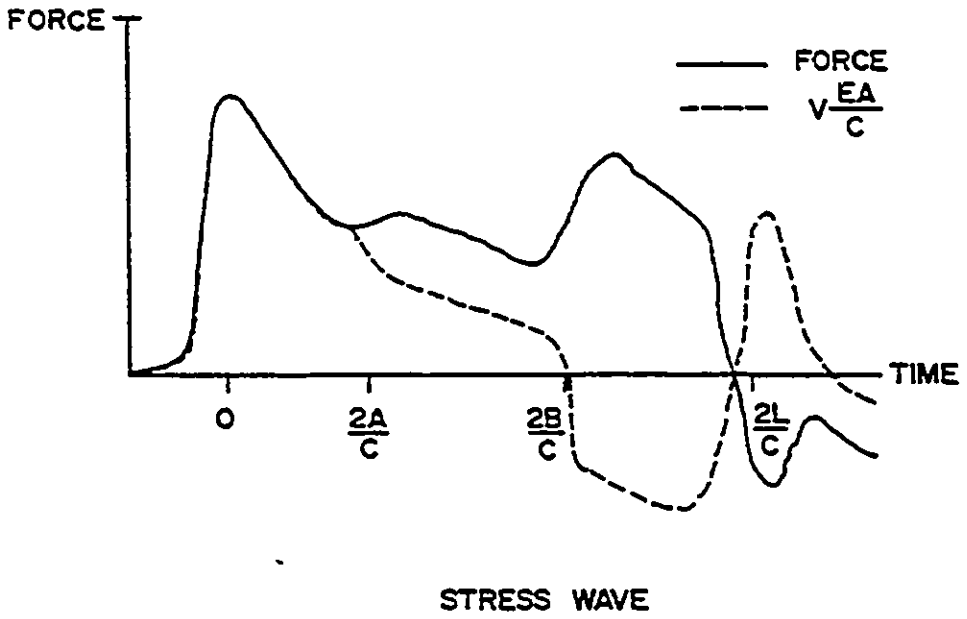

Fig. 2.28 Effects of soil resistance on force and VEA/c (after Likins and Hussein, 1988)

RSP

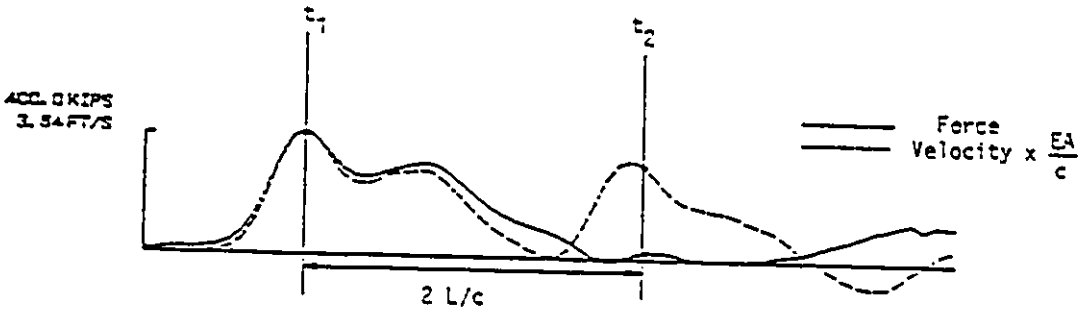

$F(t_1) = F1 = 415$ kips

$F(t_2) = F2 = 70$ kips

$V(t_1) = V1 = 415$ kips

$V(t_2) = V2 = 350$ kips

$RTL = 1/2\ (F1 + F2 + V1 - V2)$

$= 1/2\ (415 + 70 + 415 - 380)$

$= 275$ kips

$RS1 = RTL - J\ (V1 + F1 - RTL)$

$= 275 - 0.3\ (415 + 415 - 275)$

$= 108$ kips

Fig. 2.29 CMES computation for RSP method (after Likins and Hussein, 1988)

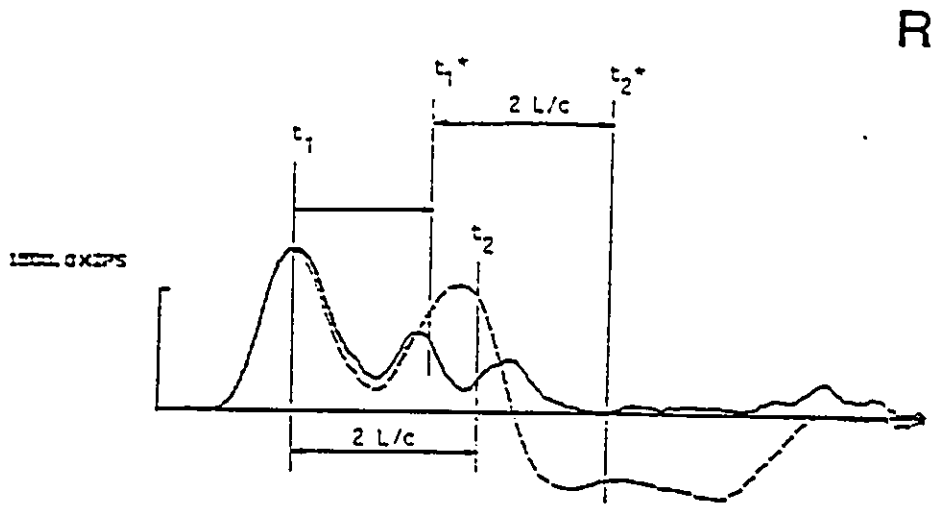

$F1 = 2045$ kips $\quad F2 = 405 \quad V1 = 2045$ kips $\quad V2 = 1427$

$F1^* = 878$ kips $\quad F2^* = 0$ kips $\quad V1^* = 1244$ kips $\quad V2^* = 842$ kips

$$RTL^* = 1/2\ (F1^* + F2^* + V1^* - V2^*)$$
$$= 1/2\ (878 + 0 + 1244 + 842)$$
$$= 1482 \text{ kips}$$

$$RSi^* = RMX = RTL^* - J\ (V1^* + F1^* - RTL^*)$$
$$= 1482 - 0.3\ (1244 + 878 - 1482)$$
$$= 1290 \text{ kips}$$

For Comparison:

$$RTL = 1/2\ (F1 + F2 + V1 - V2)$$
$$= 1/2\ (2045 + 405 + 2045 - 1427)$$
$$= 1534$$

$$RS1 = RTL - J\ (V1 + F1 - RTL)$$
$$= 1534 - .3\ (2045 + 2045 - 1534)$$
$$= 767 \text{ kips}$$

Fig. 2.30 CMES computation for RMX method (after Likins and Hussein, 1988)

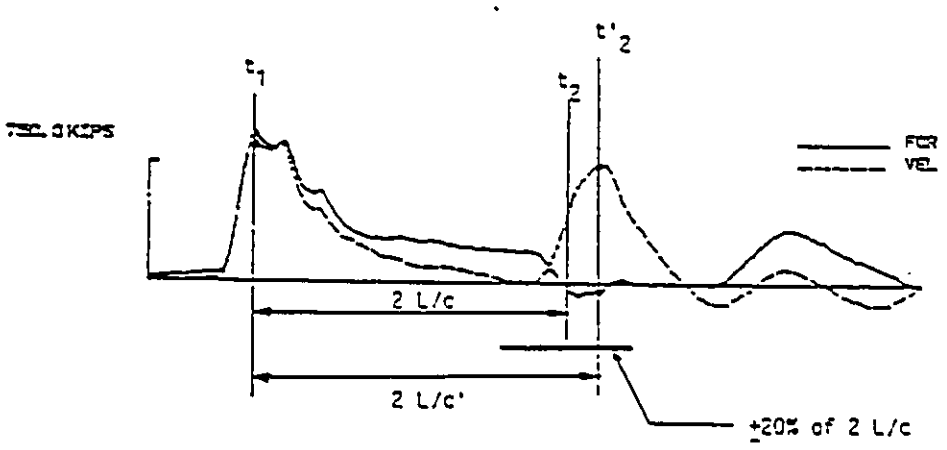

F1 = 937 kips V1 = 892 kips F2' = -60 kips V2' = 750 kips

RTL' = 1/2 (F1 + F2 + V1' - V2')

= 1/2 (937 - 60 + 892 - 750)

= 509.5 kips

assume J = 0.2

RS1' = RMN = RTL' - J (F1 + V1 - RTL')

= 509.5 - 0.2 (937 + 892 - 509.5)

= 246 kips

Fig. 2.31 CMES computation for RMN method (after Likins and Hussein, 1988)

RUN

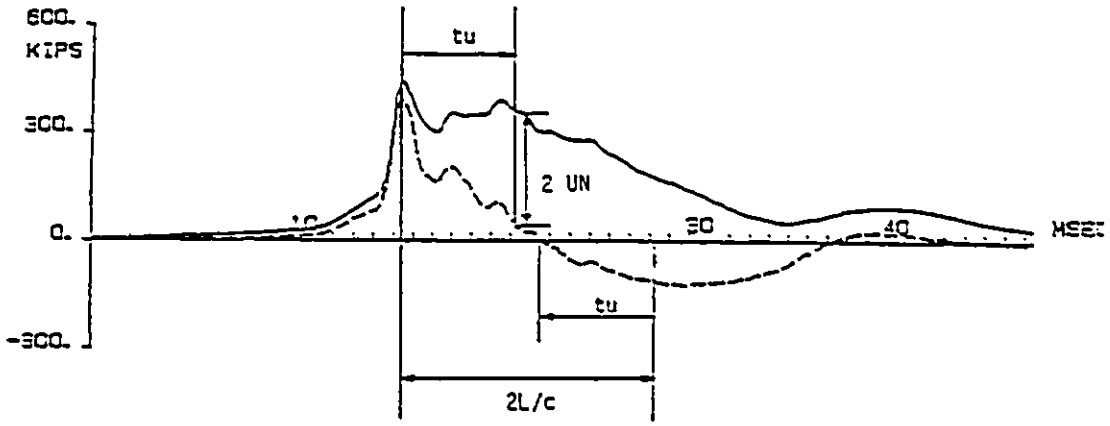

F1 = 450 kips F2 = 183 kips V1 = 400 kips V2 = 117 kips 2UN = 317 kips

RTL = 1/2 (F1 + F2 + V1 - V2)

= 1/2 (450 + 183 + 400 + 117)

= 575 kips

RSU = RTL + UN - J (2F1 - RTL - UN)

= 575 + 158.5 - 0.5 (2 x 450 - 575 - 158.5)

= 650.25 kips

For Comparison:

RS1 = RTL - J (V1 + F1 - RTL)

= 575 - 0.5 (400 + 450 - 575)

= 437.5 kips

Fig. 2.32 CMES computation for RSU method (after Likins and Hussein, 1988)

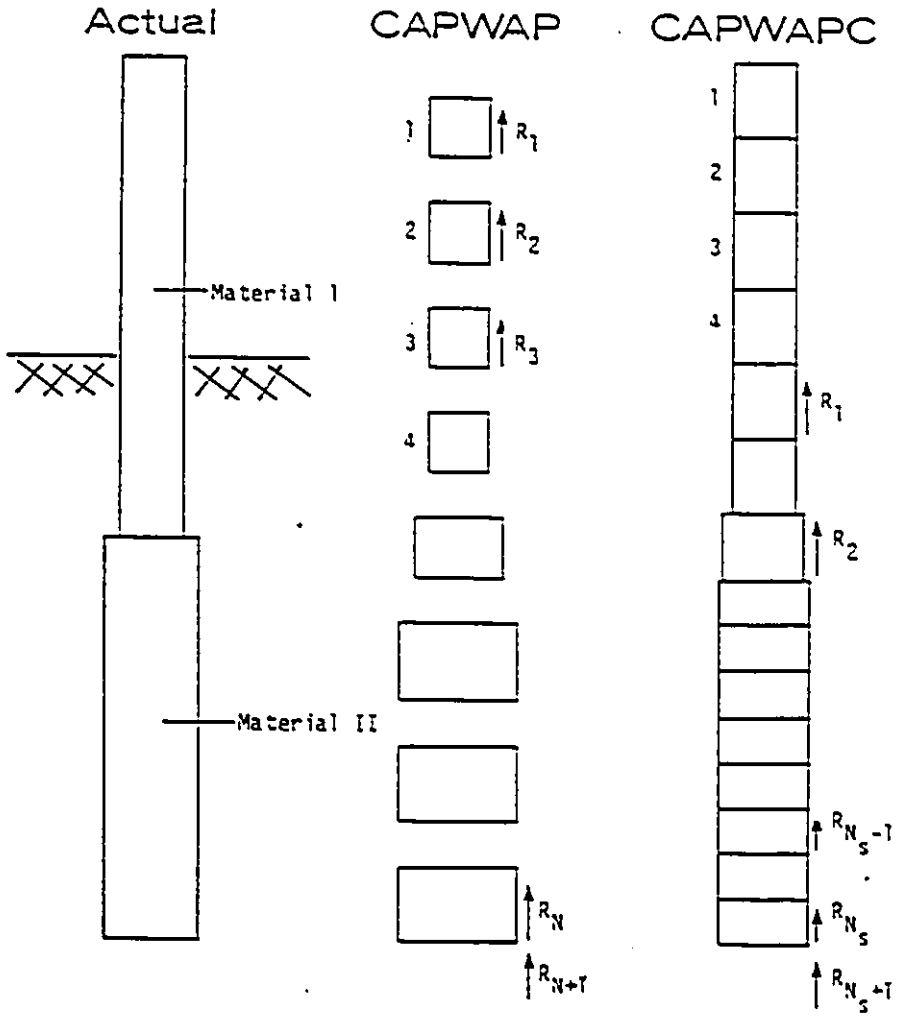

Fig. 2.33 Comparison of Smith and continuous pile model (after CAPWAPC manual, 1989)

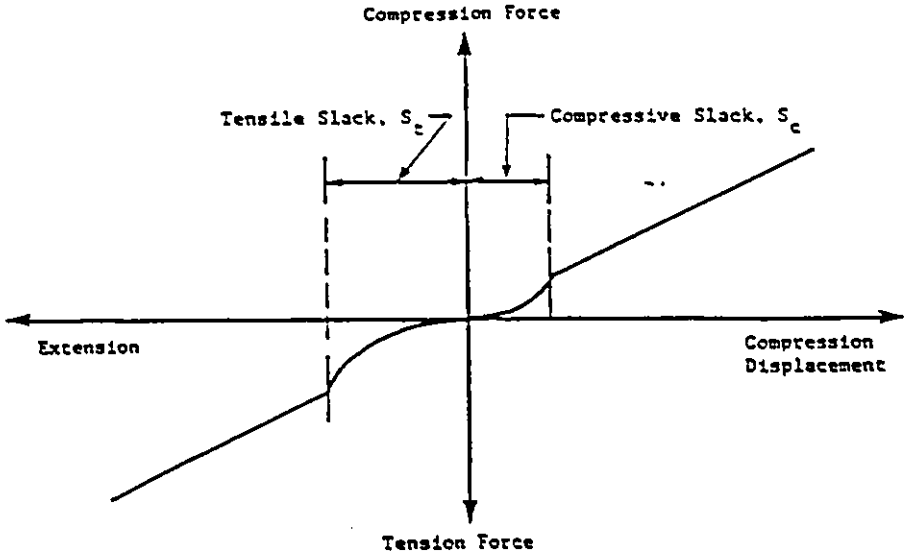

Fig. 2.34 Slack model (after CAPWAPC manual, 1989)

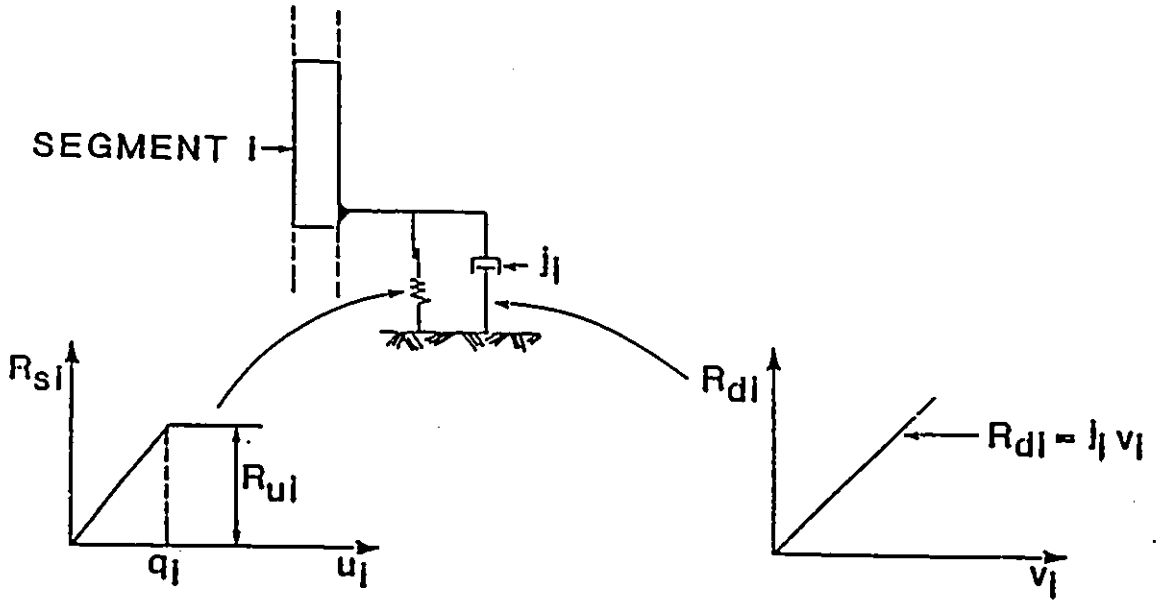

Fig. 2.35 Comparison of Smith soil model (left) and CAPWAPC viscous damping model (right) (after CAPWAPC manual, 1989)

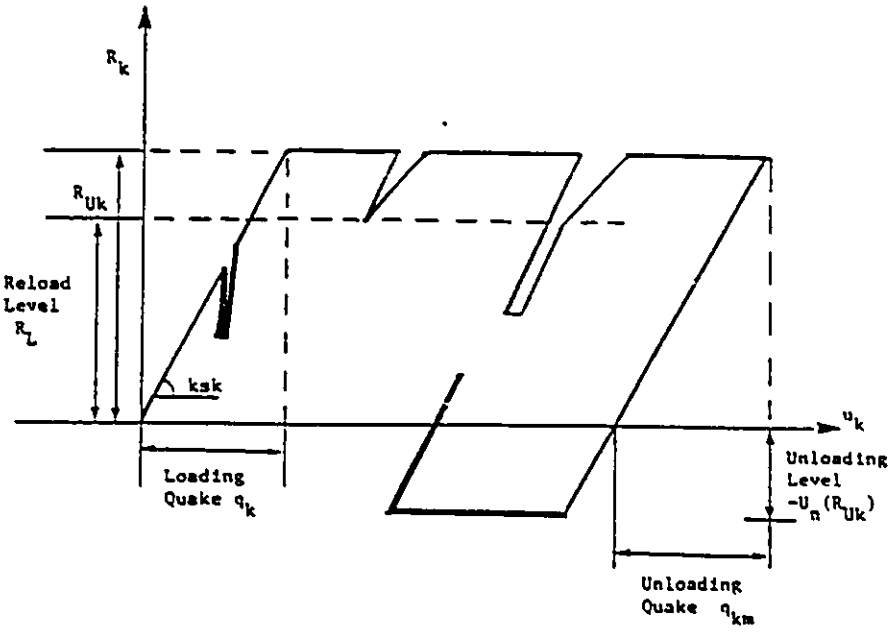

Fig. 2.36 Static shaft resistance (after CAPWAPC manual, 1989)

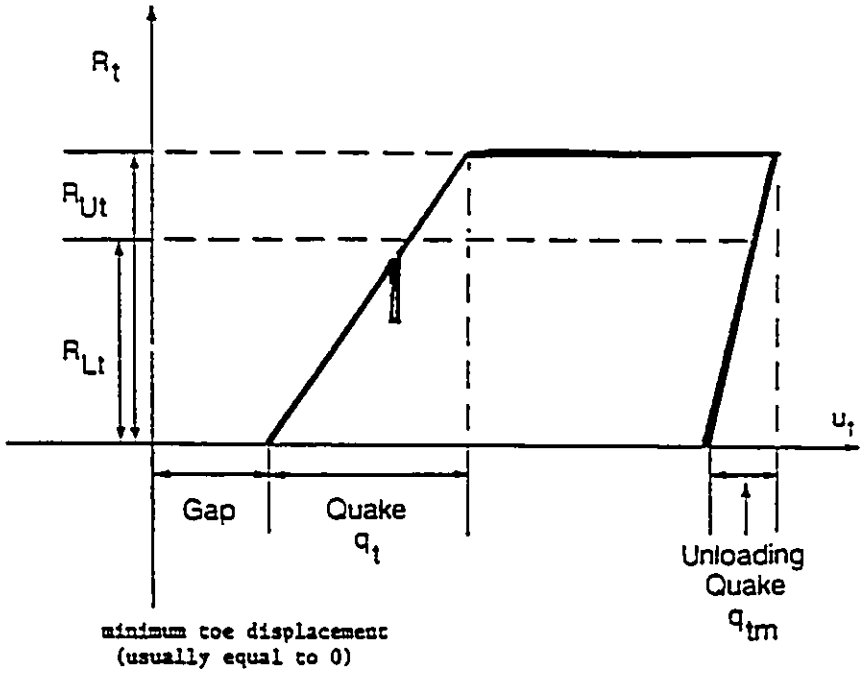

Fig. 2.37 Static toe resistance (after CAPWAPC manual, 1989)

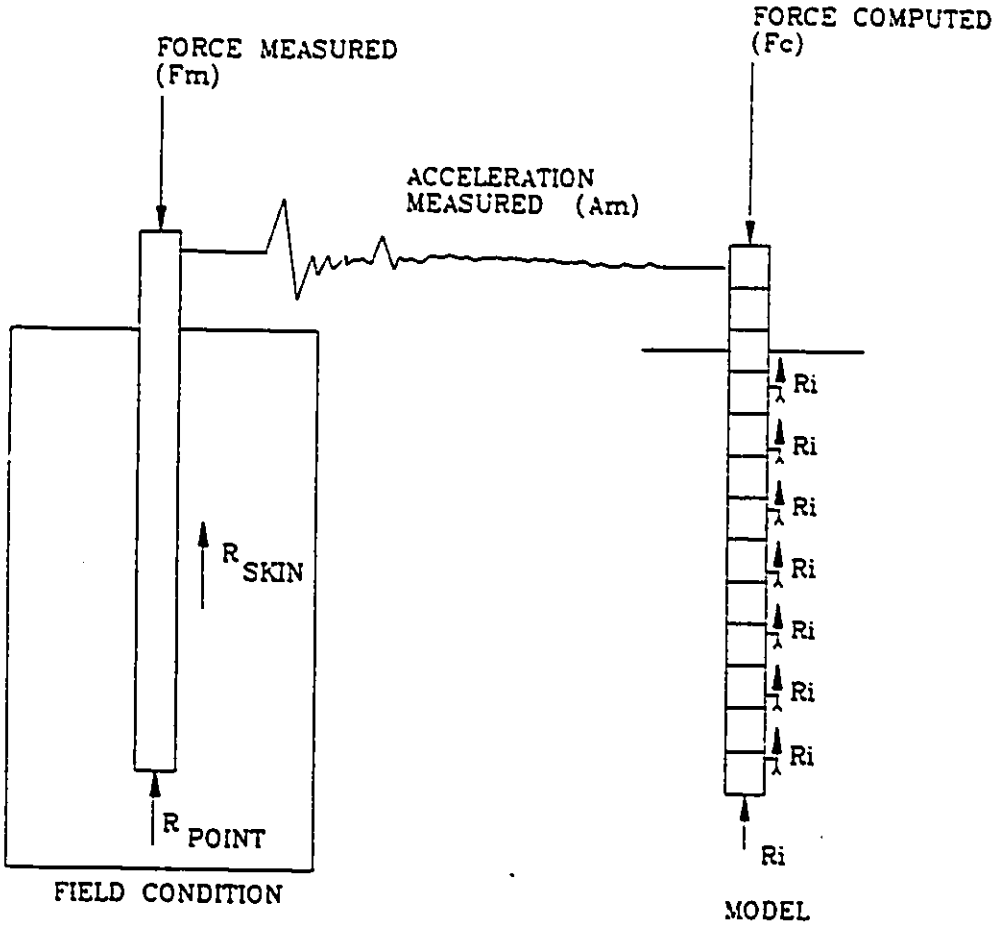

1. MEASURE Fm, Am
2. COMPUTE Fc = Fc(Am, Ri)
3. COMPARE Fm — Fc
4. CORRECT Ri
5. ITERATE (GO TO 2.)

Fig. 2.38 CAPWAPC simulation and iteration procedure (after Hanningan, 1990)

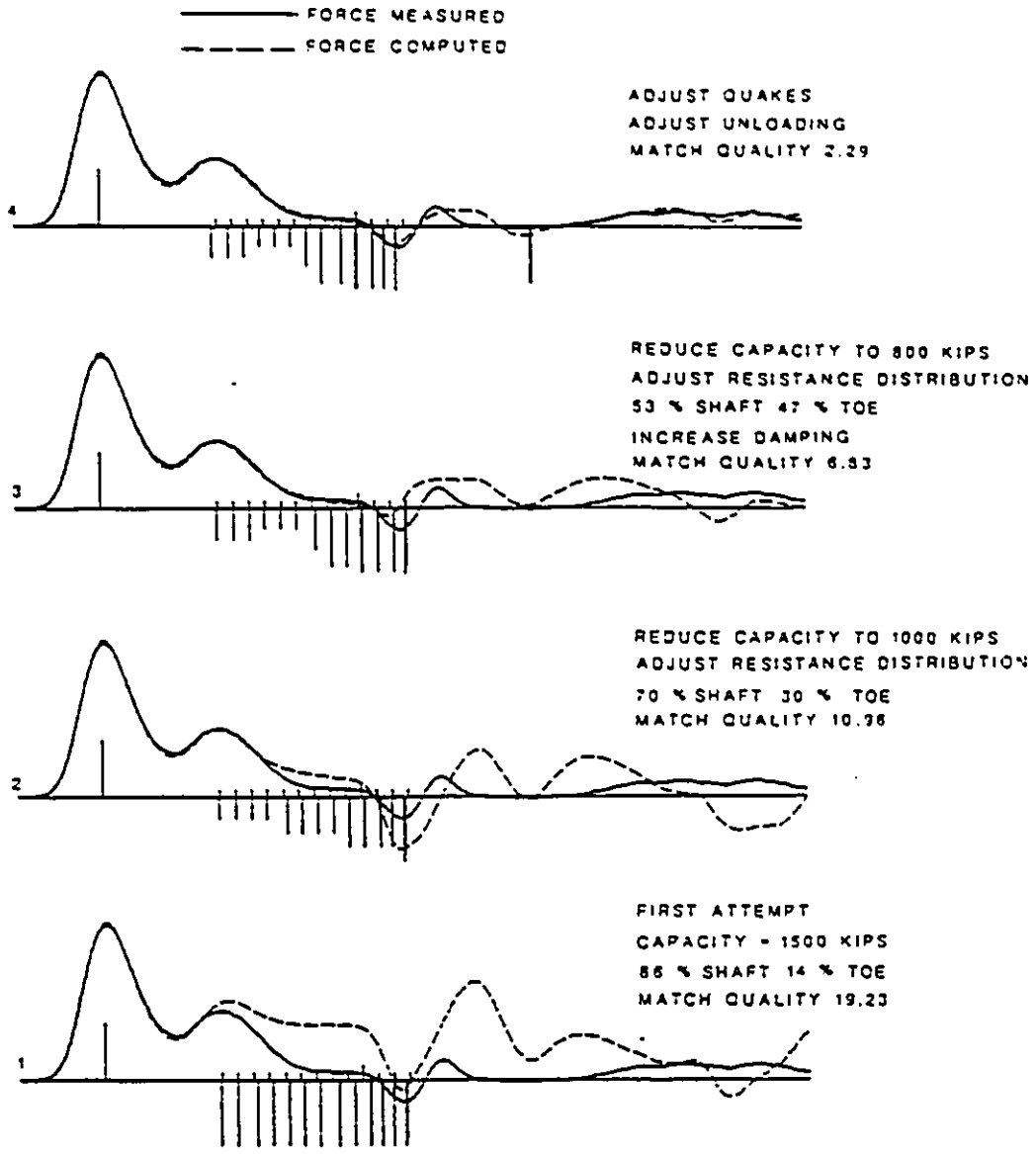

Fig. 2.39 CAPWAPC wave matching procedure (after CAPWAPC manual, 1989)

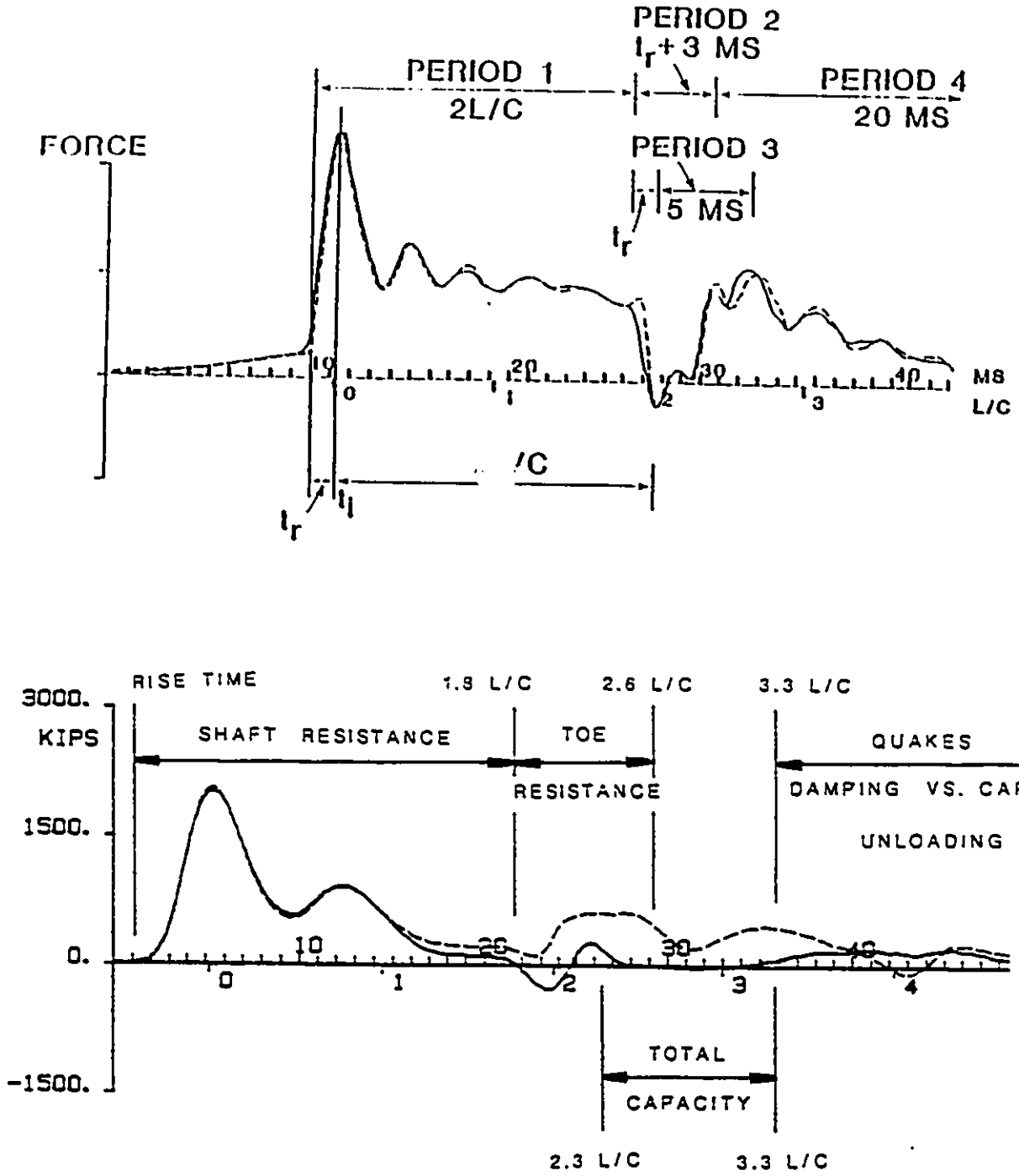

Fig. 2.40 CAPWAPC wave matching intervals (after CAPWAPC manual, 1989)

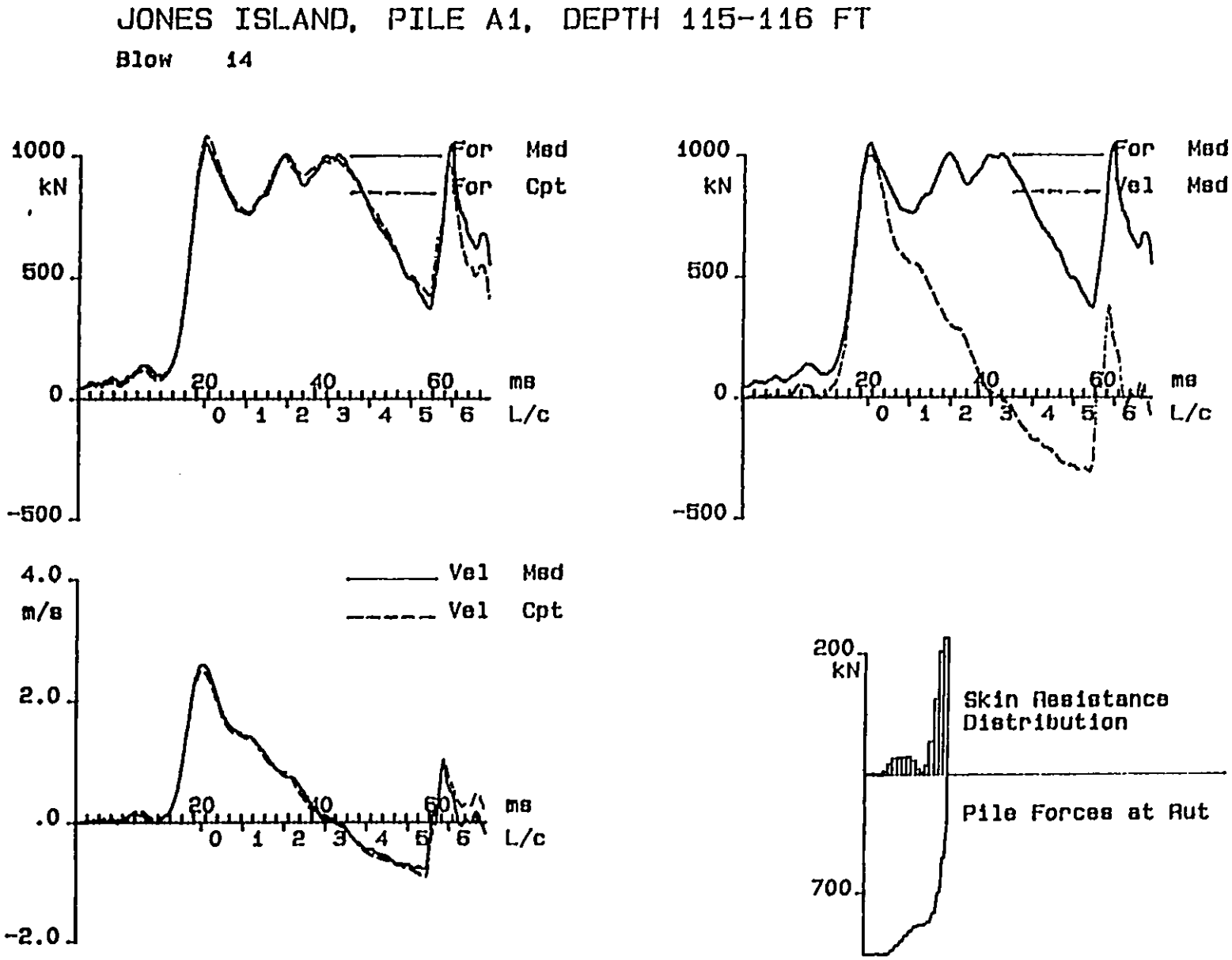

Fig. 2.41 Graphical output of CAPWAPC results

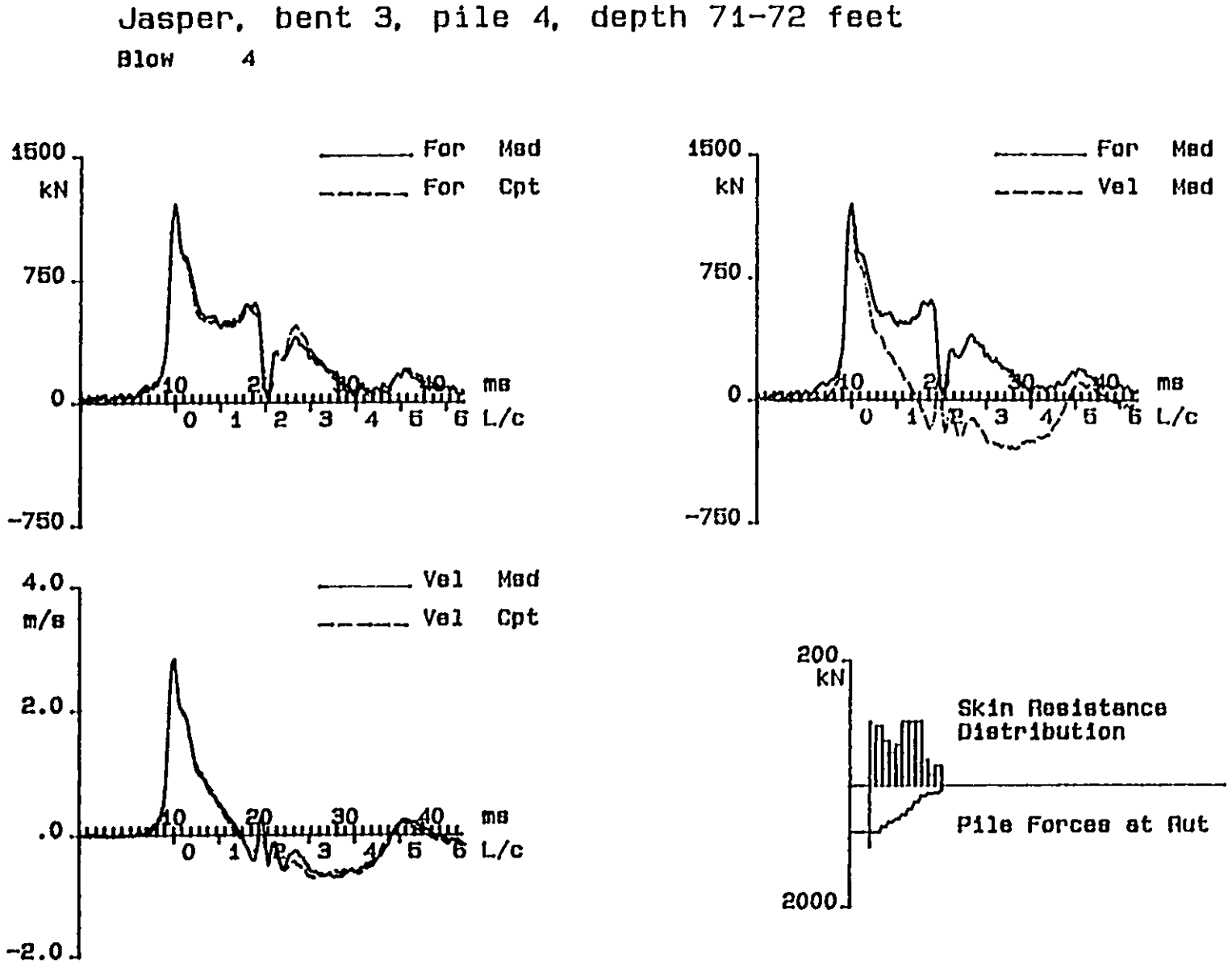

Fig. 2.42 Graphical output of CAPWAPC results

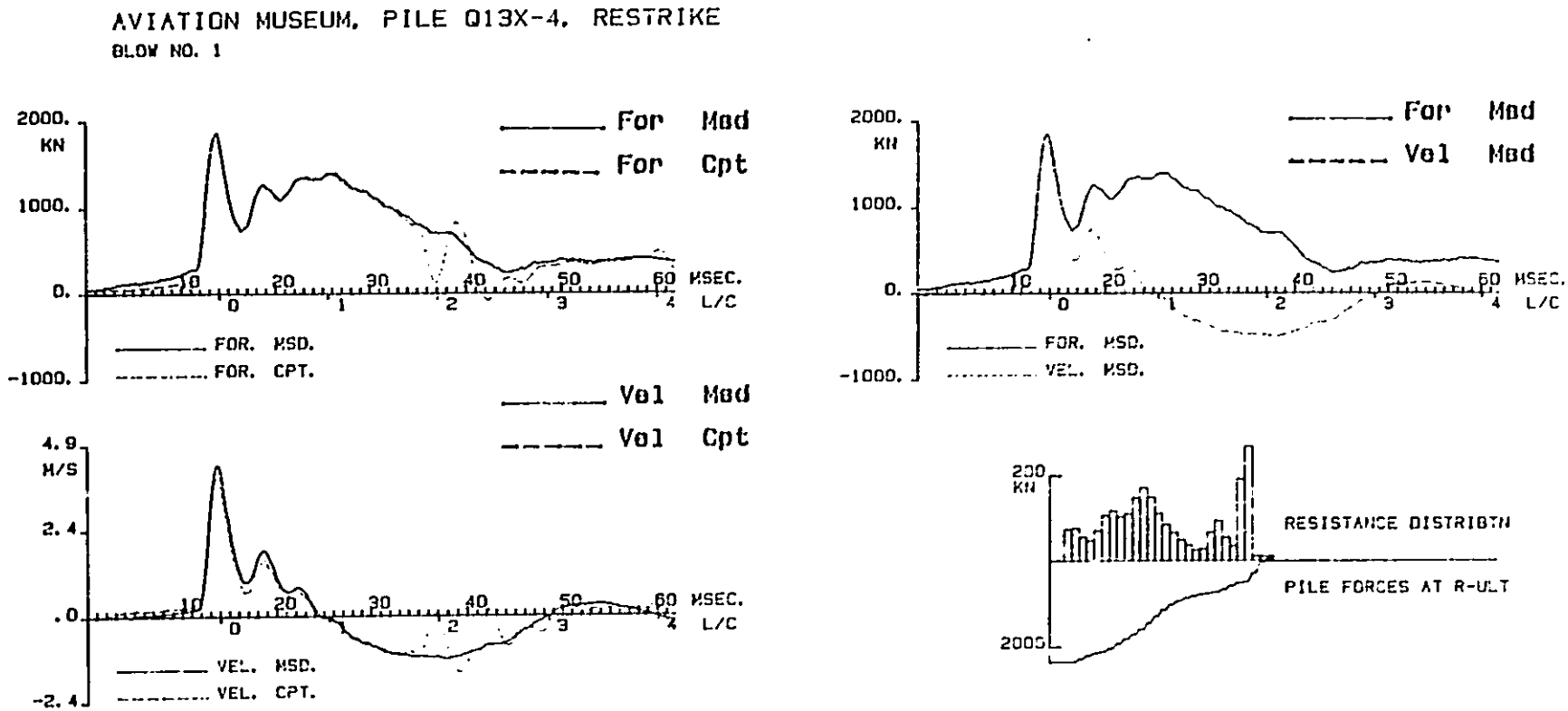

Fig. 2.43 Graphical output of CAPWAPC results

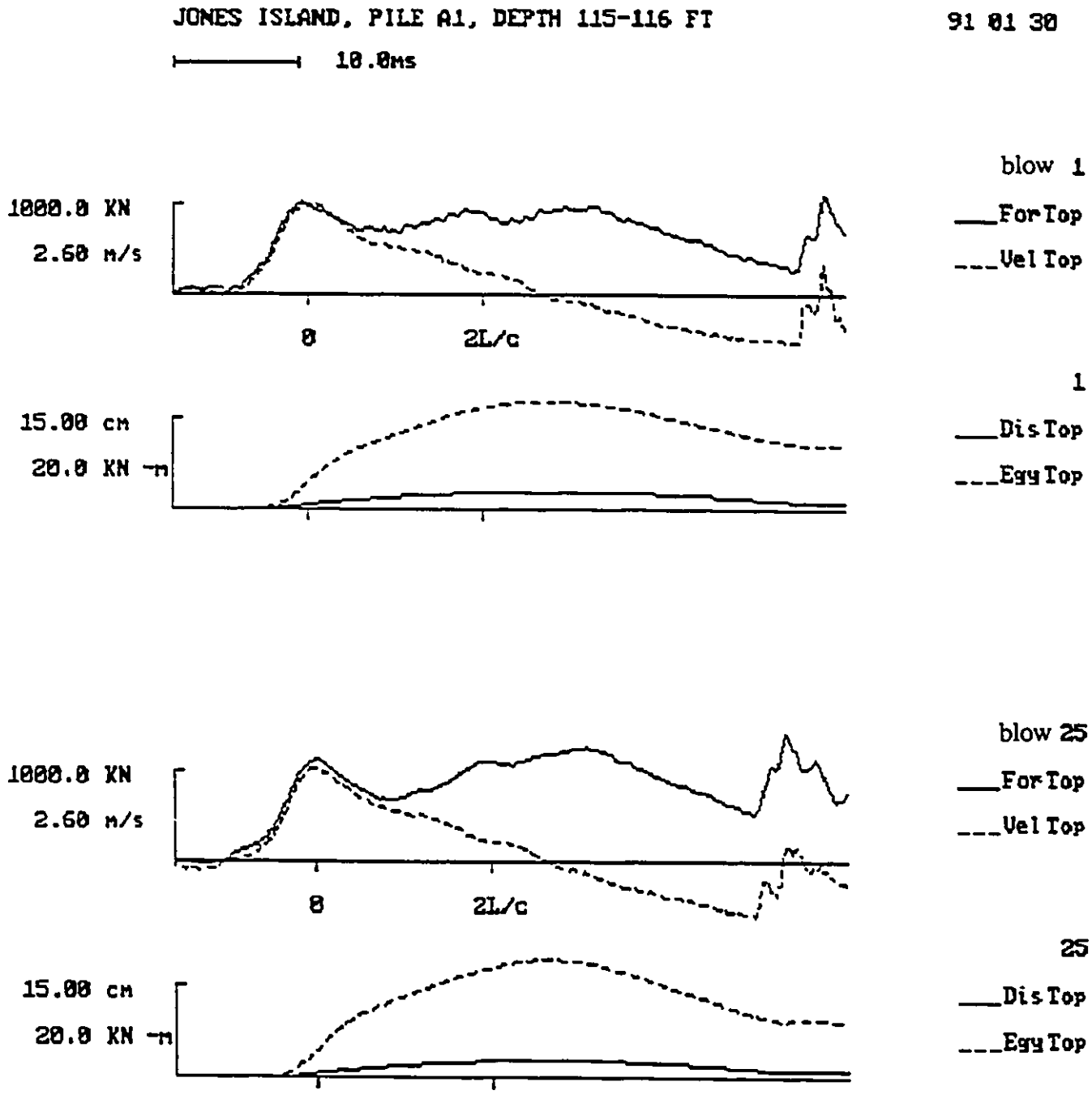

Fig. 3.1 Dynamic measurement records

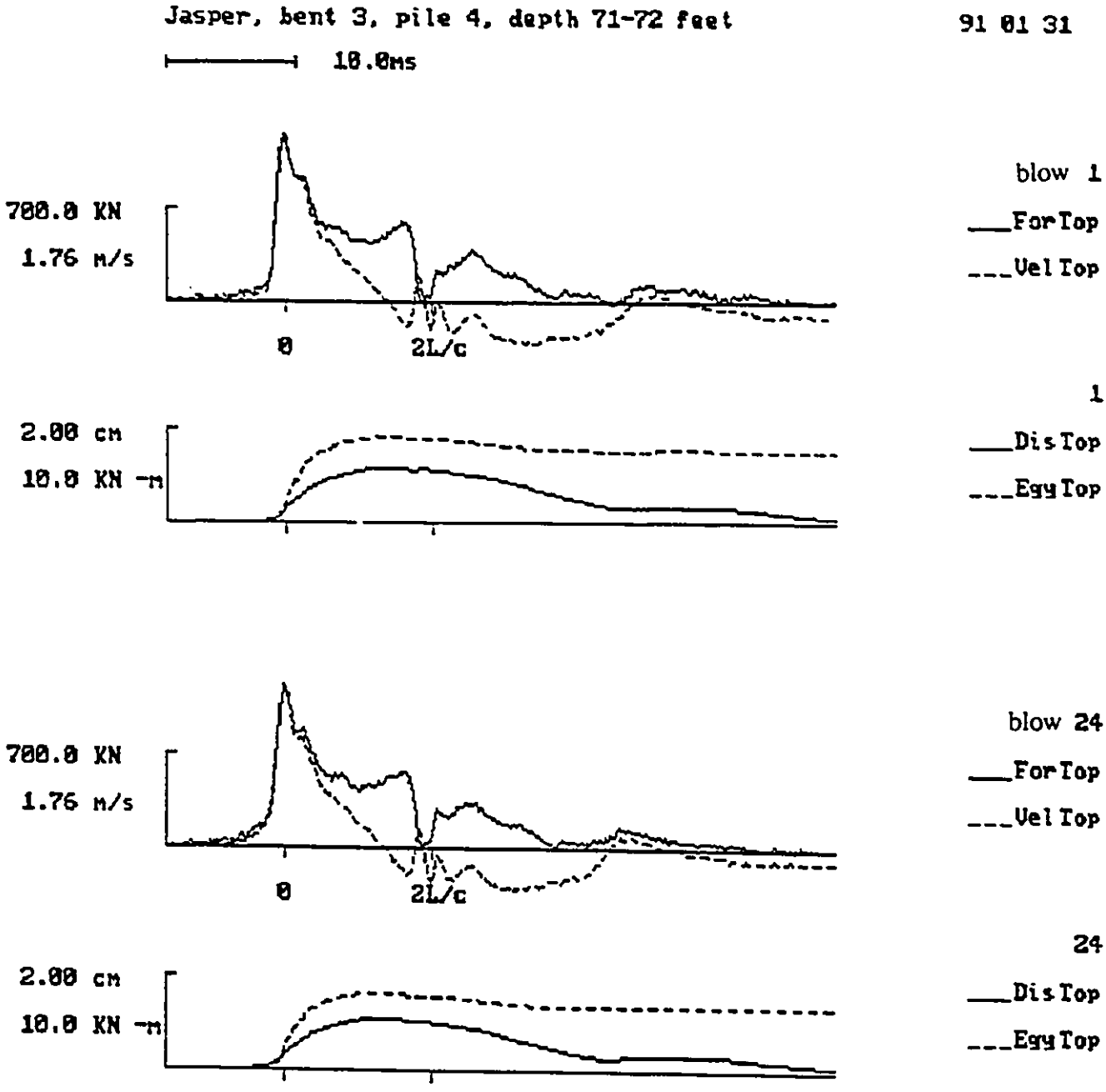

Fig. 3.2 Dynamic measurement records

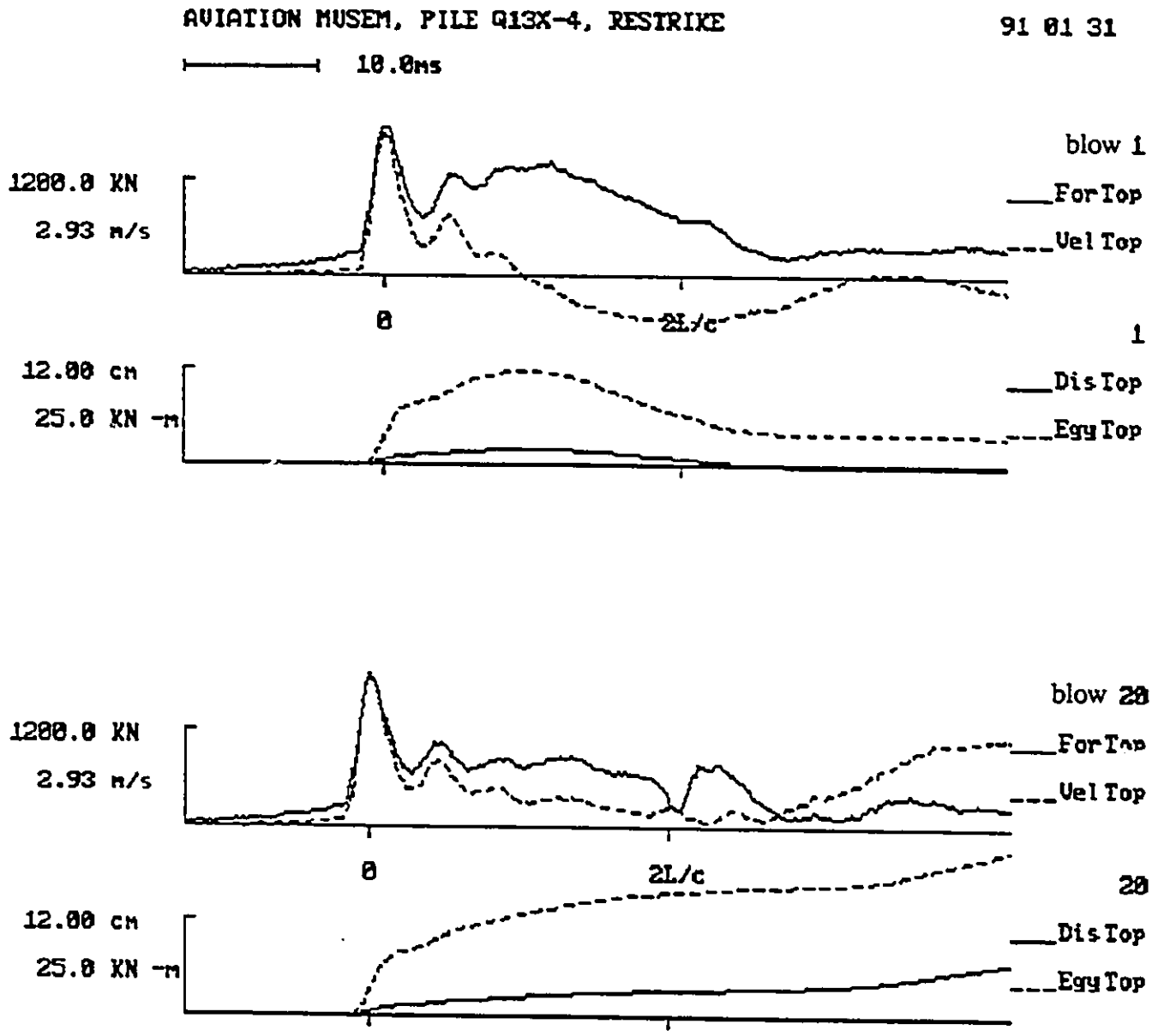

Fig. 3.3 Dynamic measurement records

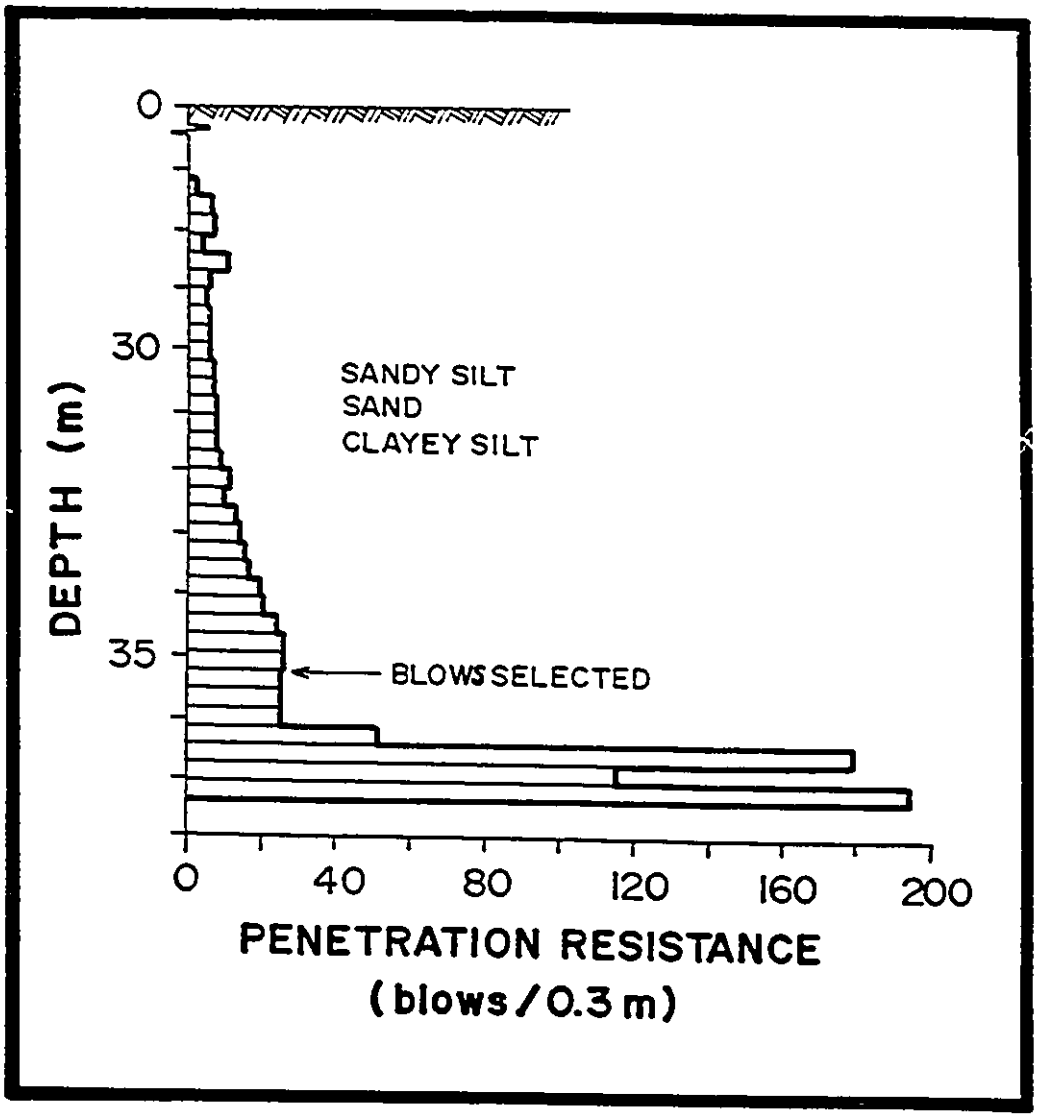

Fig. 3.4 Driving log diagram, Jones Island

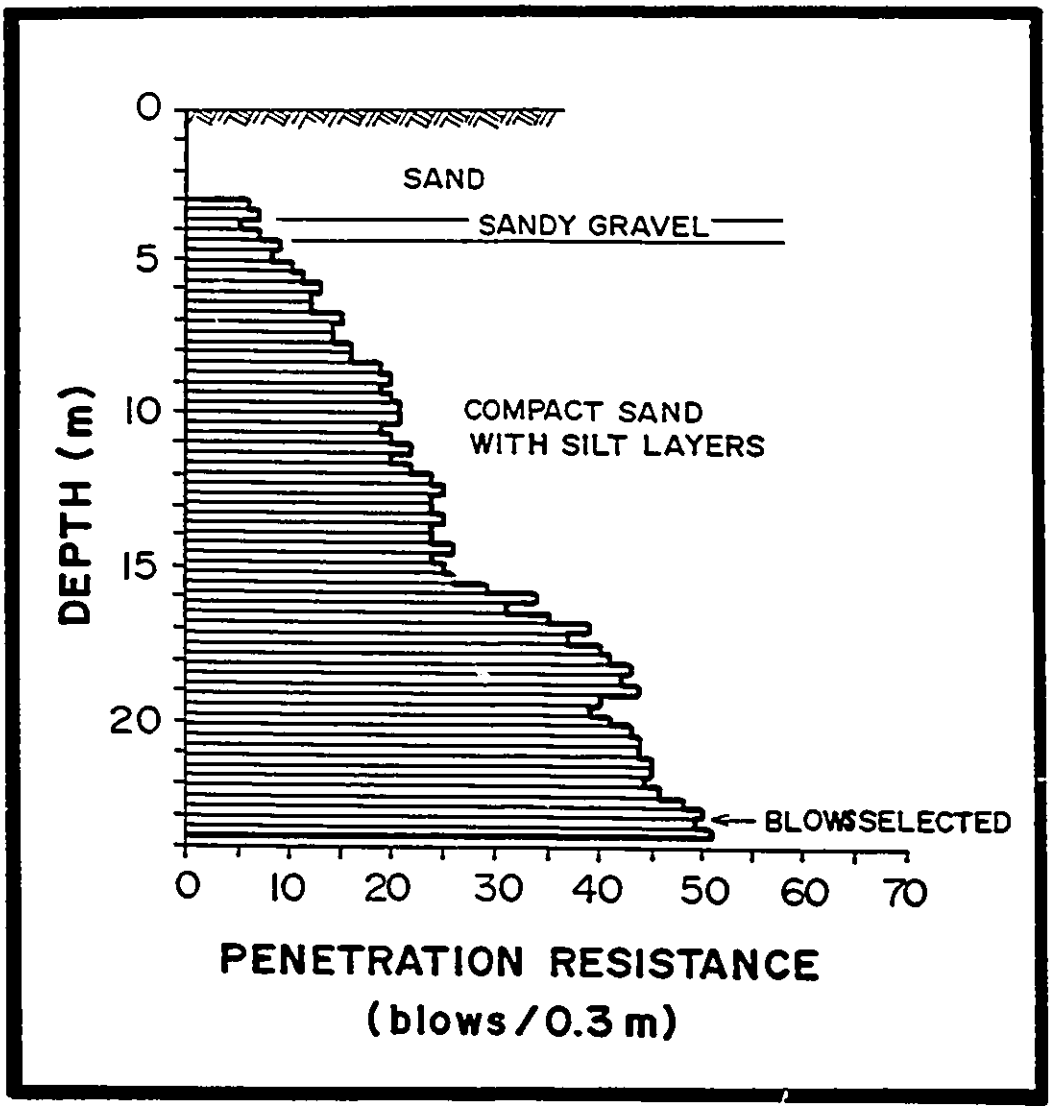

Fig. 3.5 Driving log diagram, CN Jasper

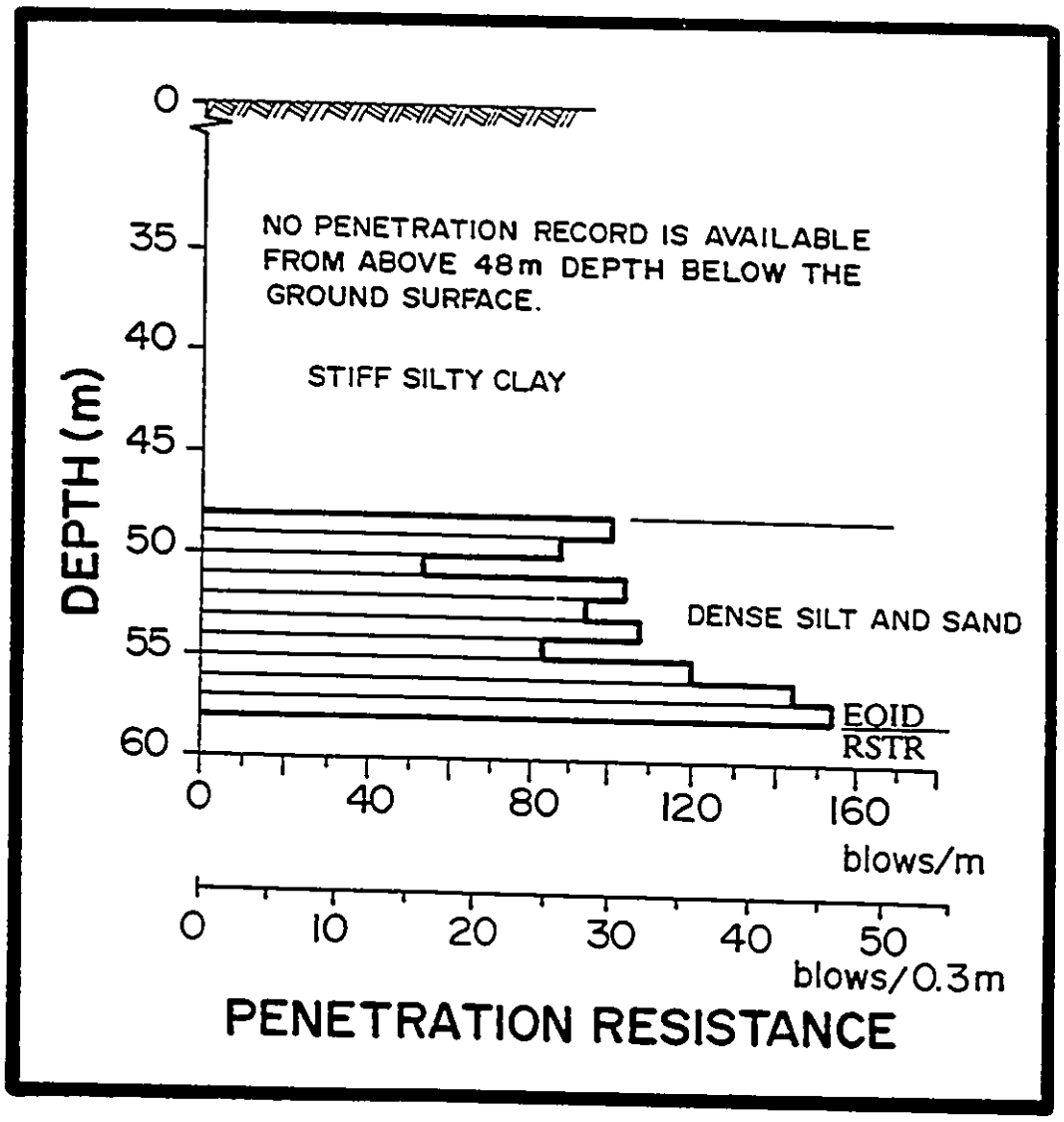

Fig. 3.6 EOID driving log diagram, National Aviation Museum

FIG. 4.1 – IMPACT FORCE

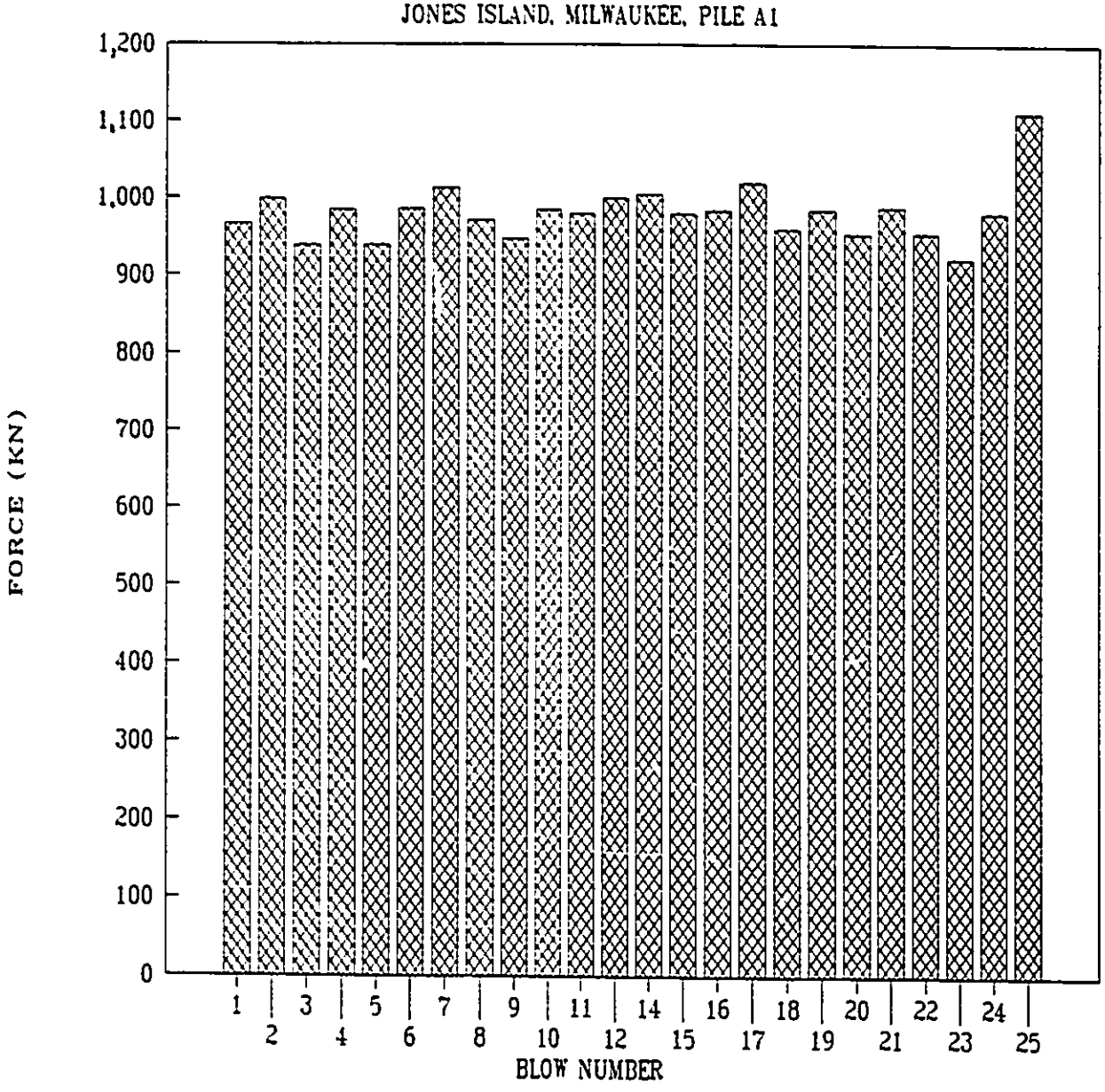

FIG. 4.2 – TRANSFERRED ENERGY

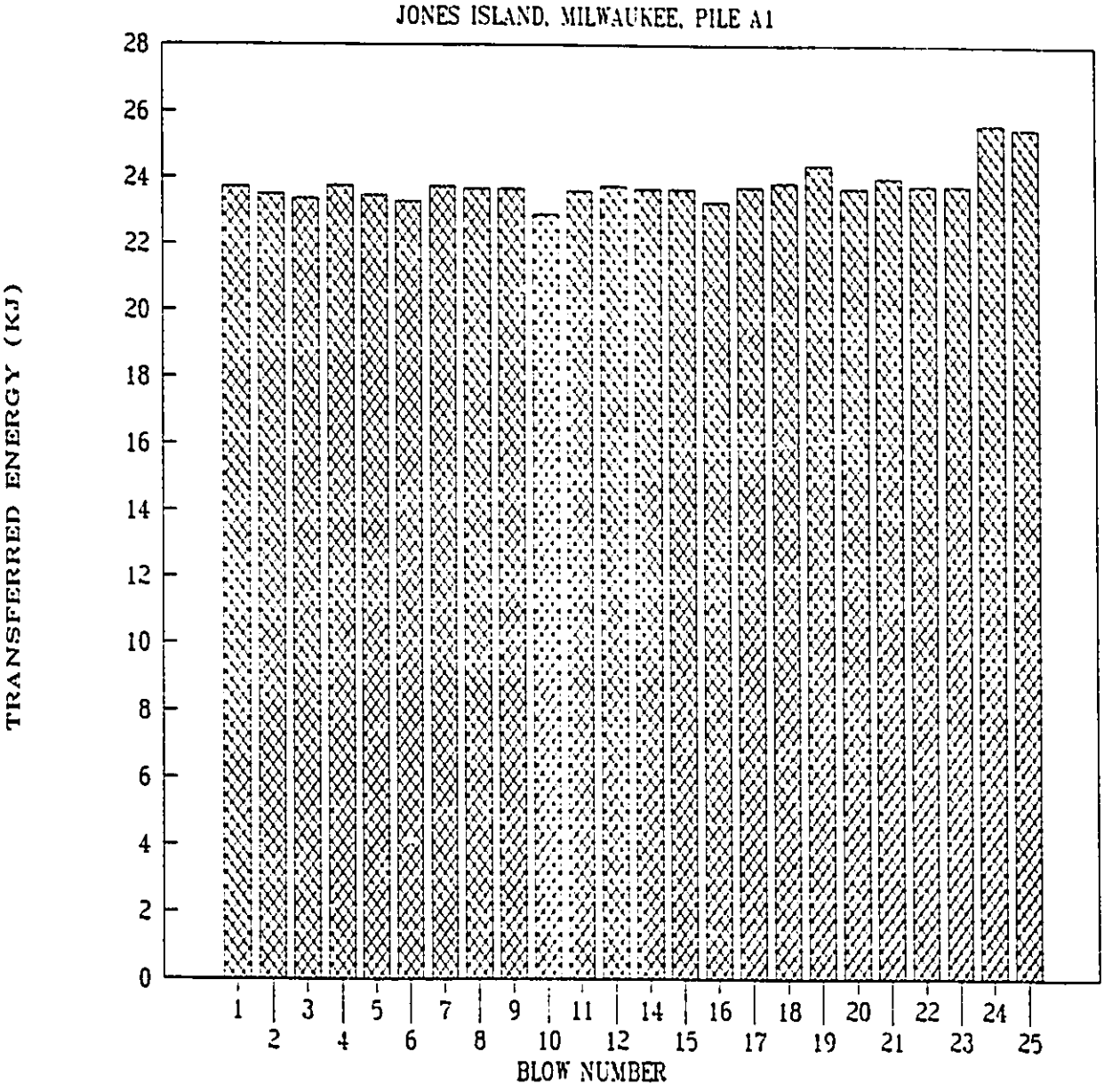

FIG. 4.3 – CMES–RMX CAPACITY

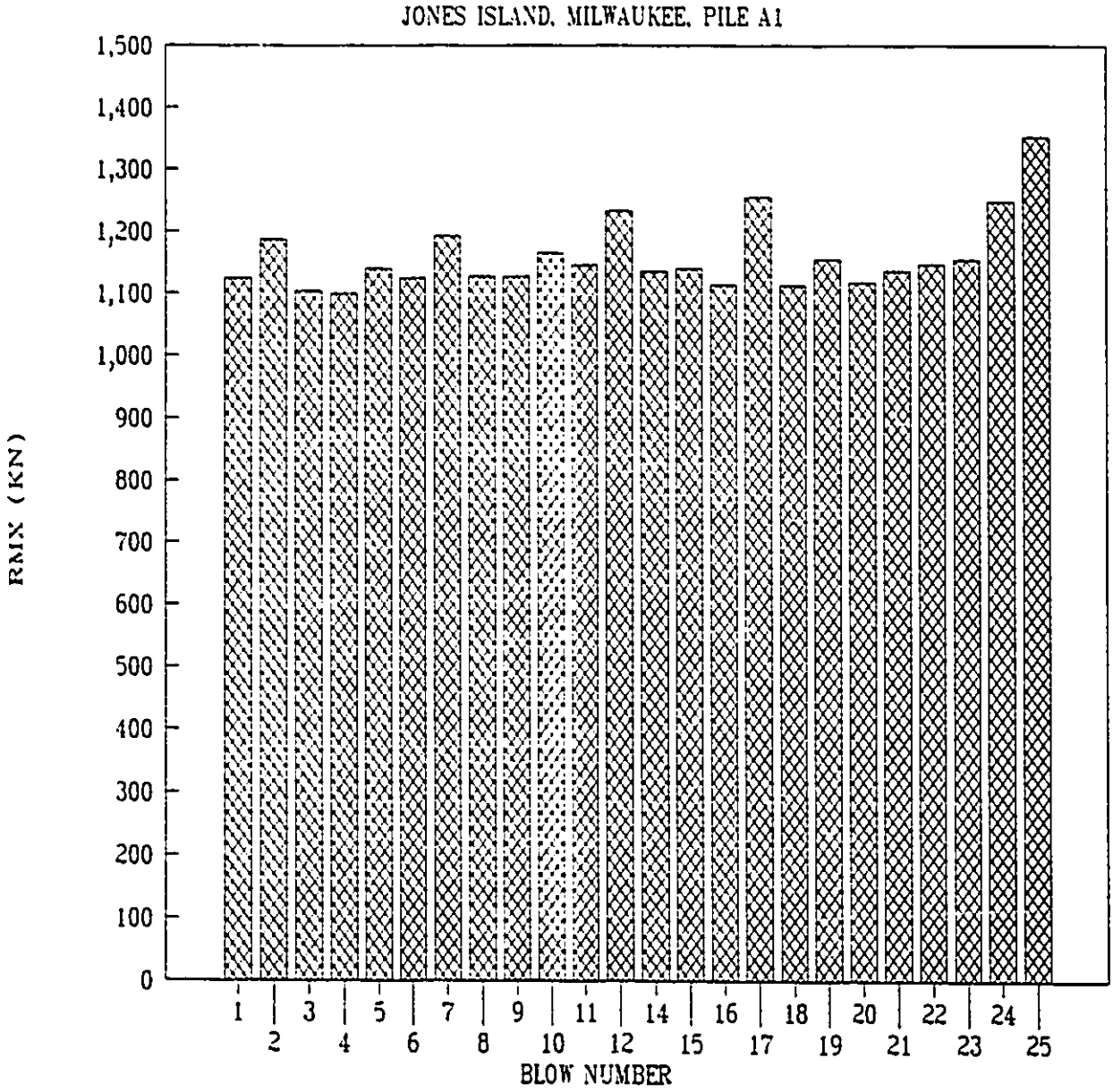

FIG. 4.4 – RMX / FIMP

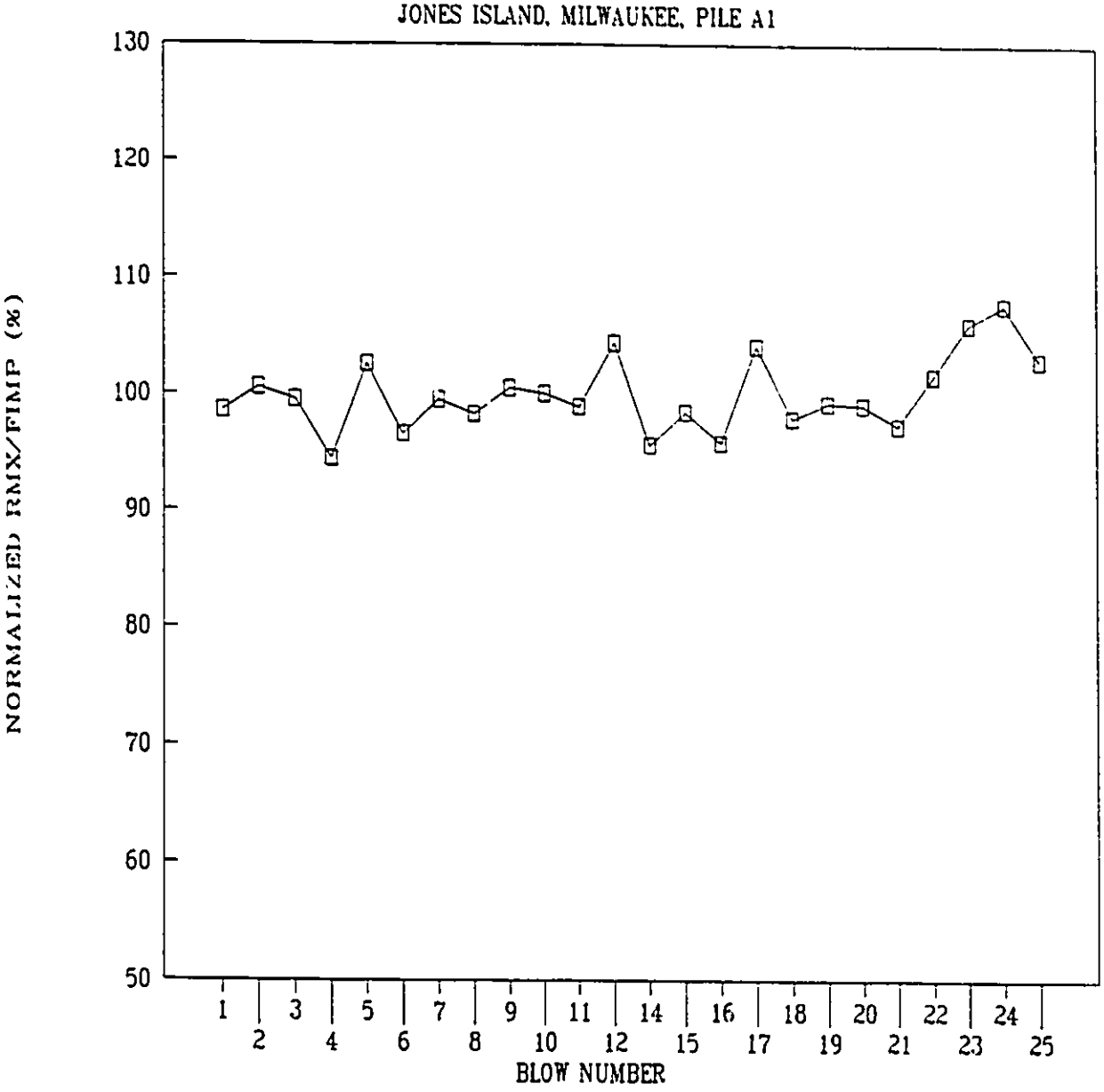

FIG. 4.5 – RMX / FIMP and EMAX

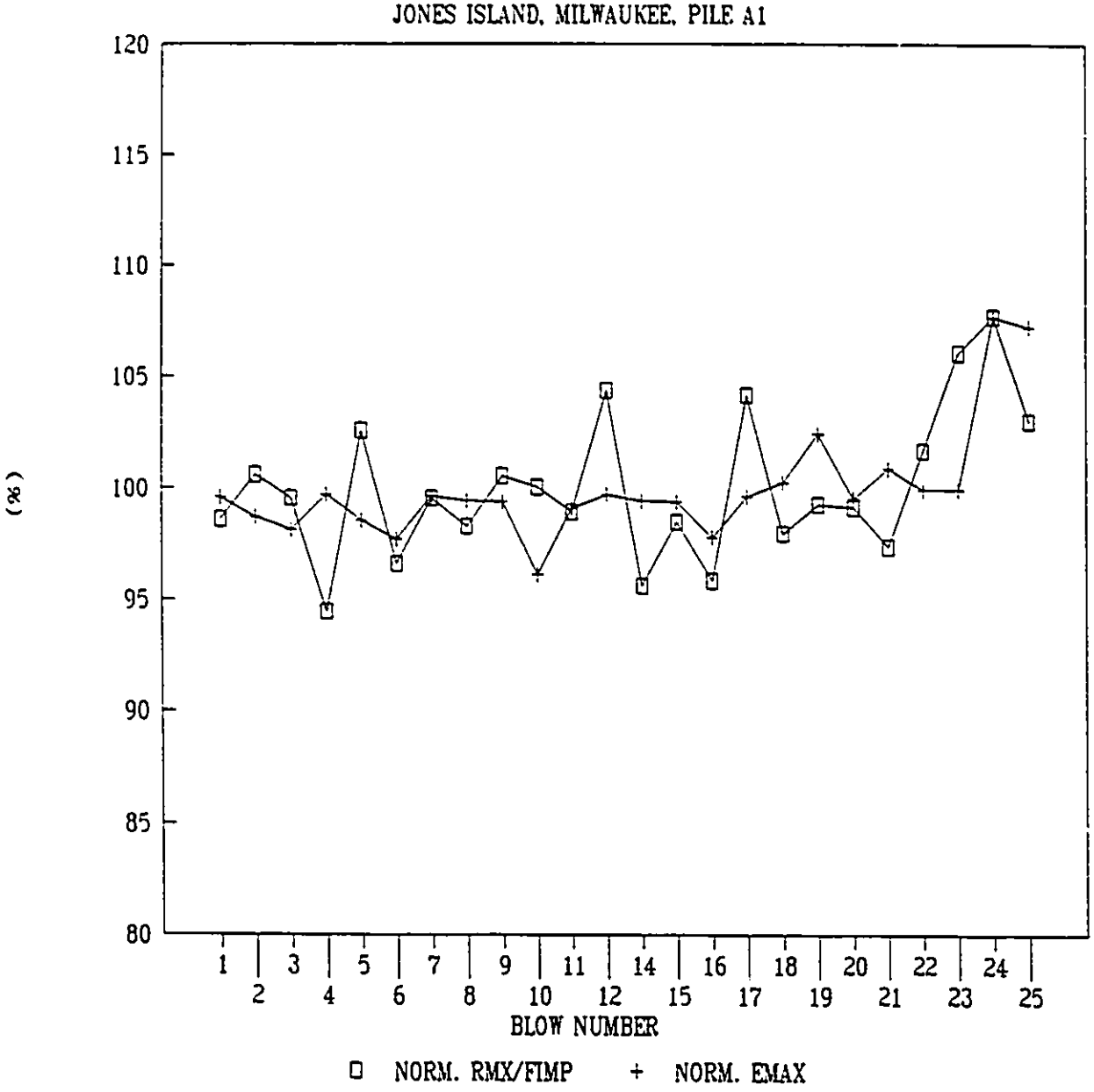

FIG. 4.6 – IMPACT FORCE

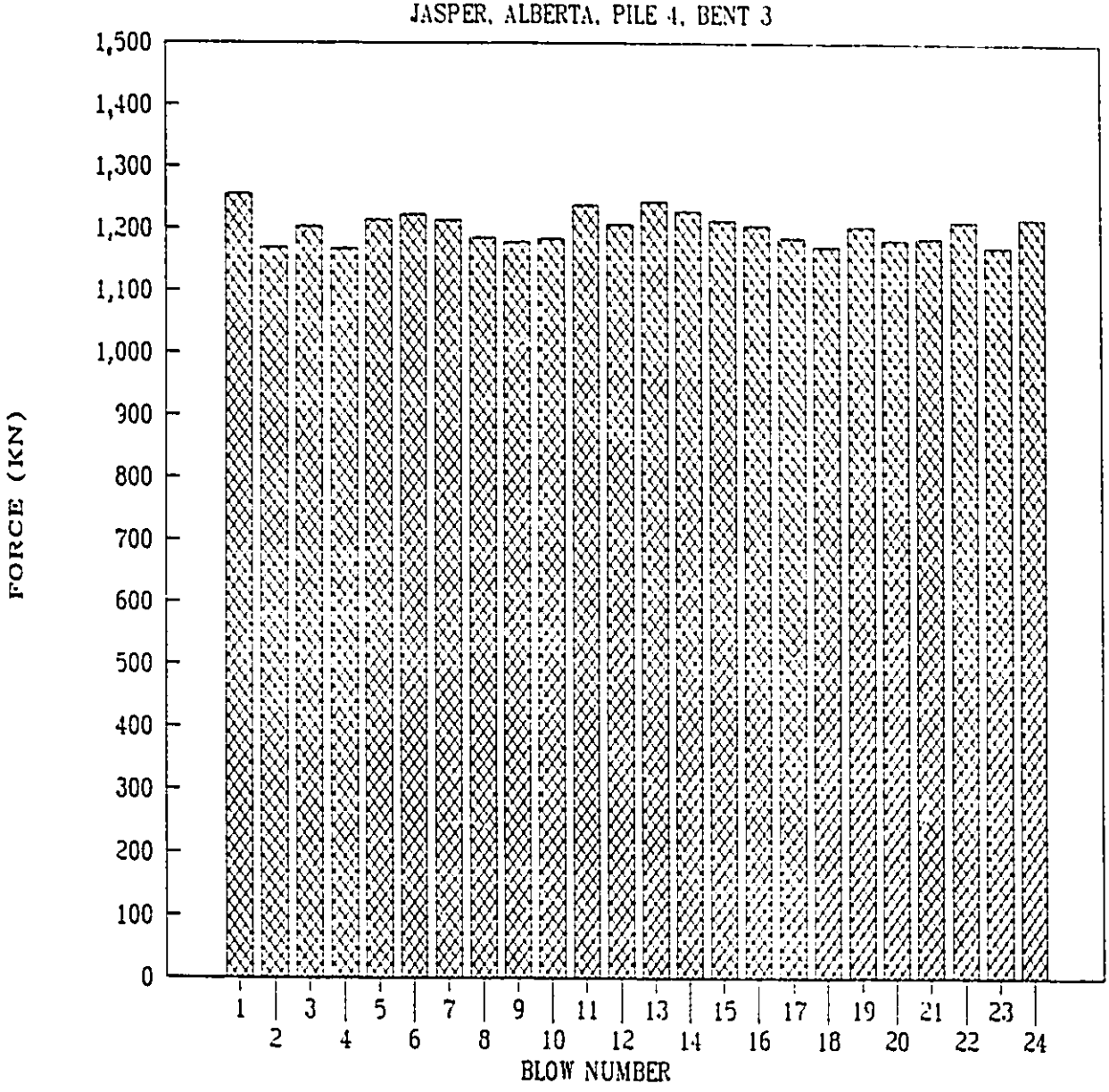

FIG. 4.7 – TRANSFERRED ENERGY

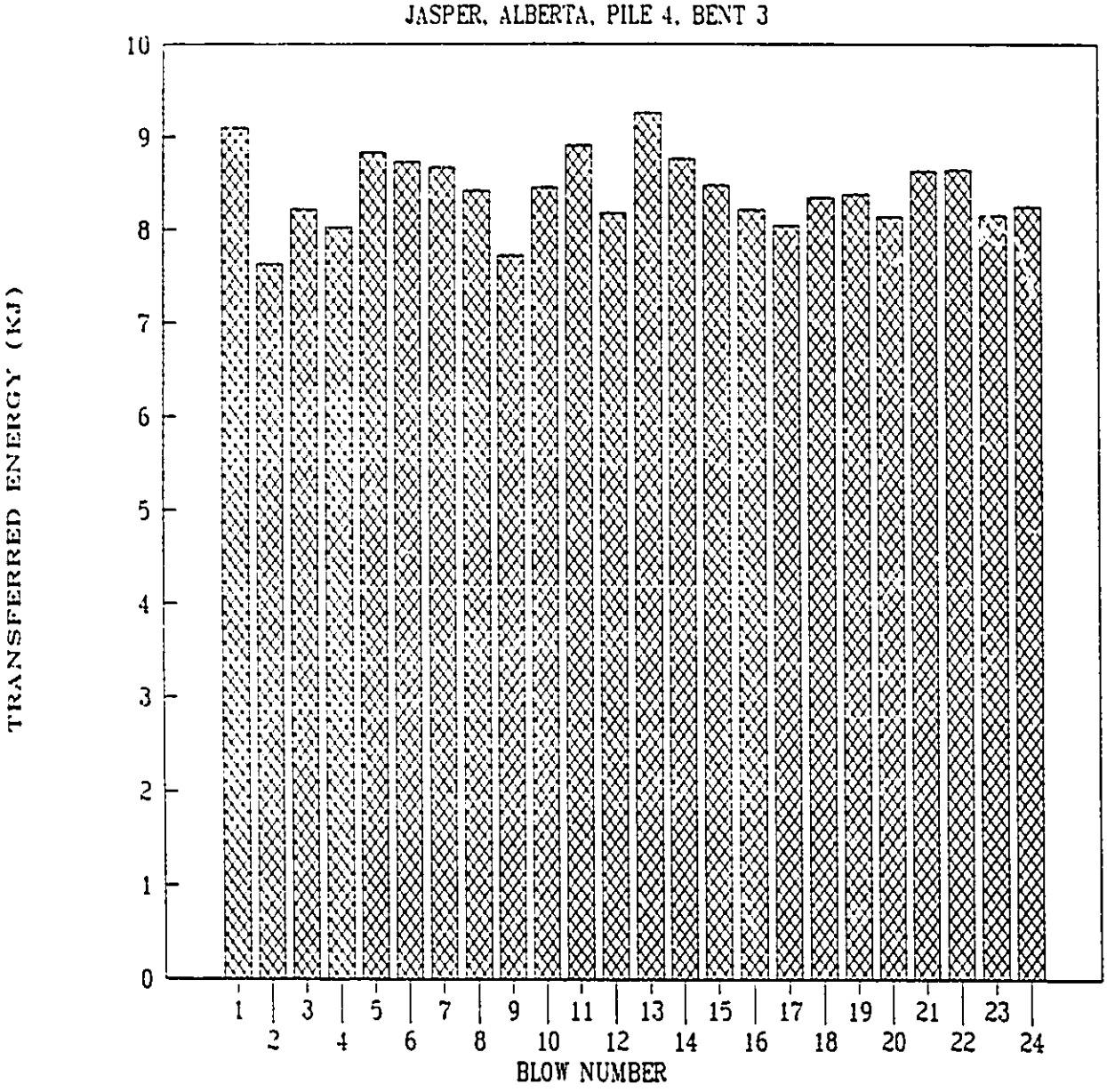

FIG. 4.8 – CMES–RMX CAPACITY

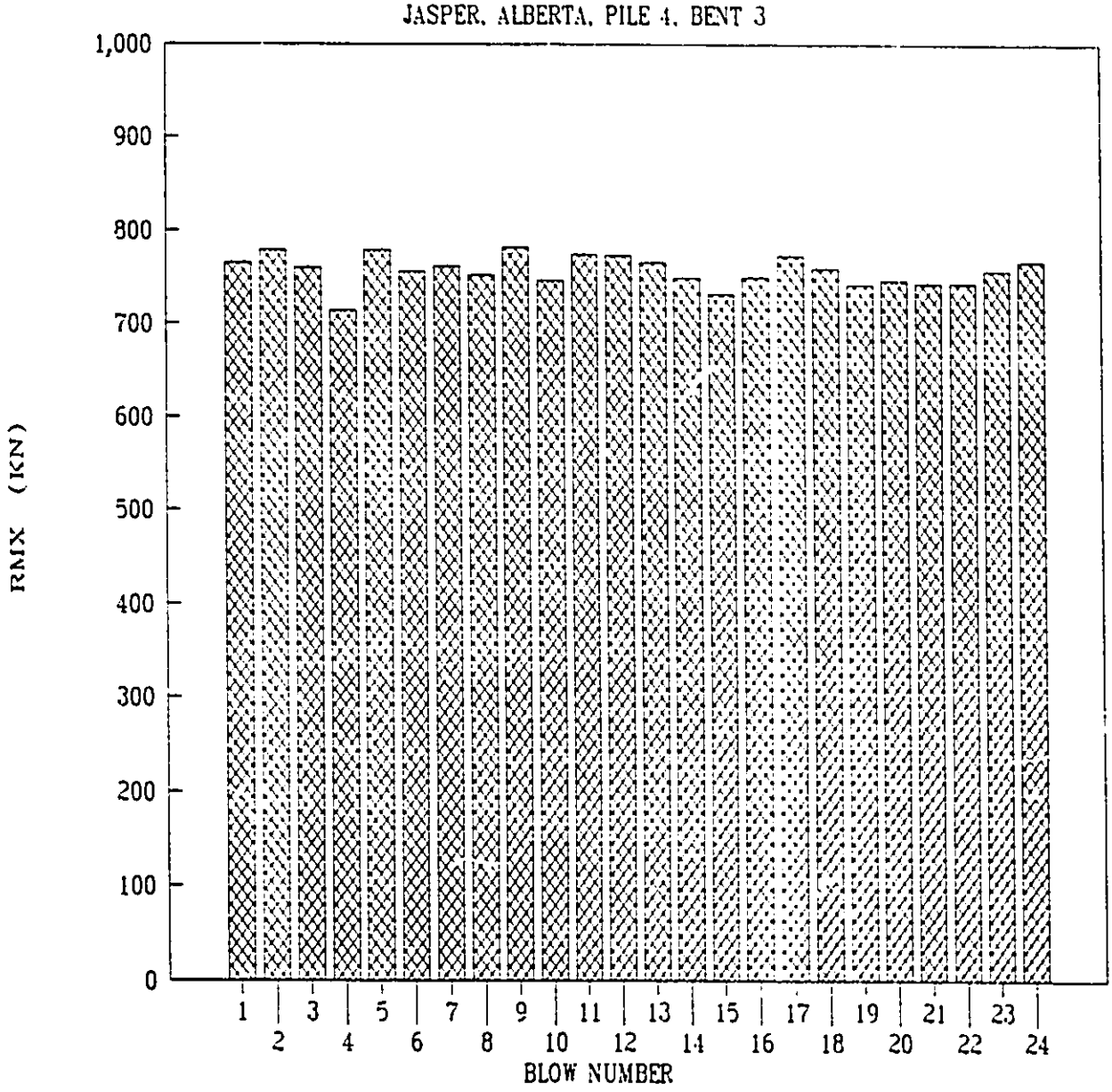

FIG. 4.9 – RMX / FIMP

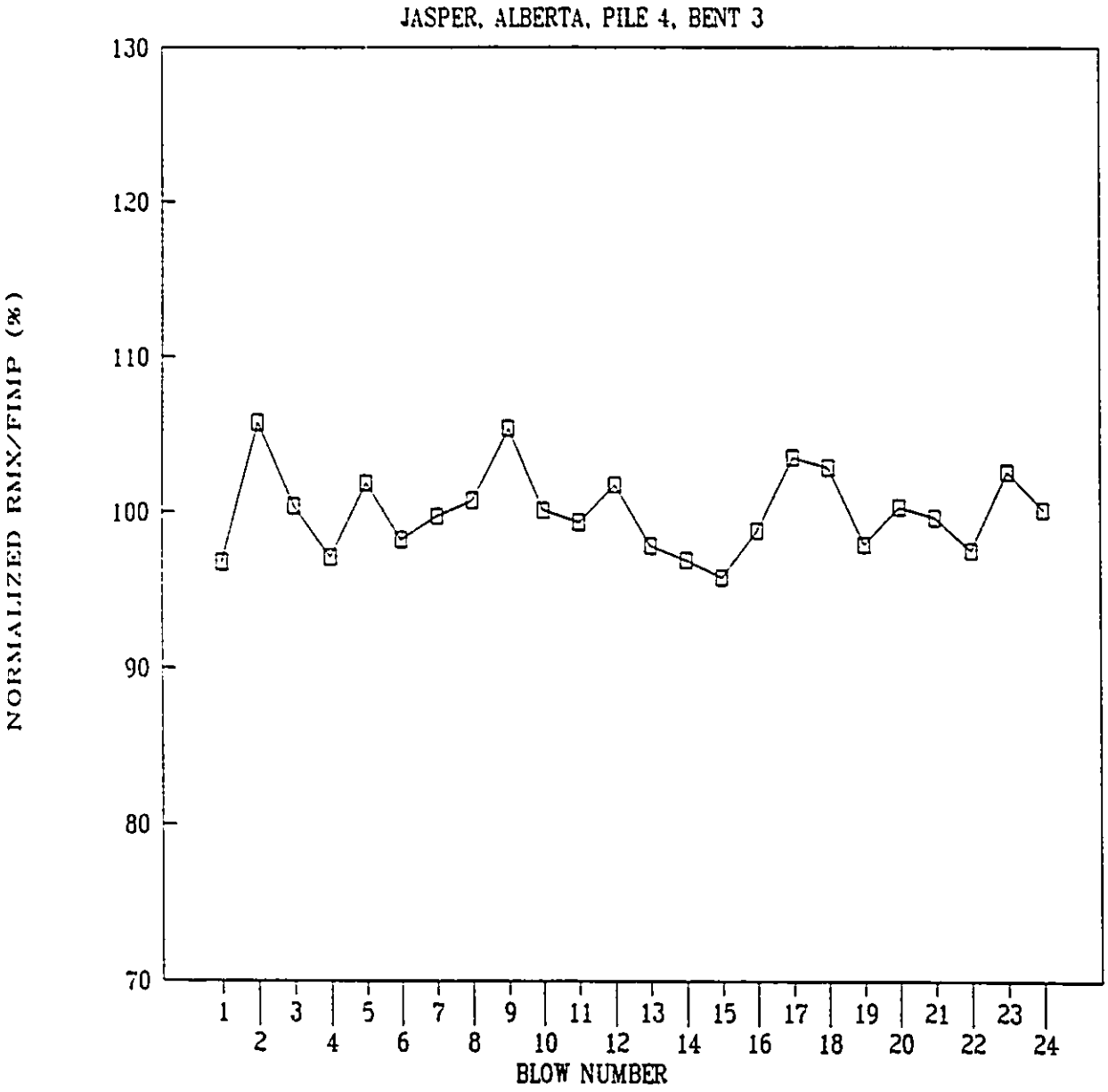

FIG. 4.10 – RMX/FIMP and EMAX

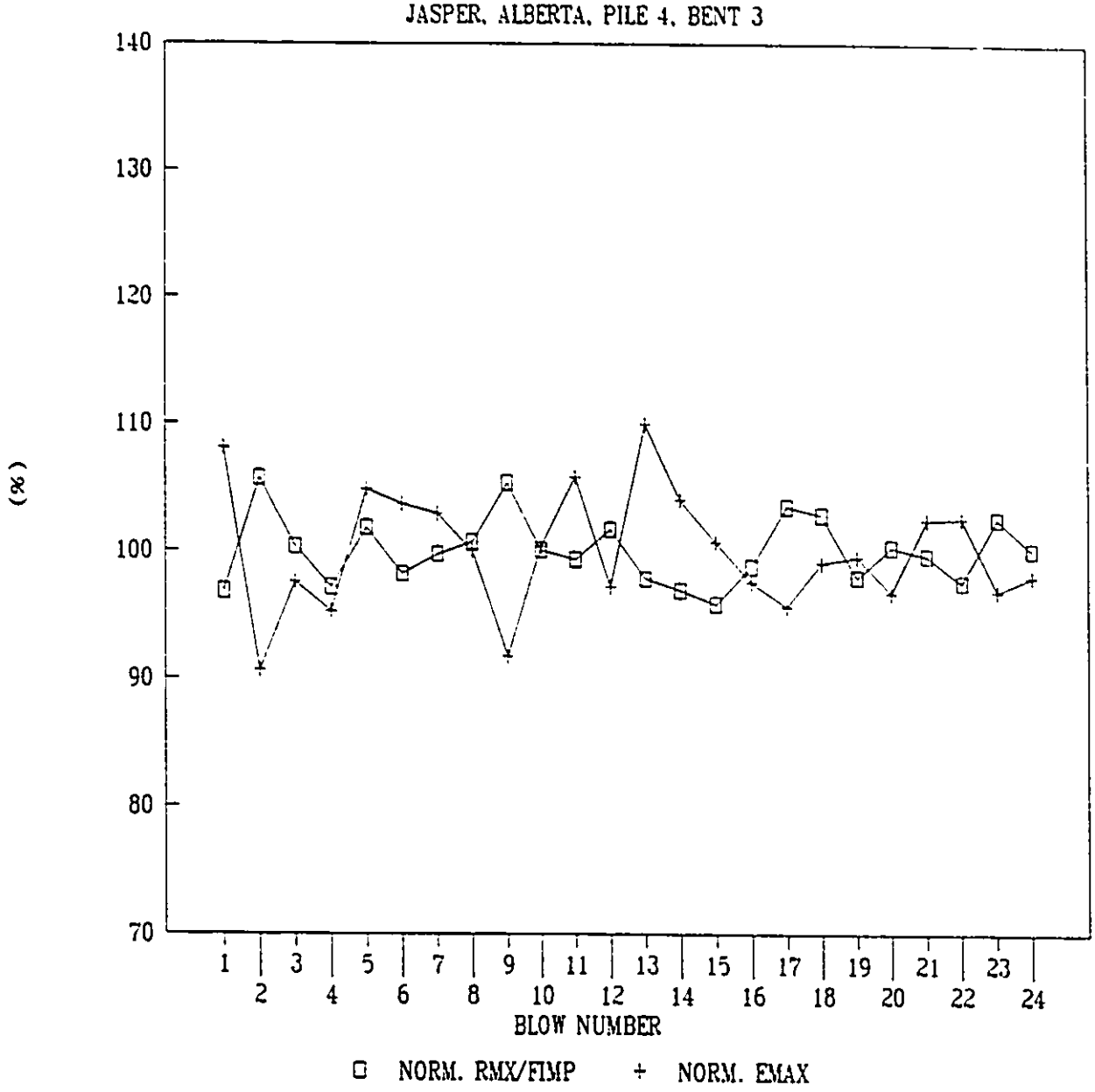

FIG. 4.11 – IMPACT FORCE

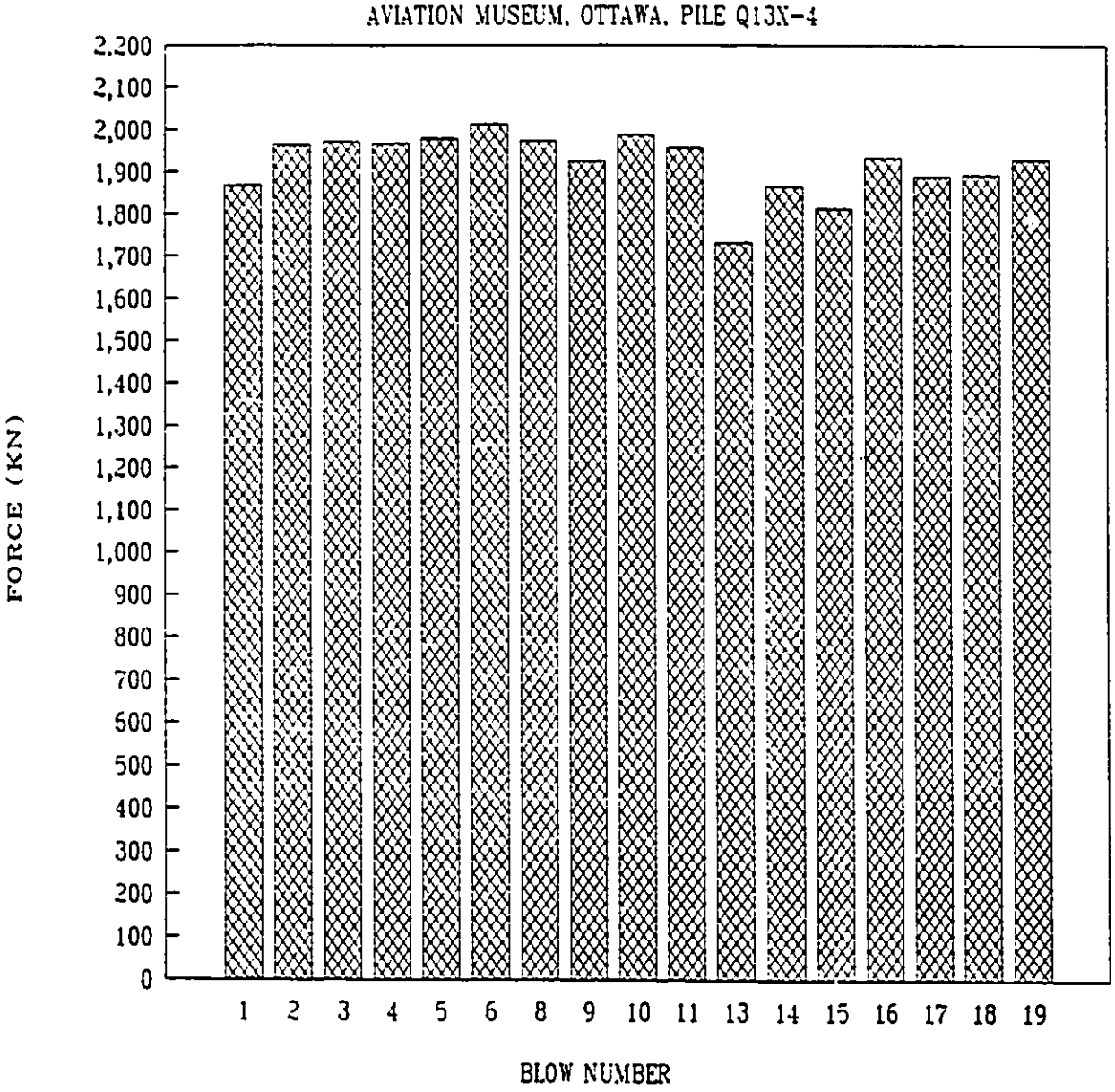

FIG. 4.12 – TRANSFERRED ENERGY

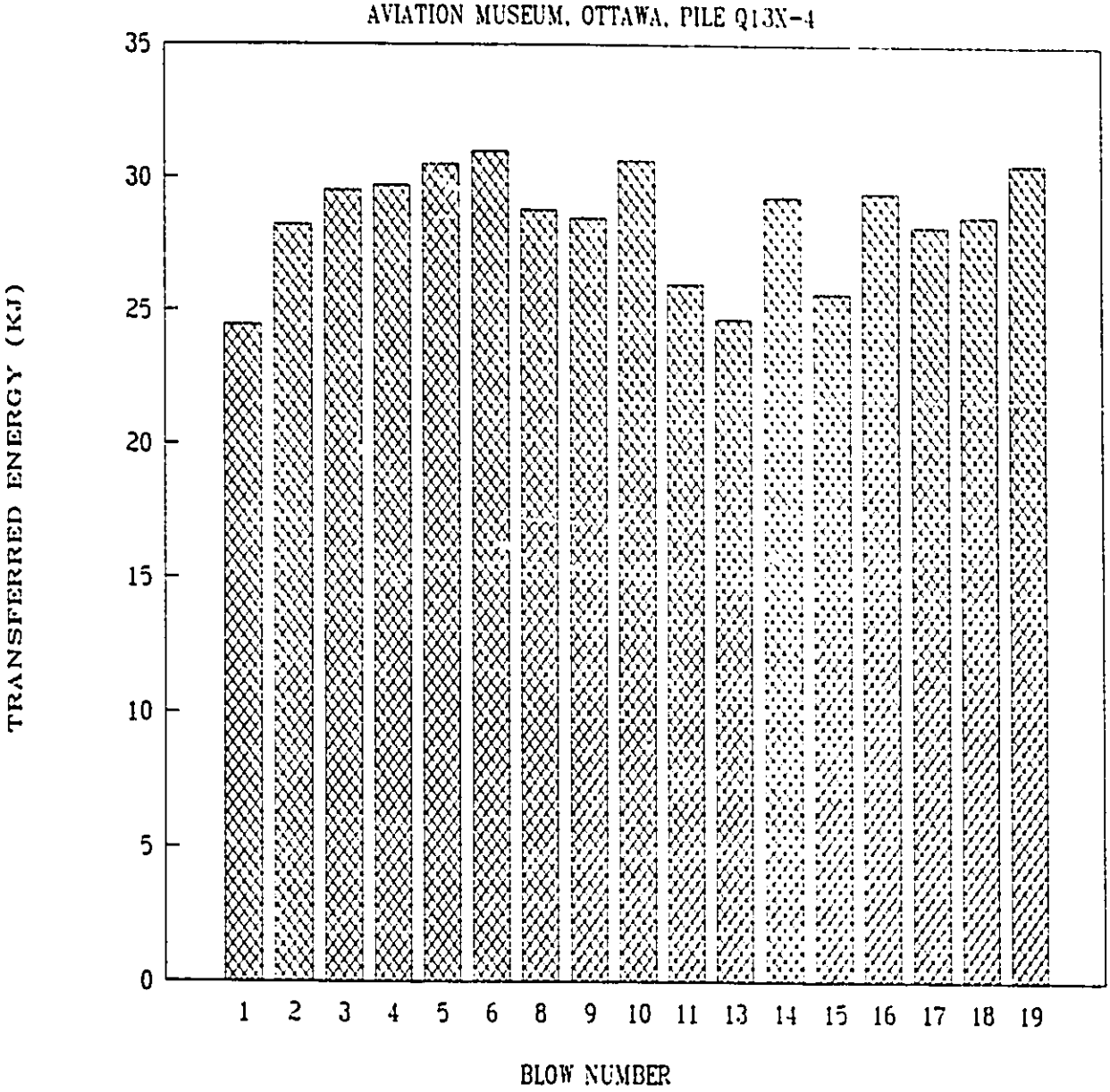

FIG. 4.13 – CMES–RMX CAPACITY

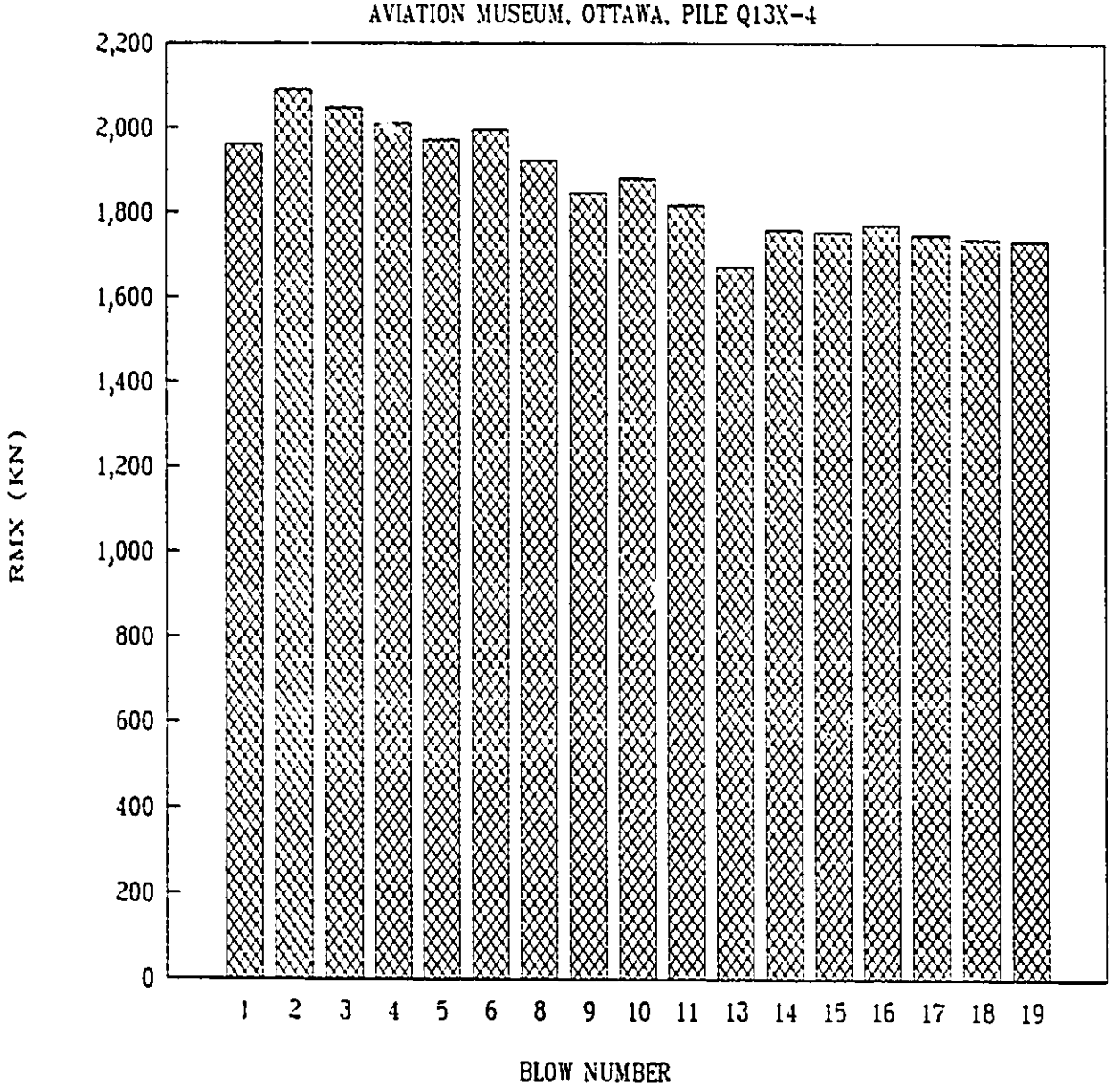

FIG. 4.14 – RMX / FIMP

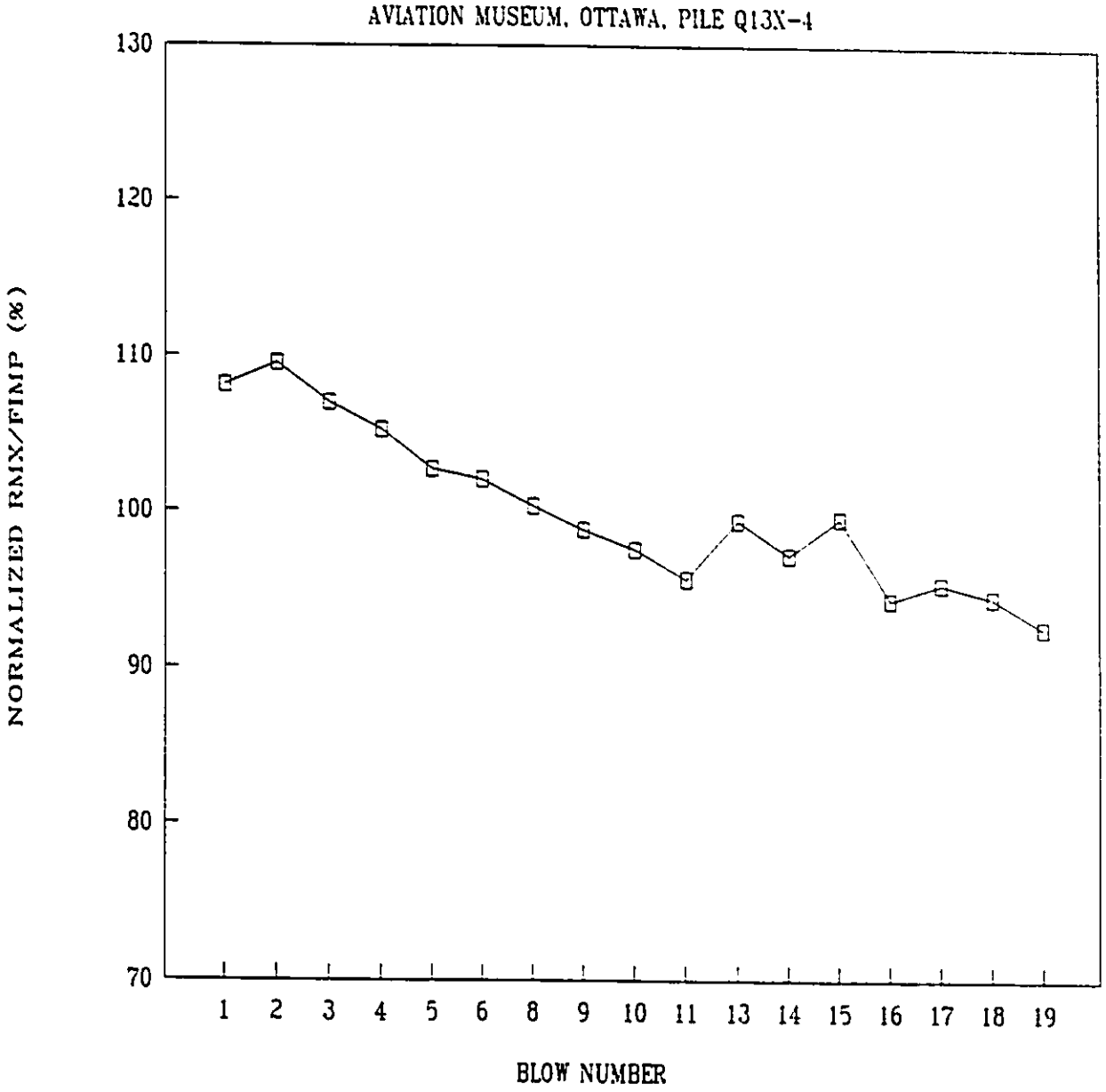

FIG. 4.15 - RMX/FIMP and EMAX

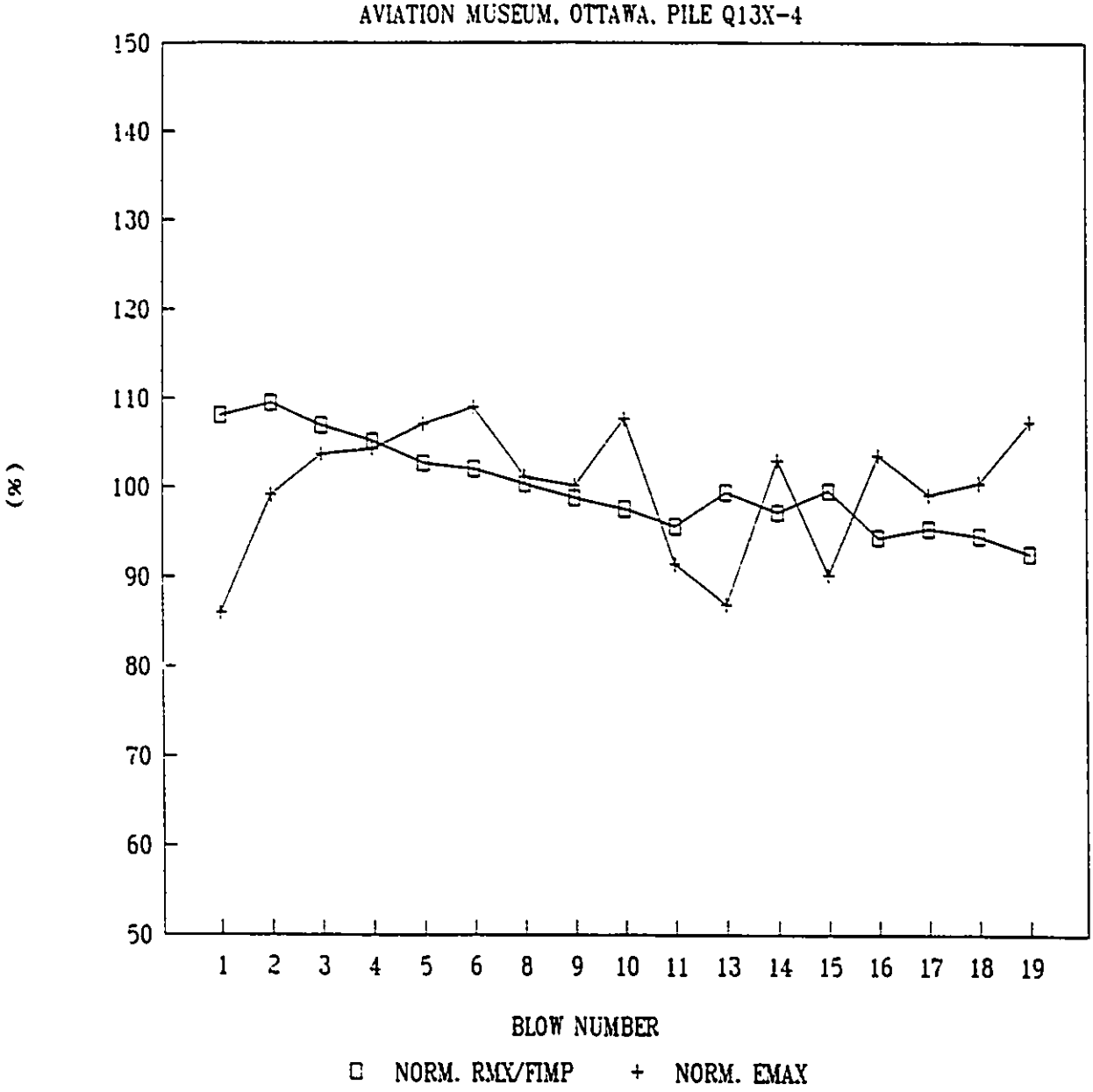

FIG. 4.16 – CAPWAPC STATIC RESISTANCE

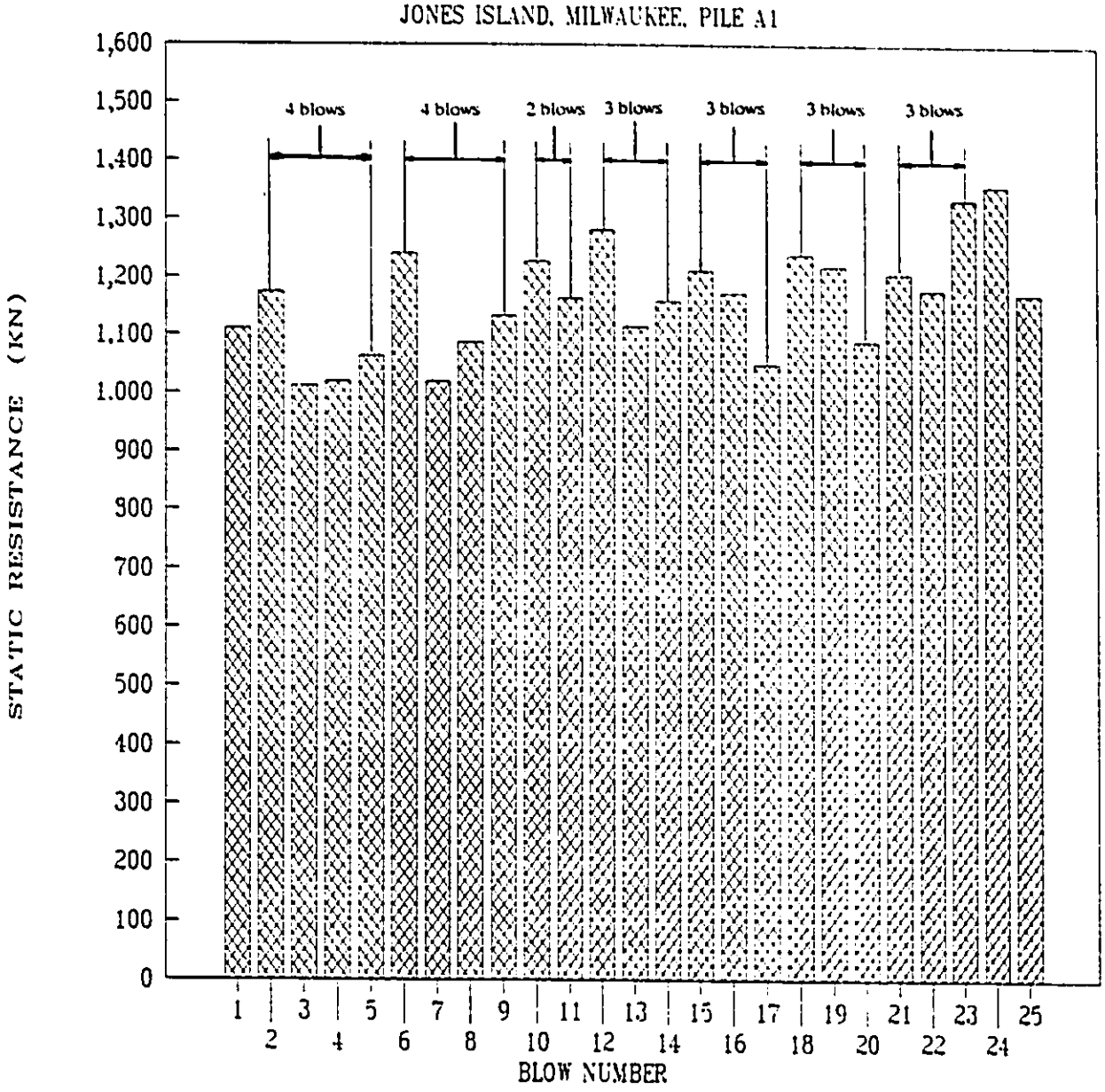

FIG. 4.17 – CAPWAPC CAPACITY / FIMP

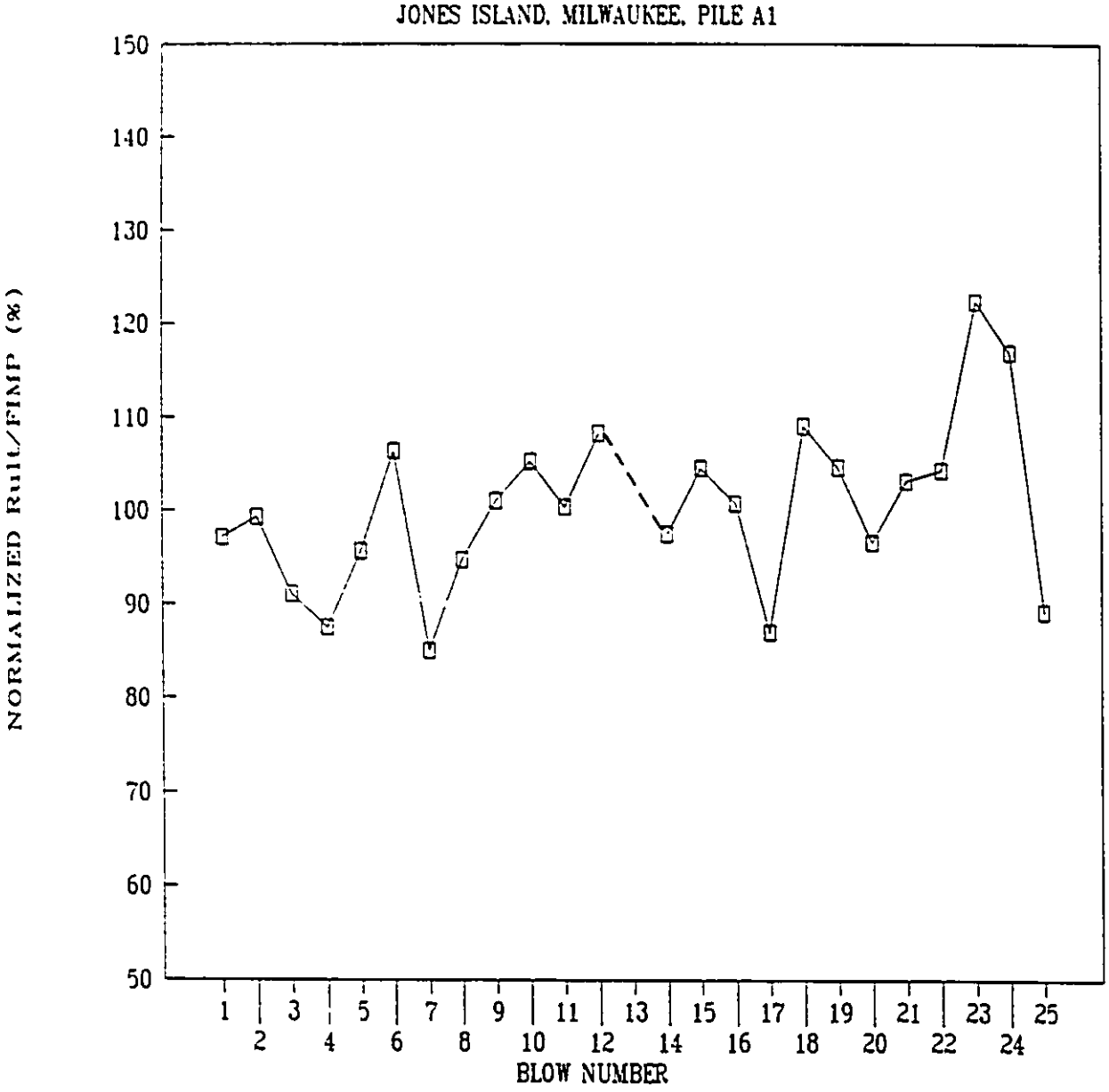

FIG. 4.18 – CAPWAPC CAPACITY AND ENERGY

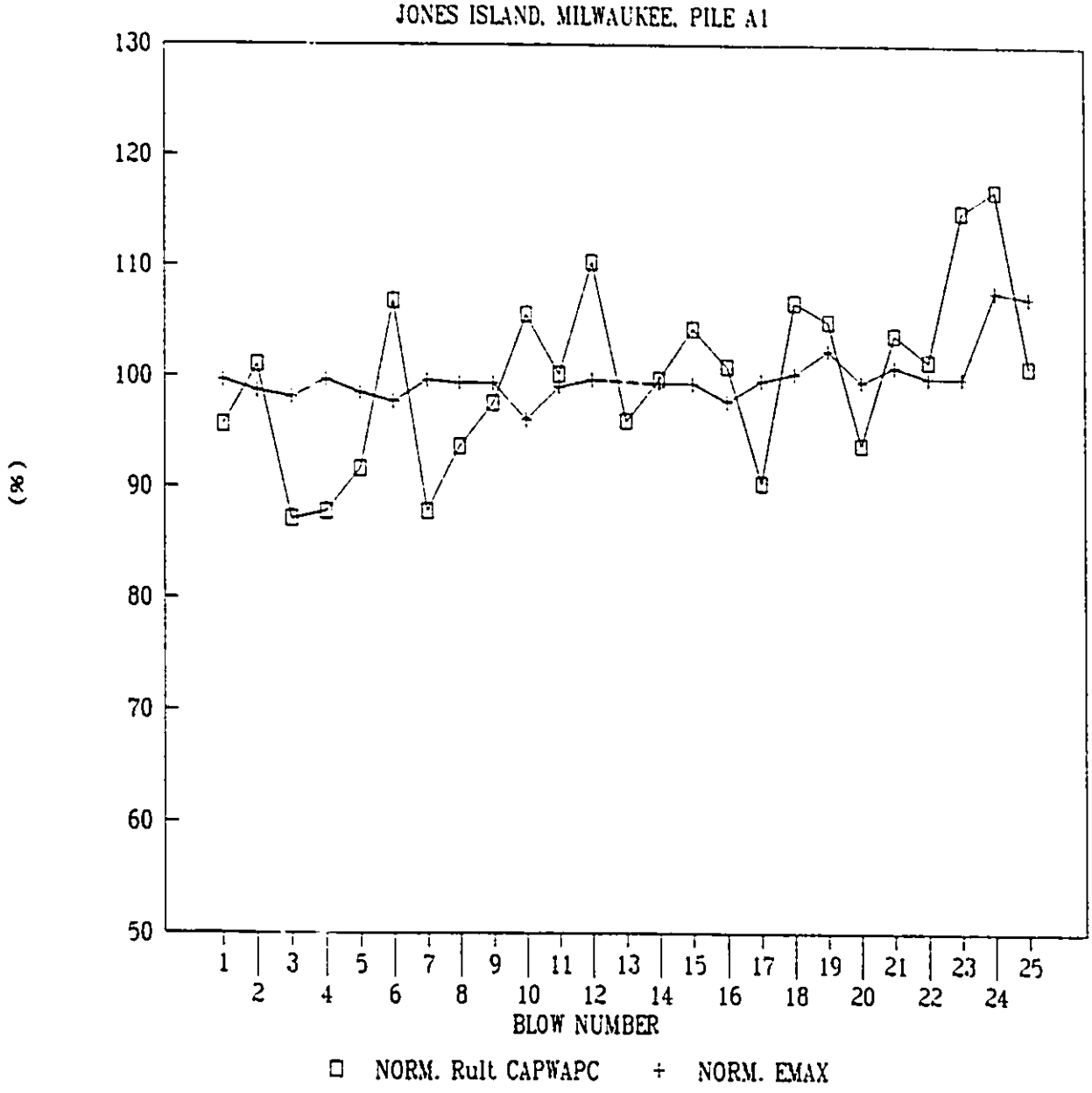

FIG. 4.19 - Rult CAPWAPC and CMES-RMX

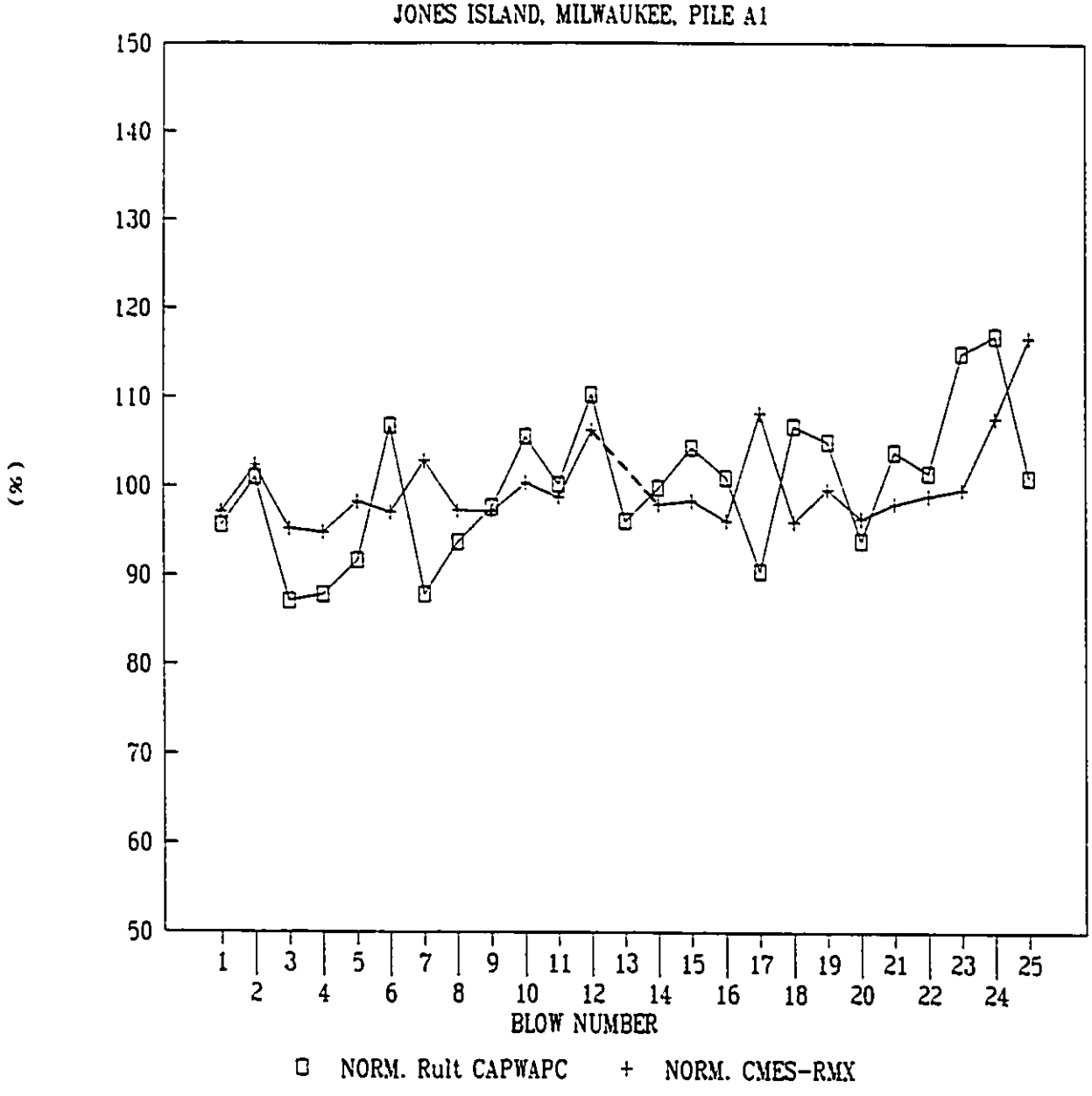

FIG. 4.20 – CAPWAPC CAPACITY

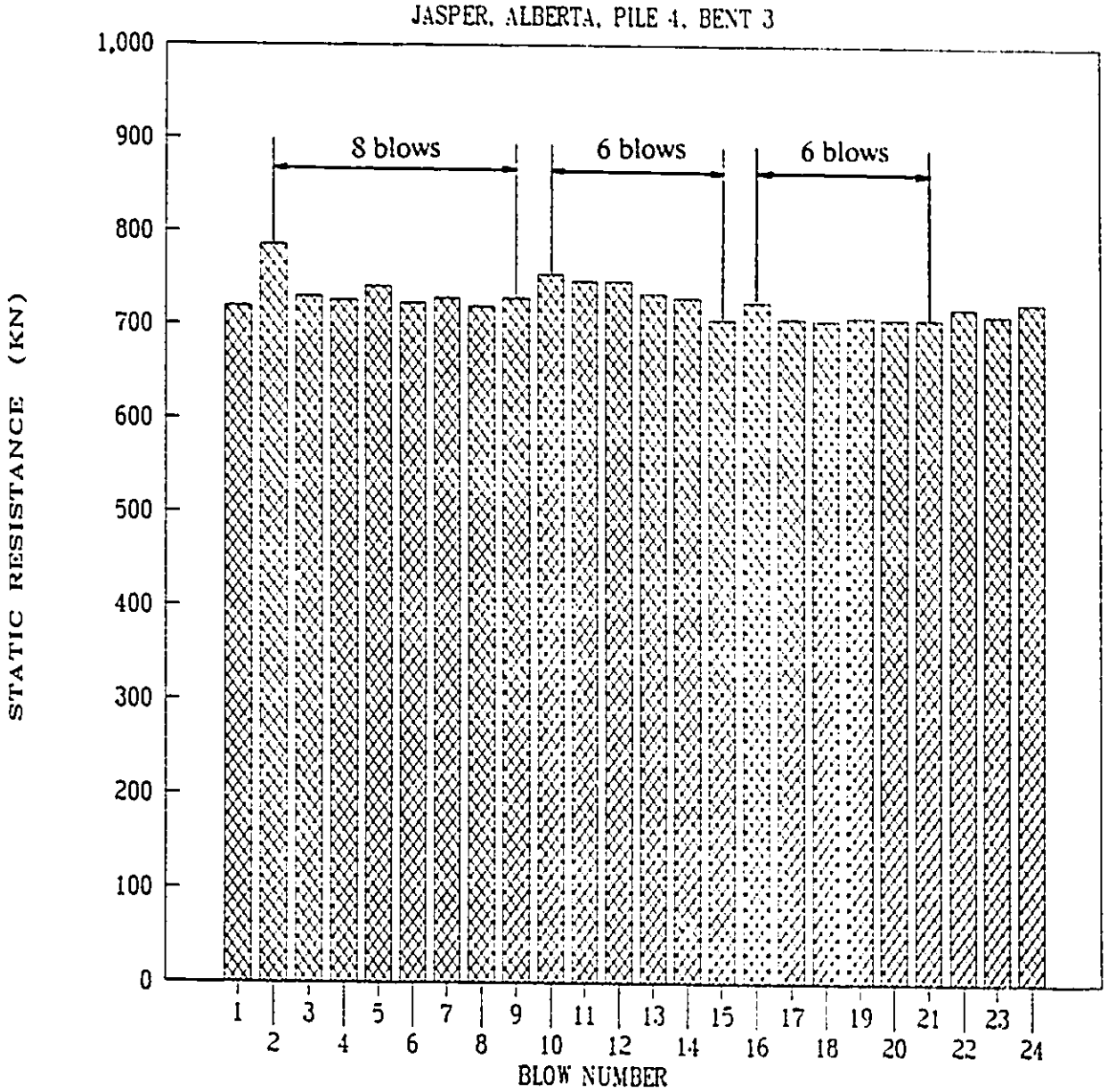

FIG. 4.21 – CAPWAPC CAPACITY / FIMP

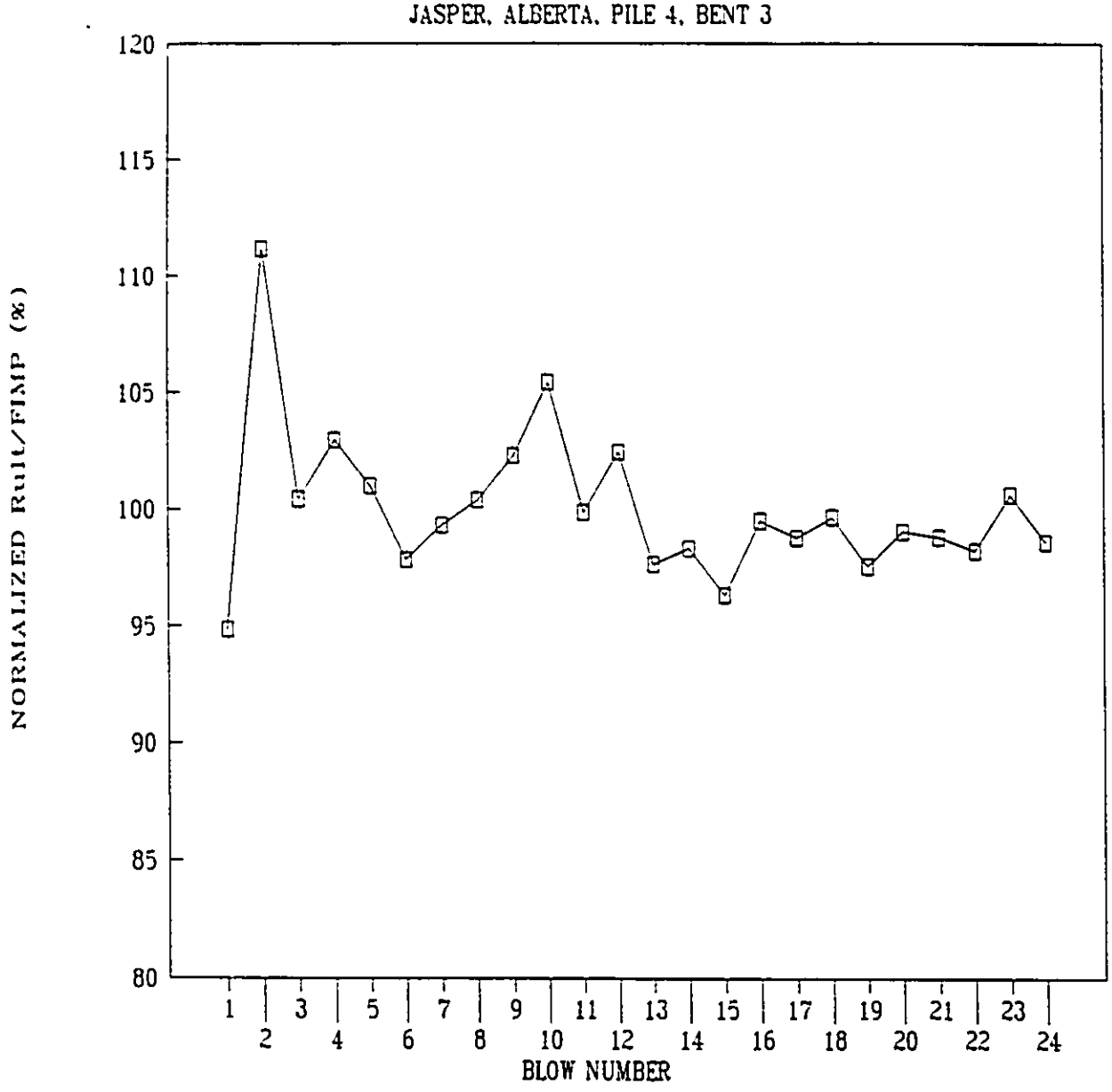

FIG. 4.22 – CAPWAPC CAPACITY AND ENERGY

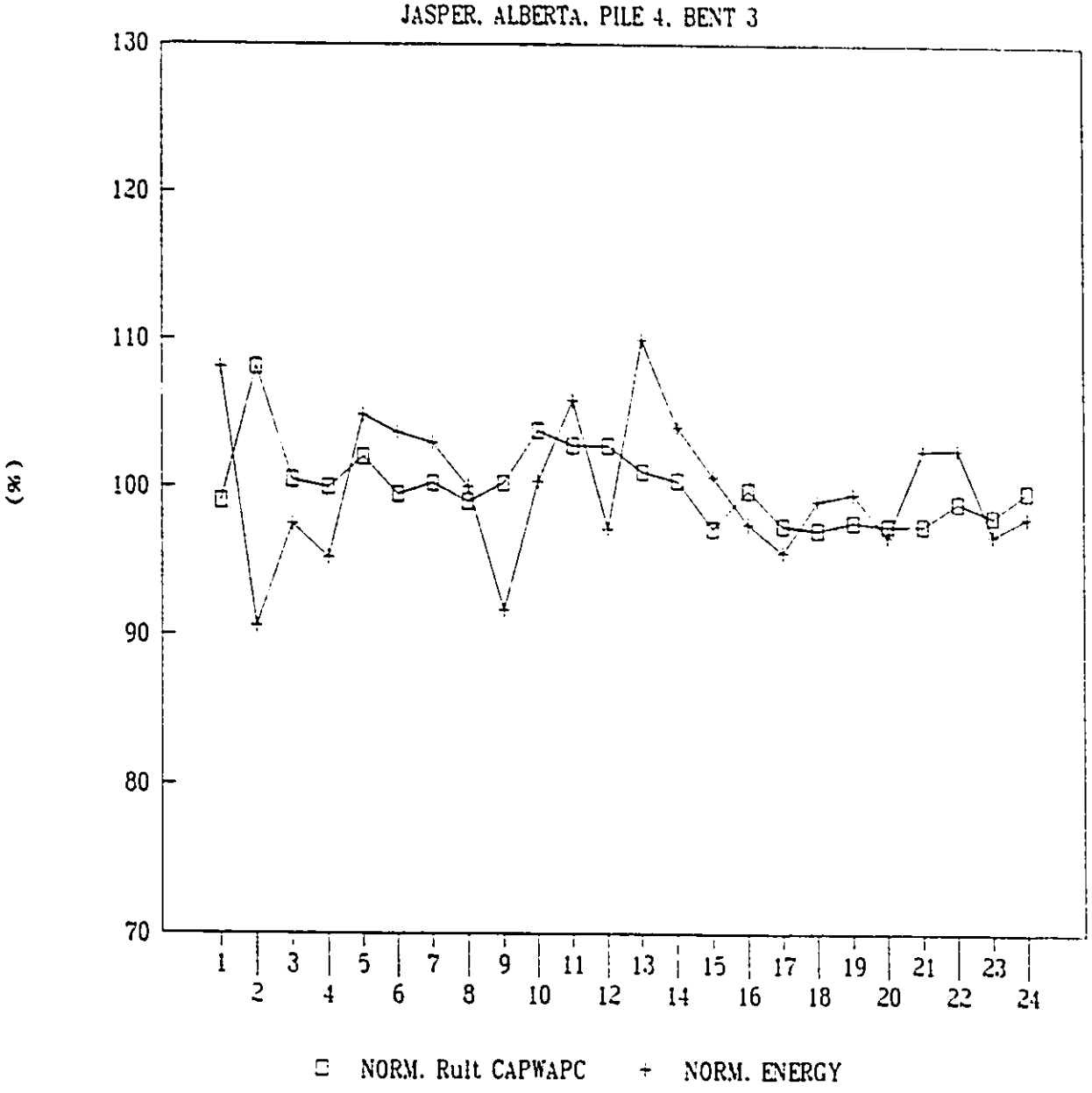

FIG. 4.23 – Rult–CAPWAPC AND CMES–RMX

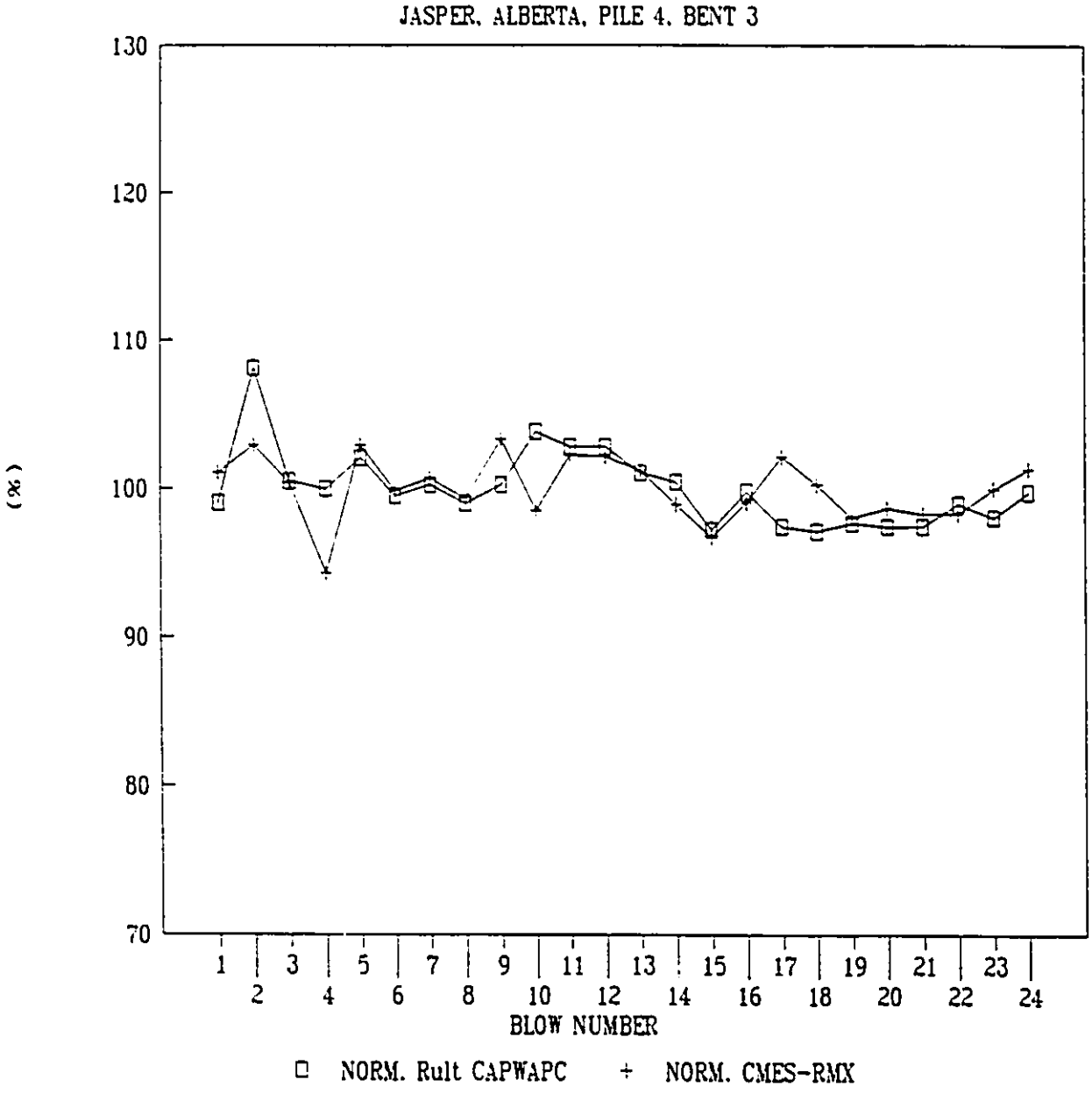

FIG. 4.24 – CAPWAPC CAPACITY

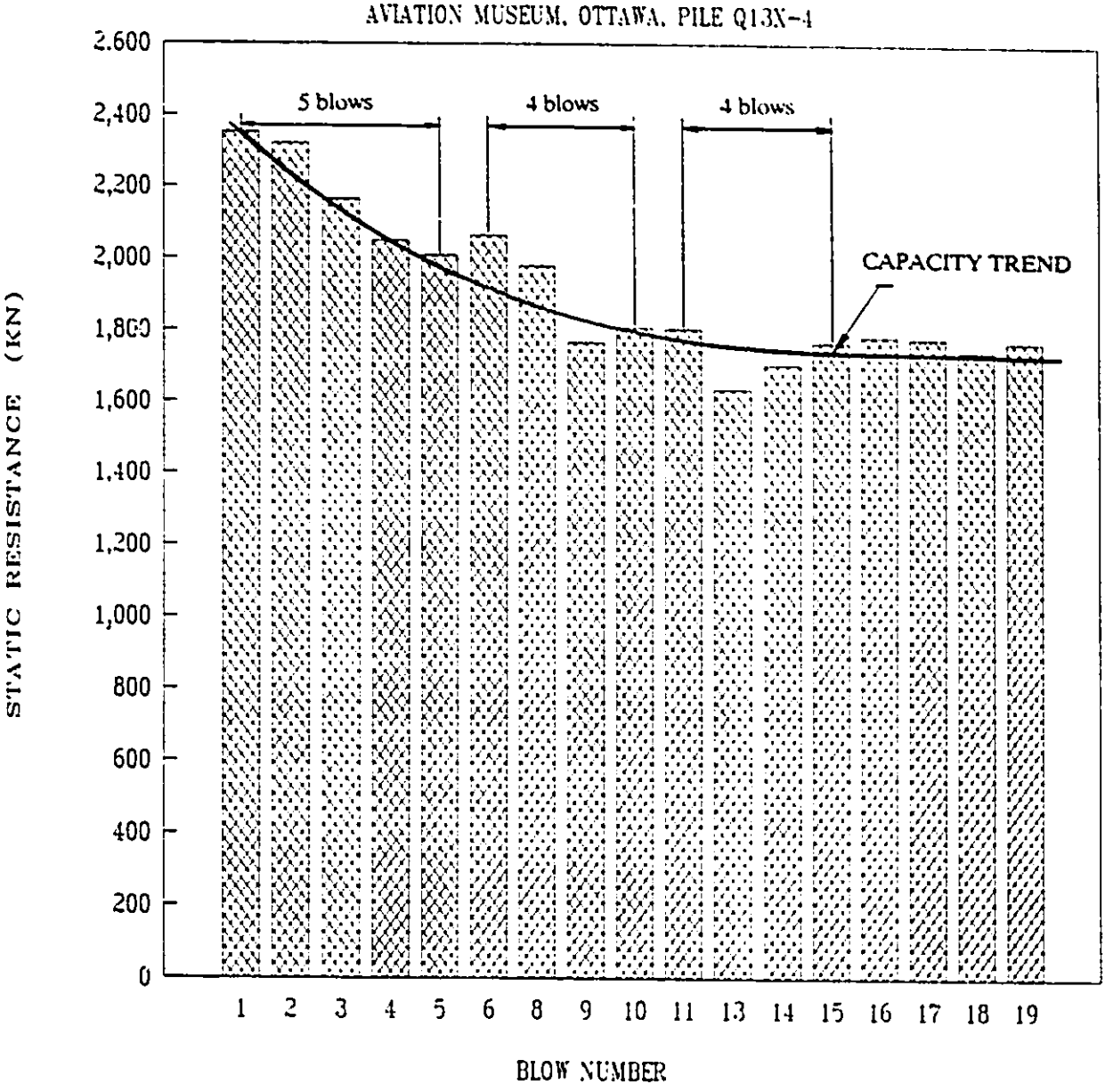

FIG. 4.25 - CAPWAPC CAPACITY / FIMP

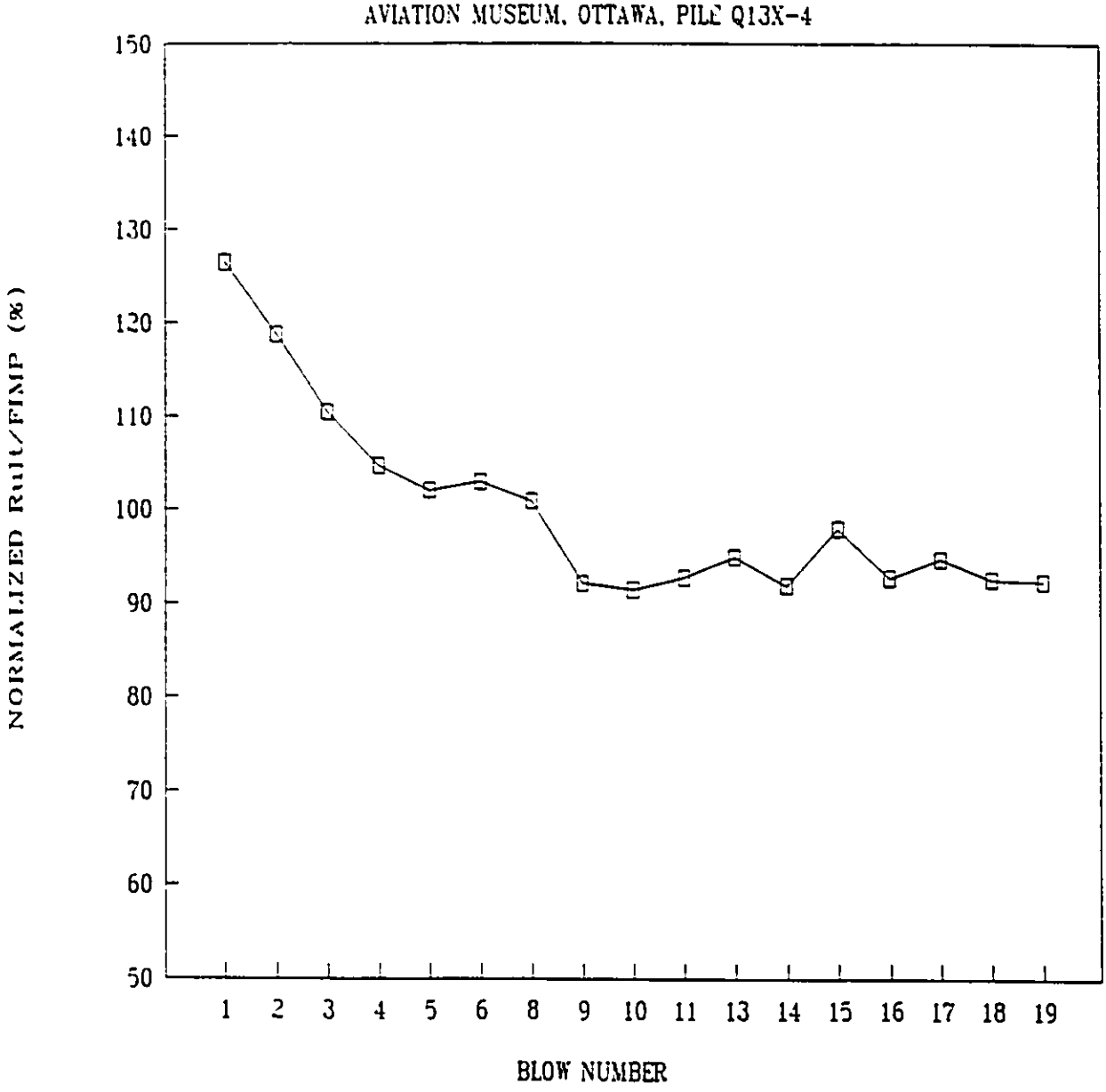

FIG. 4.26 – CAPWAPC CAPACITY AND ENERGY

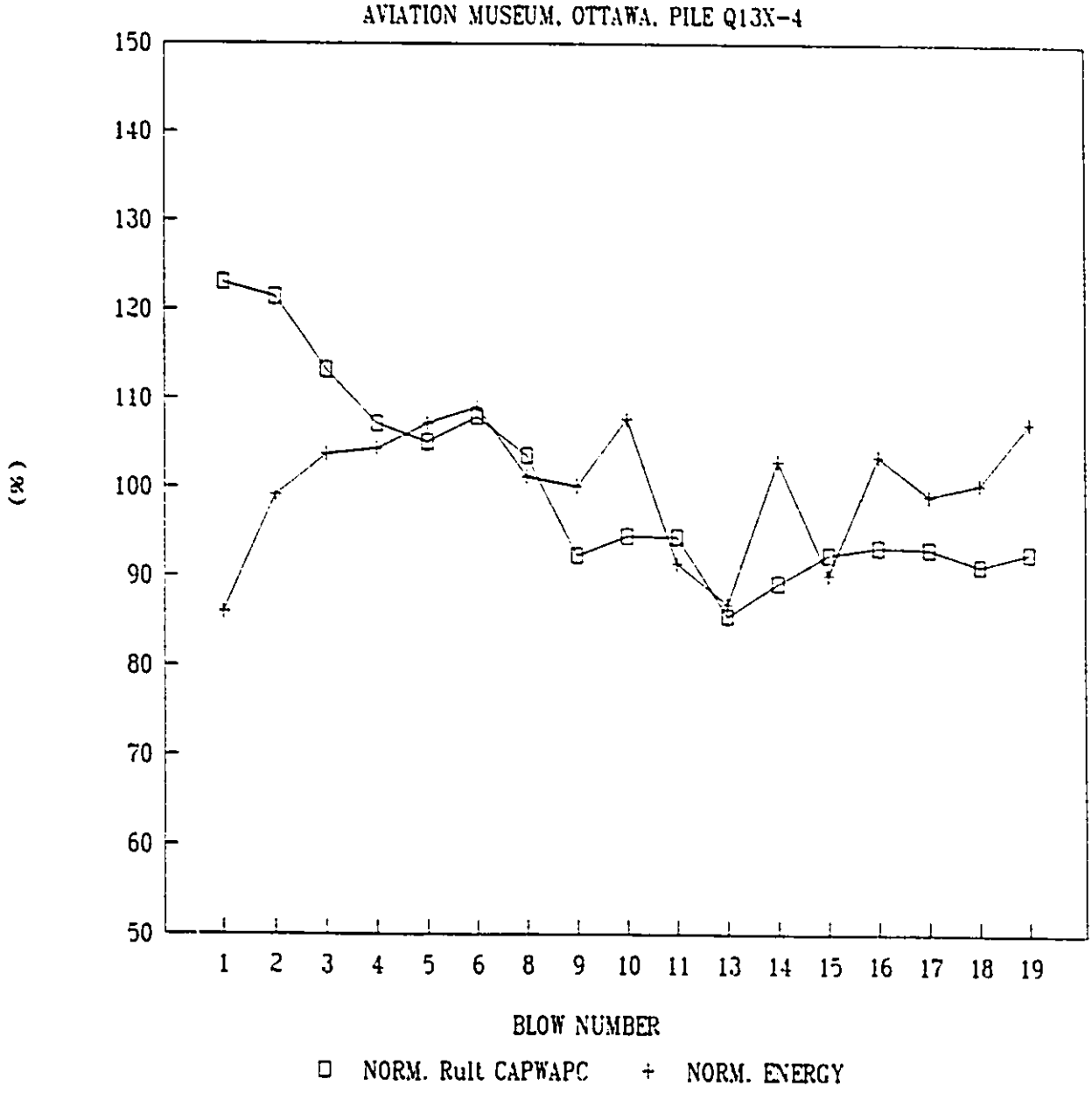

FIG. 4.27 - Rult CAPWAPC and CMES-RMX

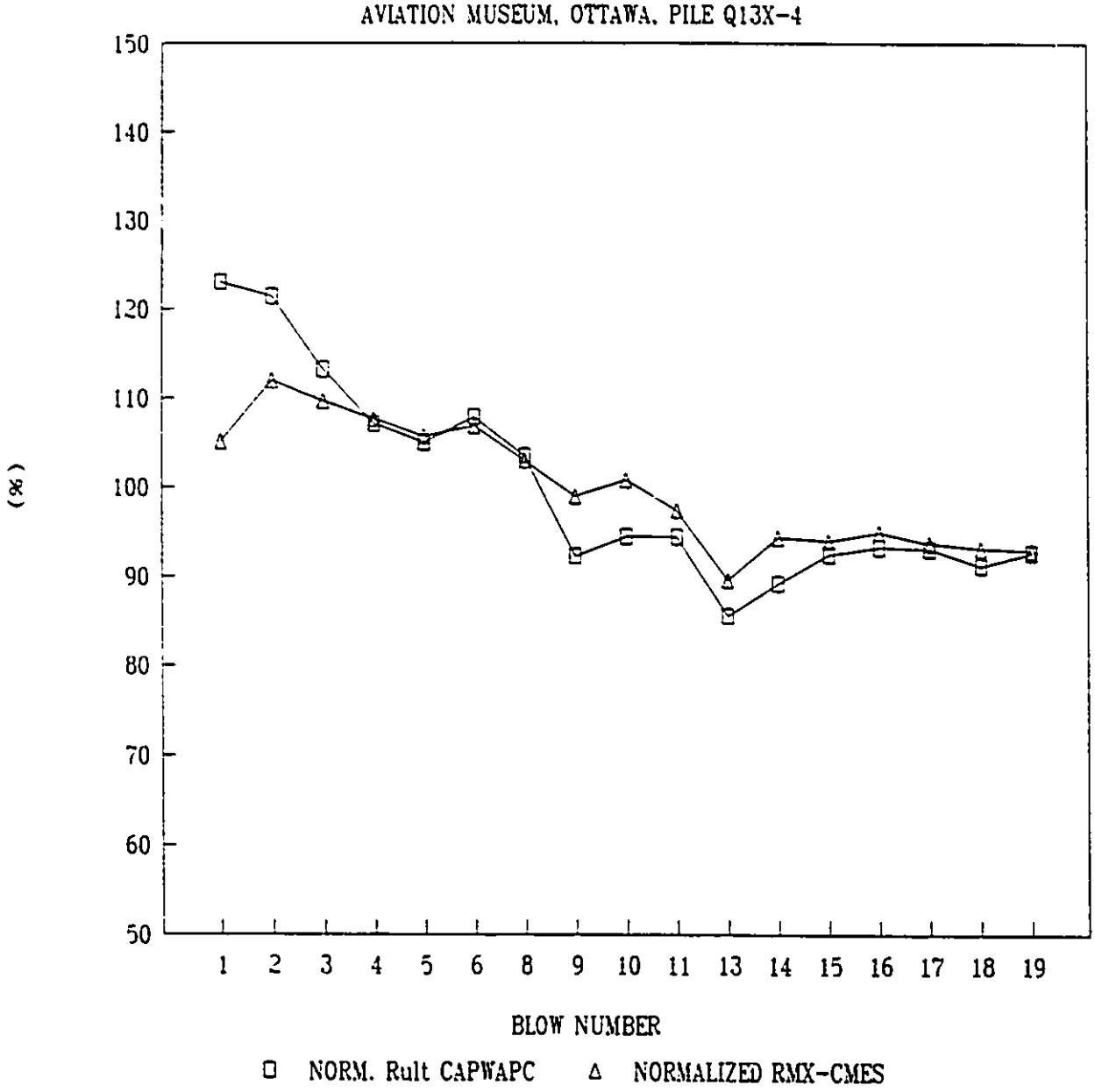

FIG. 4.28 – SHAFT AND TOE CAPACITY

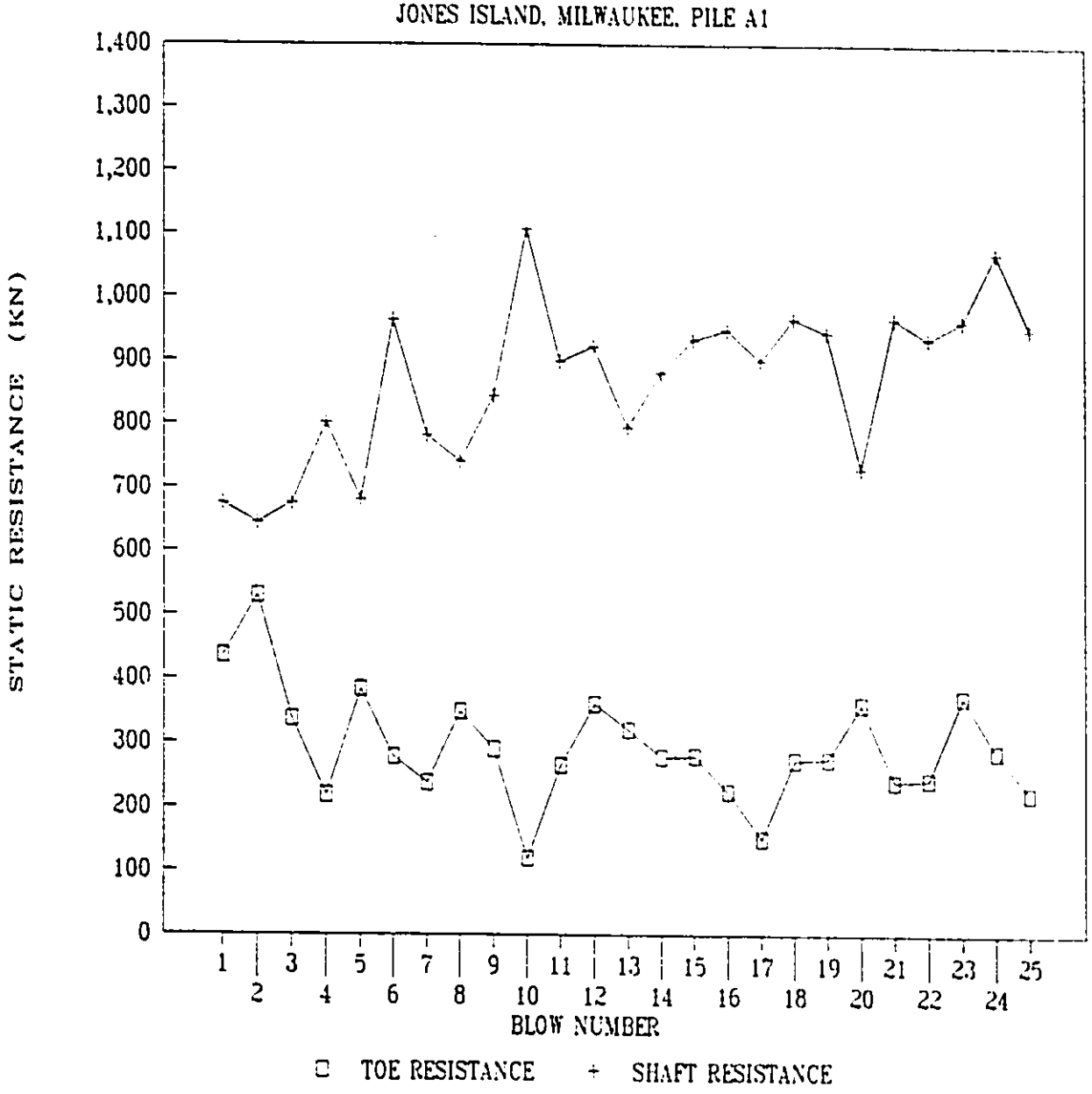

FIG. 4.29 – SHAFT AND TOE RATIO

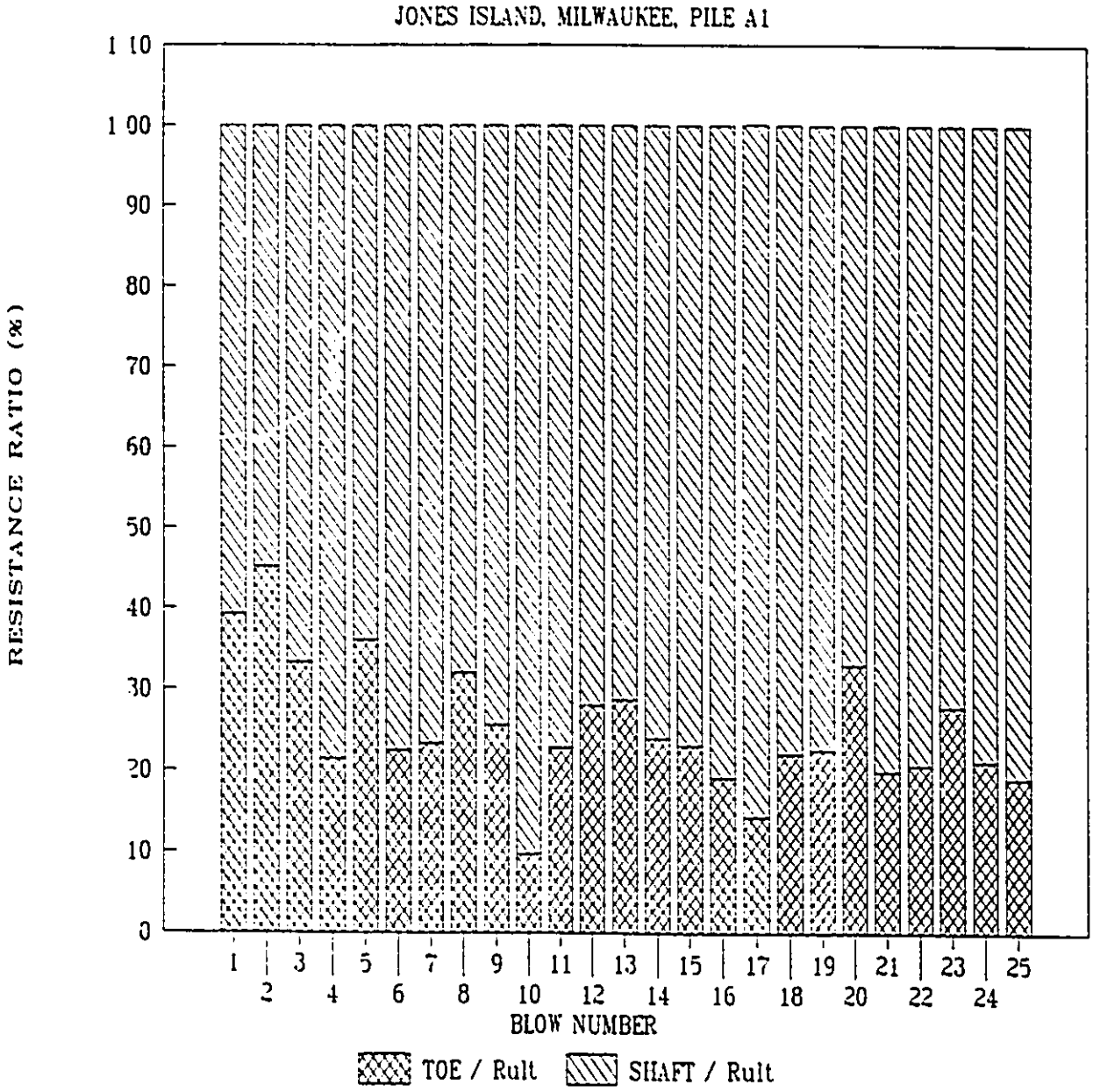

FIG. 4.30 – SHAFT AND TOE CAPACITY

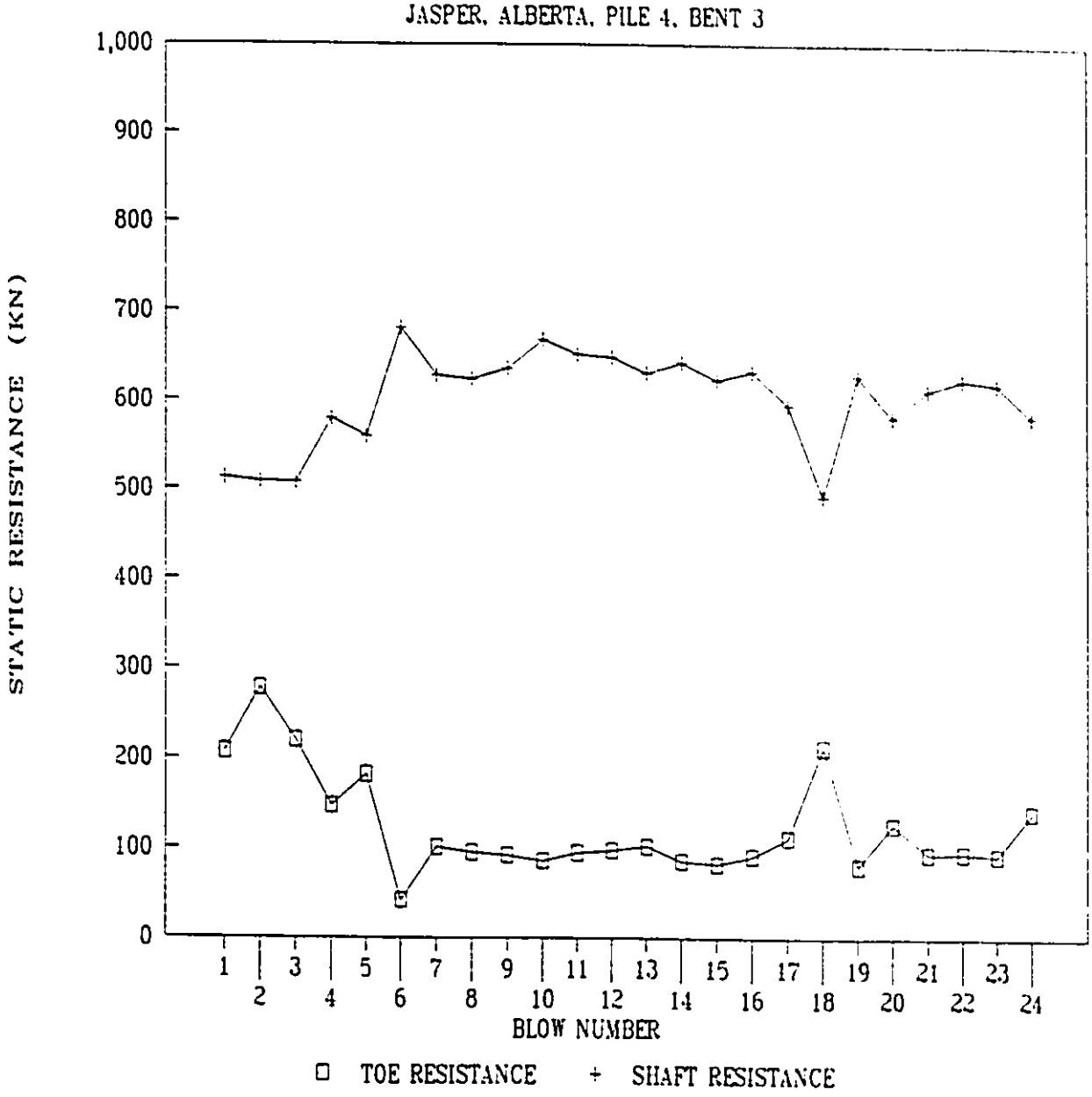

FIG. 4.31 – SHAFT AND TOE RATIO

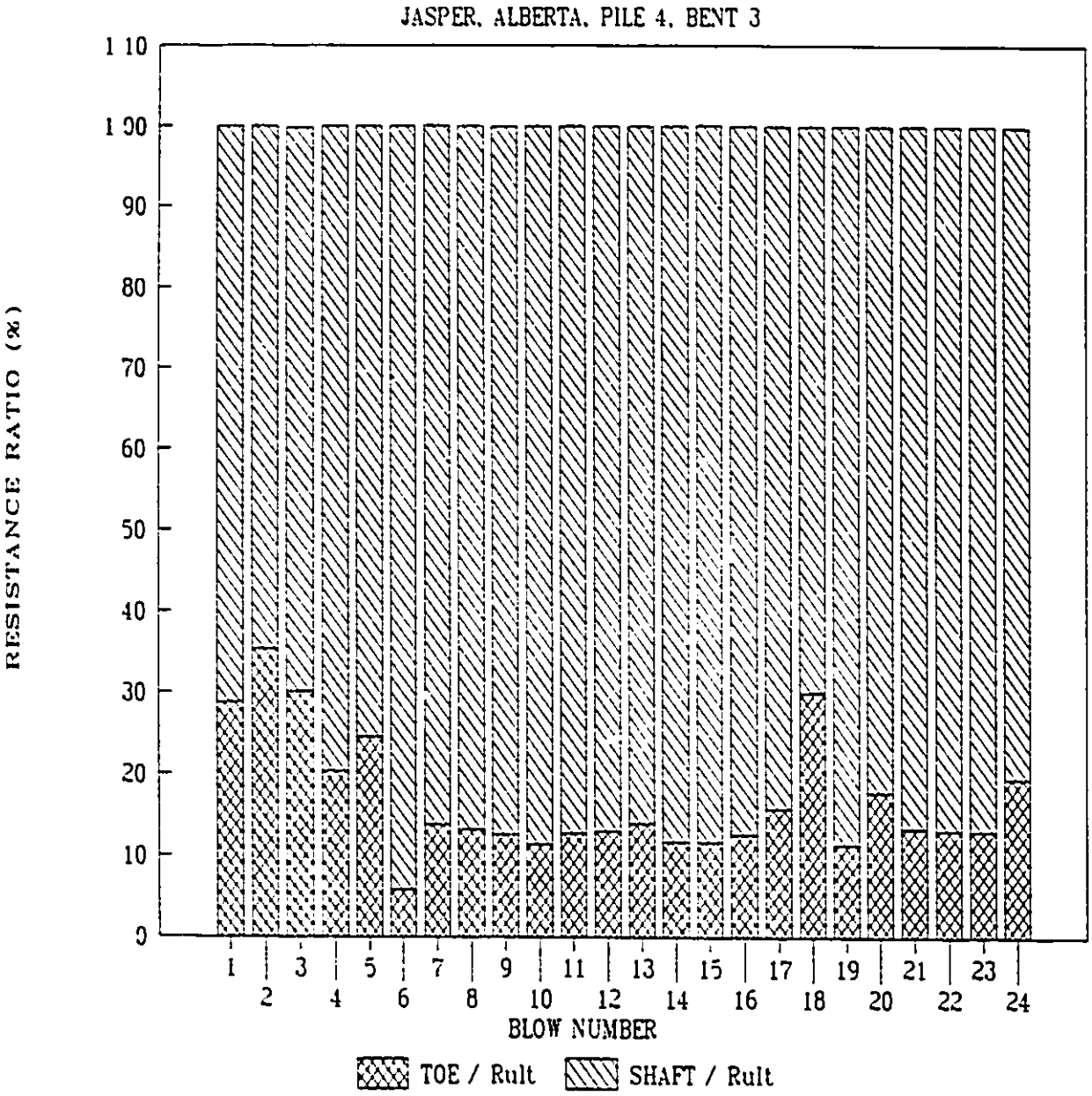

FIG. 4.32 – SHAFT AND TOE CAPACITY

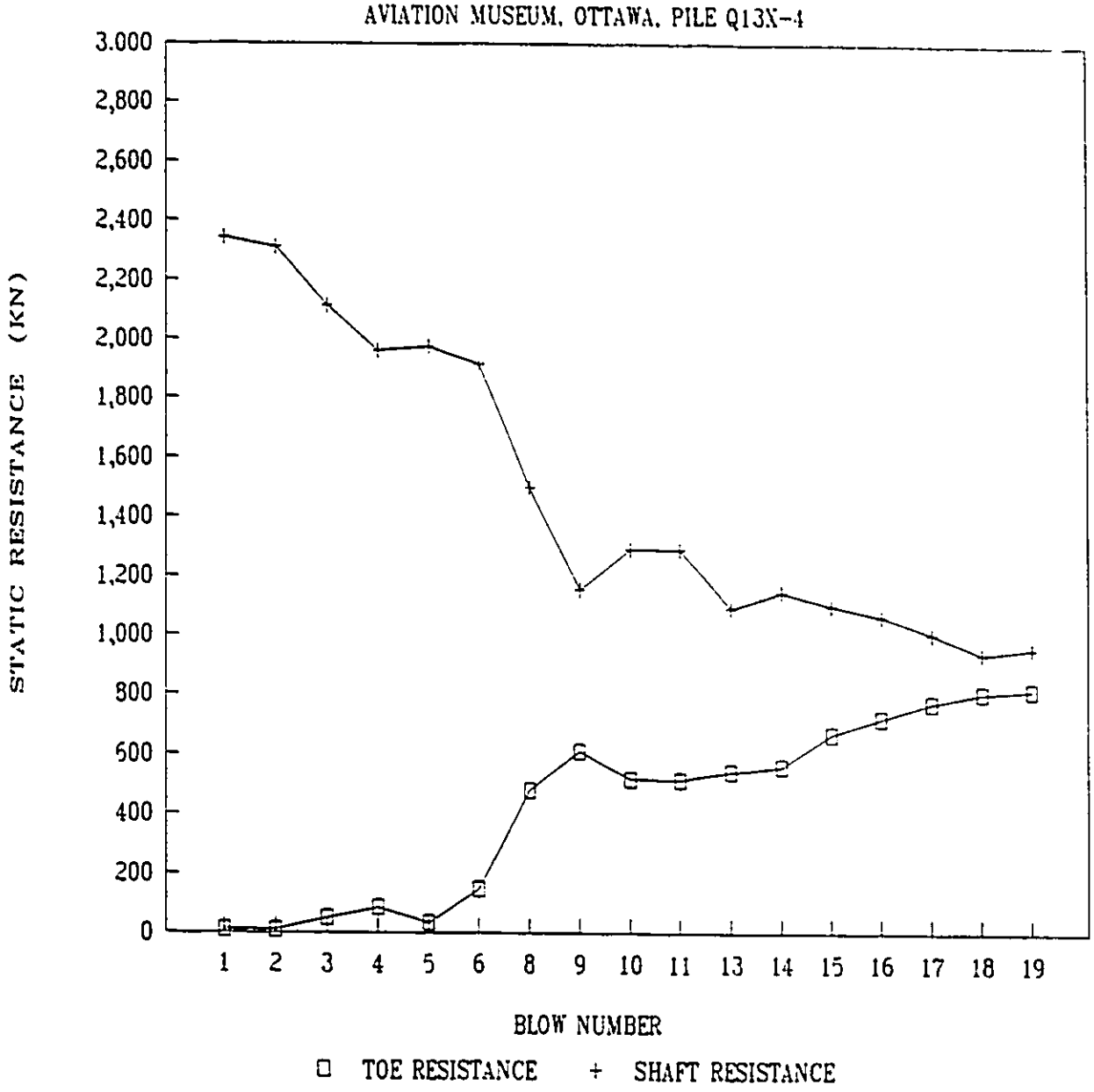

FIG. 4.33 – SHAFT AND TOE RATIO

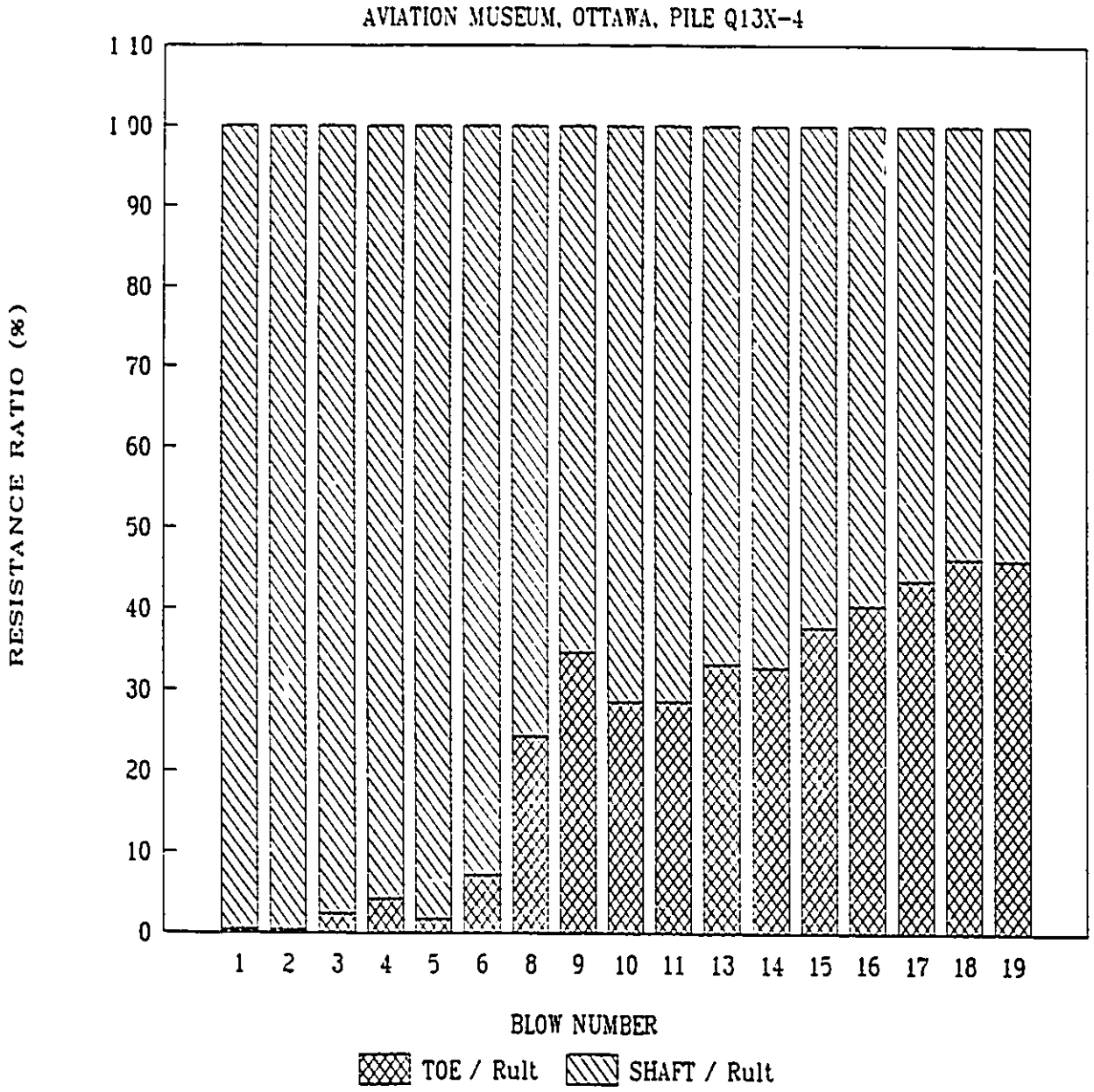

FIG. 4.34 – SHAFT DYNAMIC PARAMETERS

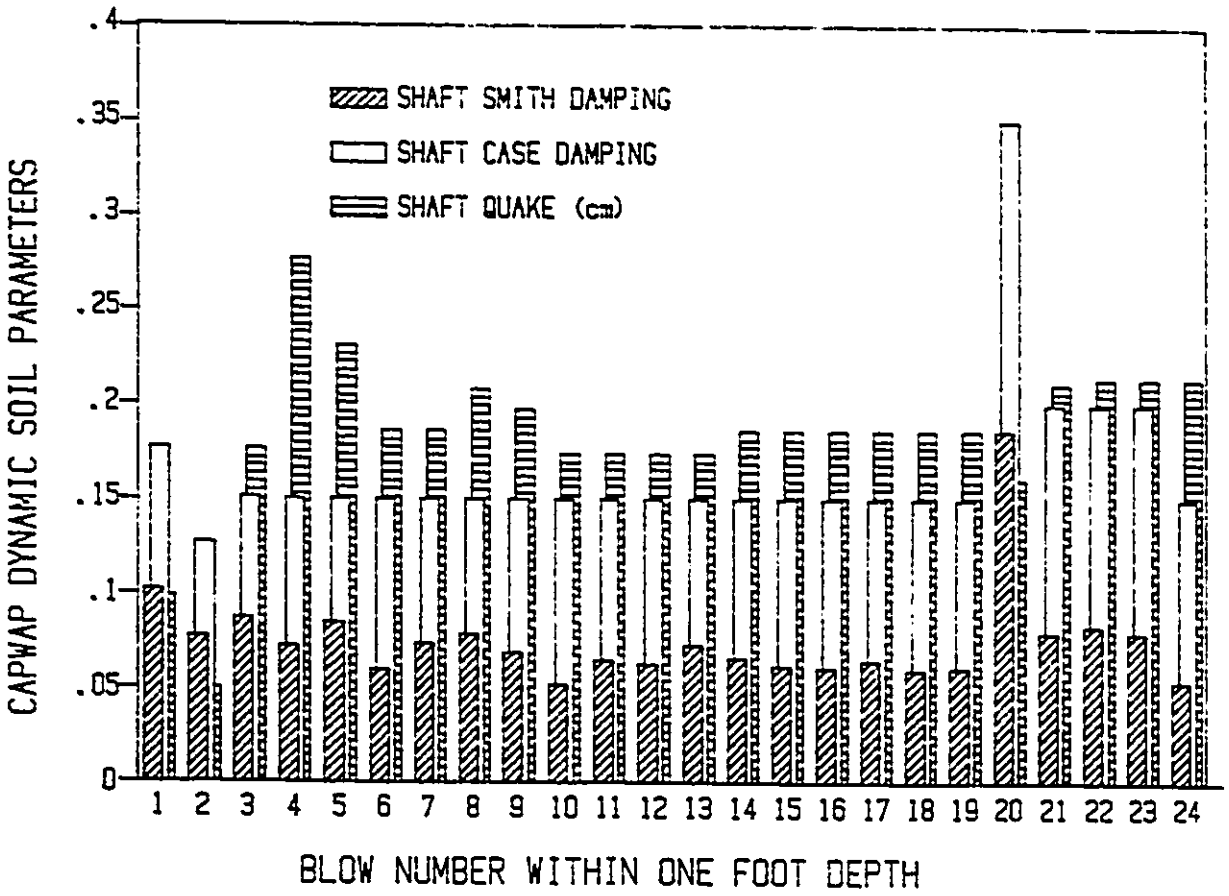

FIG. 4.35 – TOE DYNAMIC PARAMETERS

JONES ISLAND, MILWAUKEE, PILE A1

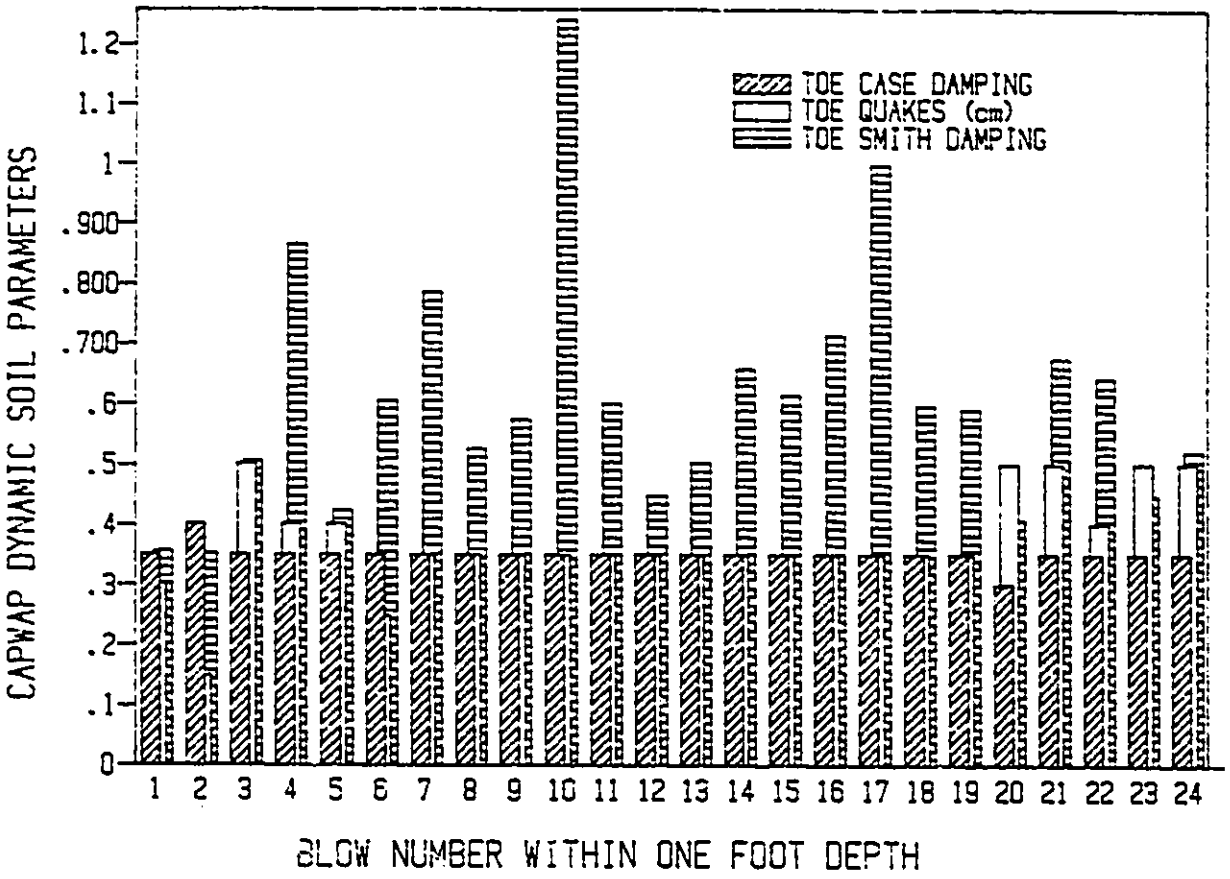

FIG. 4.36 – SHAFT DYNAMIC PARAMETERS

JASPER, ALBERTA, PILE 4, BENT 3

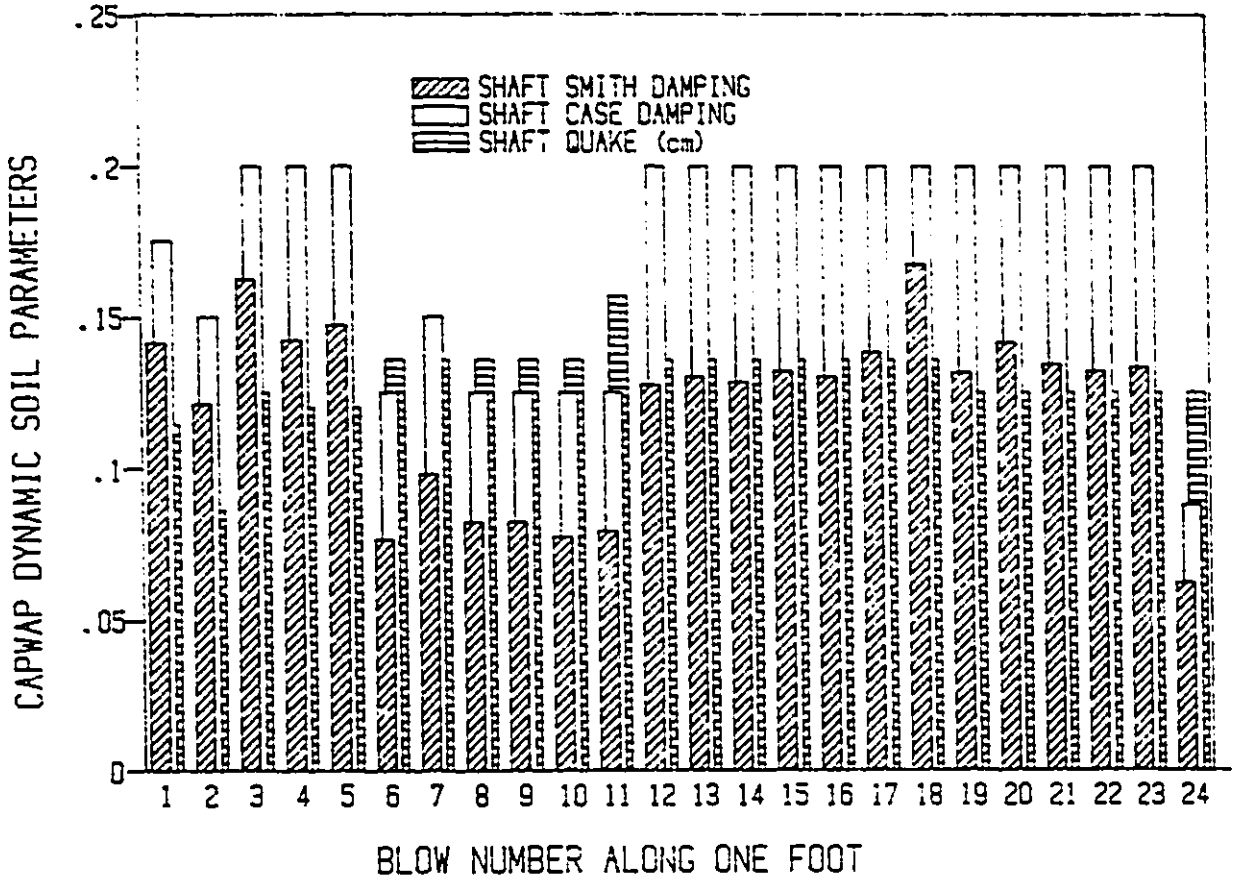

FIG. 4.37 – TOE DYNAMIC PARAMETERS

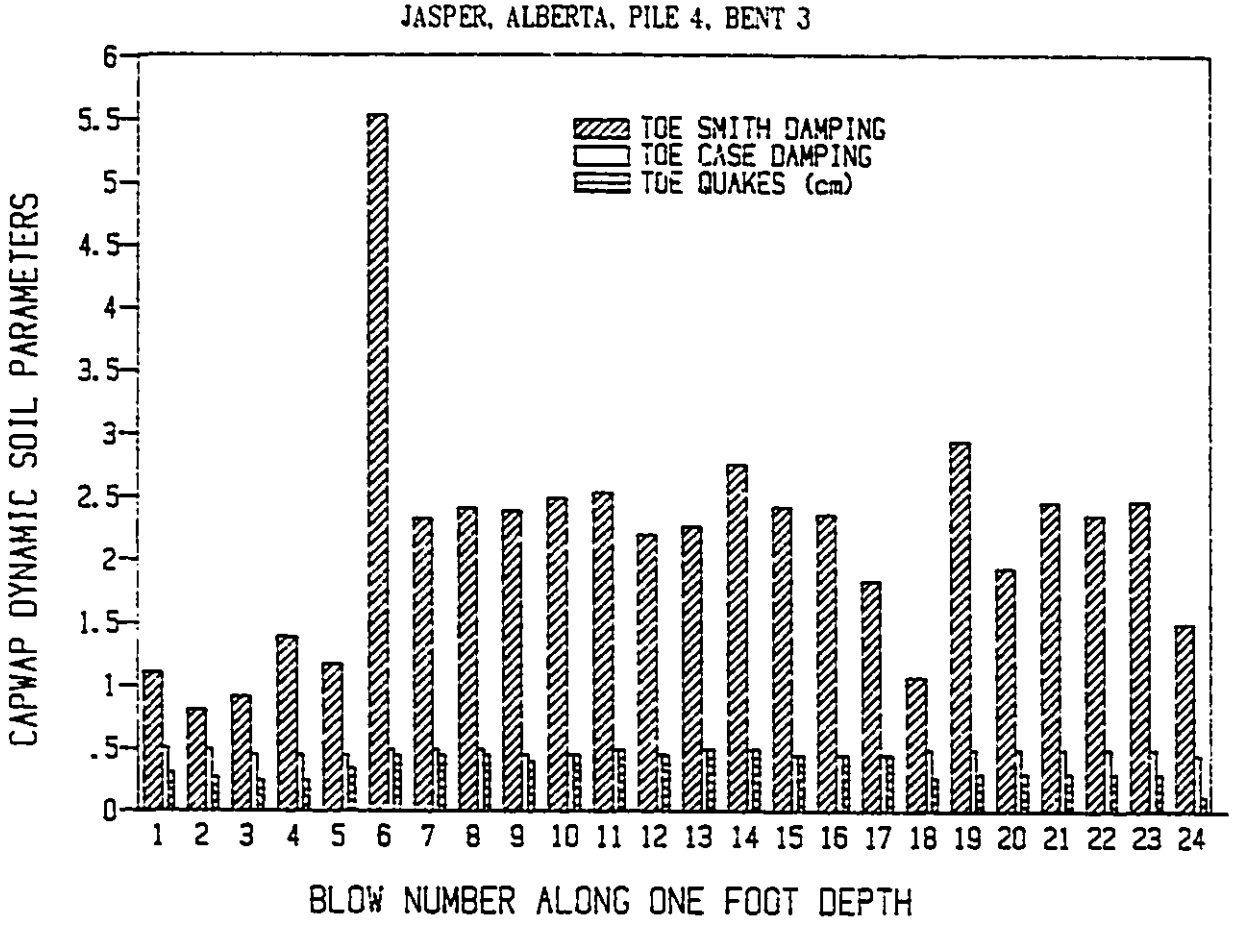

FIG. 4.38 – SHAFT DYNAMIC PARAMETERS

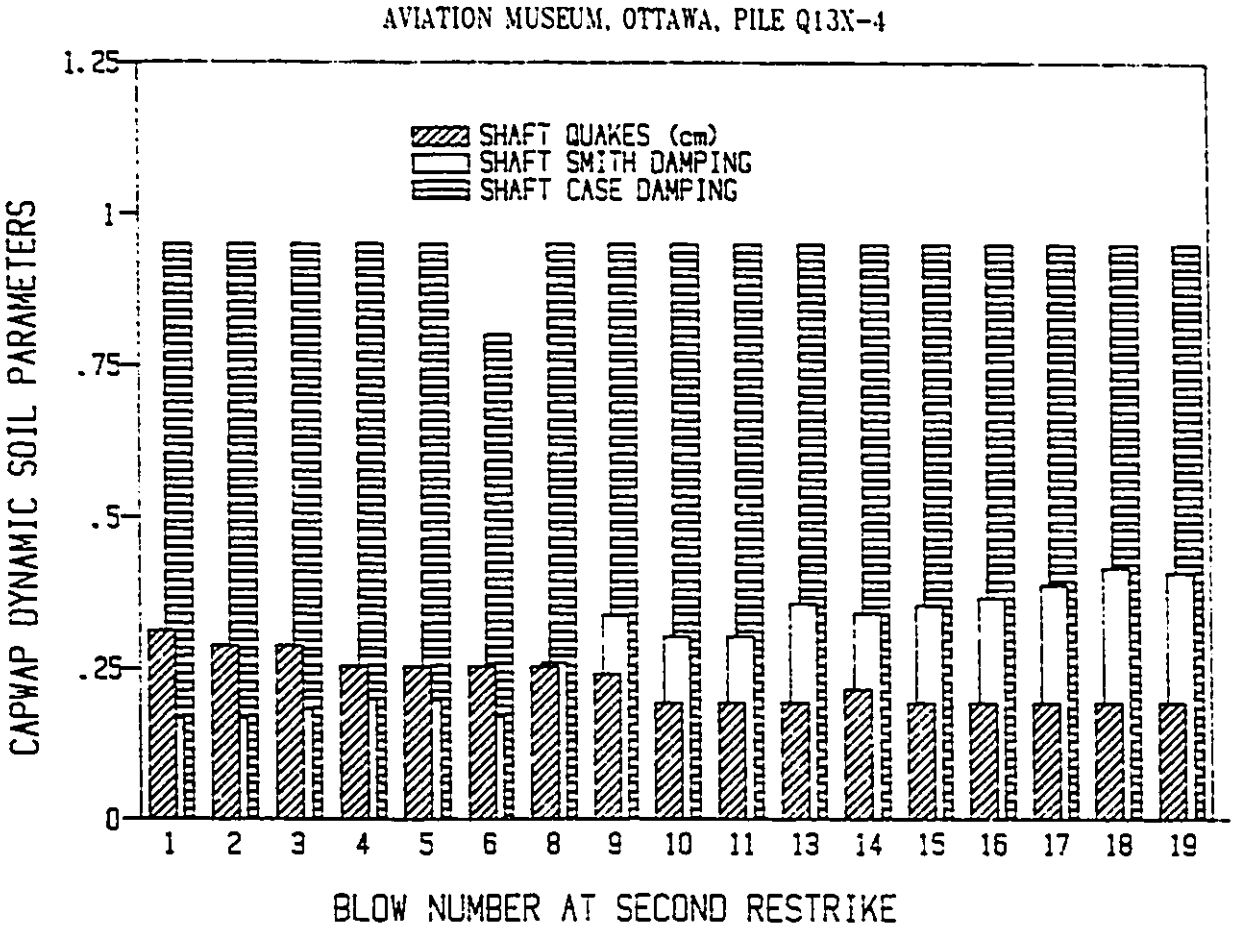

FIG. 4.39 – TOE DYNAMIC PARAMETERS